DEVELOPMENT OF HIGH PERFORMANCE REDOX FLOW BATTERIES FOR ENERGY STORAGE

Thesis submitted to the

University of Calicut
in partial fulfillment of the requirements
for the award of the degree of
Doctor of Philosophy in Chemistry
under the Faculty of Science
by

JEENA C.B.

Under the supervision of

Dr. V.T. JOY
Associate Professor & HOD
Post Graduate & Research Department of Chemistry
Christ College (Autonomous)
Irinjalakuda, Kerala, India-680125

MAY 2022

CERTIFICATE

This is to certify that the thesis entitled "**Development of high performance redox flow batteries for energy storage**" is an authentic record of the research work carried out by **Jeena C.B.** under my supervision in partial fulfillment of the requirements for the award of the degree of Doctor of Philosophy in Chemistry under the faculty of Science, University of Calicut, Kerala, India. The contents of this thesis, in full or parts have not been submitted to any other Institute or University for the award of any Degree or Diploma.

Dr. V.T. JOY
Assistant Professor & Head
Department of Chemistry
Christ College
Irinjalakuda, Pin: 680125

Place: Irinjalakuda

Date: 06-05-2022

Research and P.G. Department of Chemistry
Christ College, Irinjalakuda 680125

Dr. V.T. Joy
Supervising Teacher
Associate Professor & HOD
Post Graduate & Research
Department of Chemistry
Christ College (Autonomous)
Irinjalakuda, 680125
Kerala, India

Format for plagiarism check certificate

UNIVERSITY OF CALICUT
CERTIFICATE ON PLAGIARISM CHECK

1.	Name of the research scholar	JEENA. C.B.		
2.	Title of thesis/dissertation	DEVELOPMENT OF HIGH PERFORMANCE REDOX FLOW BATTERIES FOR ENERGY STORAGE		
3.	Name of the supervisor	Dr. V.T. JOY		
4.	Department/Institution	POST GRADUATE AND RESEARCH DEPARTMENT OF CHEMISTRY, CHRIST COLLEGE IRINJALAKUDA		
5.	Similar content (%) identified	Introduction/ Review of literature: 4%	Materials and Methods: 0%	Result/ Discussion/Summary/ Conclusion: 1%
	Acceptable maximum limit (%)	25 /35	25	10
6.	Software used	Oriqinal		
7.	Date of verification	25/4/2022		

**Report on plagiarism check, specifying included/excluded items with % of similarity to be attached.*

Dr. VINOD. V. M
Assistant Librarian(Sr.Scale)
University of Calicut

Checked by (with name, designation & signature)

Name & Signature of the Researcher JEENA. C.B.

Name & Signature of the Supervisor Dr. V.T. Joy

Dr. V.T. JOY
Assistant Professor & Head
Department of Chemistry
Christ College
Irinjalakuda, Pin: 680125

The Doctoral Committee* has verified the report on plagiarism check with the contents of the thesis, as summarized above and appropriate measures have been taken to ensure originality of the Research accomplished herein.

Dr. Jolly Andrews

Assistant Professor-
In-Charge
Christ College (Autonomous)
Irinjalakuda

Name & Signature of the HoD/HoI (Chairperson of the Doctoral Committee)

** In case of languages like Malayalam, Tamil, etc. on which no software is available for plagiarism check, a manual check shall be made by the Doctoral Committee, for which an additional certificate has to be attached*

DECLARATION

I hereby declare that the thesis entitled **"Development of high performance redox flow batteries for energy storage"** is the bonafide report of the original work carried out by me under the supervision of Dr. V.T. Joy, Associate Professor and HOD, Post Graduate & Research Department of Chemistry, Christ College, Irinjalakuda, Kerala, India for the award of the degree of Doctor of Philosophy in Chemistry, University of Calicut, Kerala, India. I further declare that the content of this thesis have not been submitted to any other Institute or University for the award of any Degree or Diploma.

Jeena C.B.

Place: Irinjalakuda

Date: 06-05-2022

ACKNOWLEDGEMENT

First and foremost, I thank God almighty who makes everything possible.

I would like to convey my deepest gratitude to my Ph.D supervisor, Dr. V.T. Joy, Associate Professor and Head of the Department of Chemistry, Christ College, Irinjalakuda, Kerala for the guidance and dependable support he provided to me during my Ph.D degree work. His enthusiasm and openness always made me feel comfortable working on several different projects during my studies.

I would also like to thank all my colleagues - Dr. Moly P.P, Elsa P.J., Ambily K.J., Daiphi Davis - for helping me with setting up experiments, giving me suggestions for new things to try, giving me feedback on my writing and presentations and most importantly for their friendship and kindness.

I want to thank my entire research committee for their time in reviewing my proposed work and thesis and for the feedback they gave me.

I express my sincere gratitude and tribute to Rev. Fr. Dr. Jose Thekkan C.M.I (Late), former Principal, Christ College Irinjalakuda for his love and support.

I wish to place on record my deep gratitude to Rev. Fr. Dr. Jolly Andrews, Principal Christ College Irinjalakuda, for the support given to me.

I am grateful for the support and help extended by Dr. Mathew Paul Ukken, former Head of the Dept. of Chemistry and all other former Heads of the Dept. of Chemistry, Christ College.

I would like to express my gratitude to Dr. Jibin A.K, Assistant Professor, Department of Chemistry, Christ College, Irinjalakuda, for helping me in charge-discharge experiments.

My gratitude also extends to Dr. Raina Jose Cherappanath, Dr. Prathibha P., Mrs. Vinitha M.S., Mrs. Priya Rajan (Late), Mrs. Sinta K.B., Dr. Sumesh N.V., Dr. Sreedevi Chakyar, Mrs. Drishya Mohan O.M and all other Research Scholars of Christ College (Autonomous), Irinjalakuda, for their helps in various ways.

I also thank all teachers and non-teaching staff members and students of Department of Chemistry, Christ College, Irinjalakuda, for their support and motivation during my research time.

I would like to express my heartfelt gratitude to the office staff, Christ College, Irinjalakuda for their support and assistance throughout my research.

I would also like to thank the Council of Scientific and Industrial Research (CSIR) of India, for providing financial support during my studies in the form of CSIR-JRF.

I convey my sincere gratitude to the University of Calicut for providing me all support during the research work.

I am thankful to SAIF-STIC, Cochin, for sample analysis.

I would like to express my gratitude to Mr. Arun Kumar, who handled the design work.

I would like to thank all of my friends for their encouragement and motivation, which has always inspired me to do my best.

I owe a sincere gratitude to all of my teachers for introducing me to the world of learning. I will be eternally grateful to my teachers at St. Thomas HSS Engandiyur, National HSS Engandiyur, Little Flower College, Guruvayur and Sree Narayana College Nattika, for their exceptional advice, support and motivation.

Lastly but most importantly, I am extremely thankful to my parents Balakrishnan, Renuka and sister Leena for their encouragement and support. Their prayers and blessing were the reason for all my achievements. I express my heartfelt gratitude to my husband Ciril Sreedhar and our lovely daughter Dhwani Sreyas, for their great love and continuous support during stressful days of my research. I would like to thank my in-laws, nephews and relatives for their support given to me.

JEENA C.B.

Dedicated

To

My Family

ABSTRACT

Keywords: Energy resources, redox flow batteries, anion exchange membranes, cyclic voltammetry, galvanostatic charge-discharge, efficiency.

Due to the rapid exploitation of nonrenewable energy sources, increasing attention has been given to the development of efficient, environmentally friendly, and economically viable energy conversion and storage systems. For grid-scale energy storage applications, flow batteries have been studied because their capacity and power delivery rate may be independently scaled.

Chapter 1 gives the details of current energy resources, classification of energy sources, the necessity of energy storage devices, batteries and their classifications, introduction and classification of flow batteries, electrochemistry, advantages and disadvantages of flow batteries, theory of electrode reaction and limitations of redox flow batteries.

Chapter 2 deals with various experimental techniques such as cyclic voltammetry, charge-discharge, electrochemical impedance spectroscopy and SEM techniques used for the characterization of the redox flow batteries developed in the present work.

Chapter 3 describes the development of a dendrite-free zinc-iron redox flow battery. Here a zinc-iron (Zn-Fe) RFB employing Zn/Zn(II) and Fe(III)/Fe(II) redox couples as negative and positive redox systems separated by a self-made anion exchange membrane is reported. The preparation of the anion exchange membrane and its properties are well discussed in this chapter. A key advancement in the present Zn-Fe hybrid redox flow battery is that there were no dendrite growth on zinc

electrodes during battery charging, which was the serious drawback of many early reported zinc-based redox flow batteries. The cell efficiencies, calculated from the charge-discharge curves and the repeated cycles, show no degradation in performance, confirming the excellent stability of the system.

Chapter 4 of this thesis describes an all-iron redox flow battery containing Fe/Fe(II) and Fe(III)/Fe(II) redox couples separated by the self-made anion exchange membrane. The charge-discharge performance of the cell was evaluated at a constant current density of 25 mA cm ^{2}. We also studied the influence of adding 0.03 M $ZnCl_2$ in the anode compartment on the electrode performance of the Fe/Fe(II) redox couple. The charge-discharge and cyclic voltammetry measurements showed an improvement in the electrochemical performance of Fe/Fe(II) redox couple after the addition of Zn^{2+} ions.

Chapter 5 of this thesis describes the development of a novel chloride-based copper-cerium flow battery employing Cu/Cu(II) and Ce(IV)/Ce(III) redox couples as reactive materials, separated by the self-made anion exchange membrane. Repeated galvanostatic charge-discharge measurements show that the system has a relatively stable electrochemical performance. Low-cost active materials and high cell performance makes the Cu-Ce flow battery a promising candidate for large-scale energy storage applications.

Chapter 6 of this thesis presents the summary and conclusions of the major findings of the studies described in previous chapters.

Chapter 7 of this thesis presents the recommendations for future studies.

CONTENTS

LIST OF FIGURES

LIST OF TABLES

CHAPTER 1

Introduction

1.1 Introduction

Energy is a vital prerequisite for global economic progress and social change in all countries [1,2]. We are consuming energy every day at home, at work and on the road, hence energy plays a crucial role in our daily life [3]. Since the industrial revolution, the fossil fuels, such as coal, petroleum, natural gas, etc., are burned to produce energy and the easy availability of fossil fuels had a significant impact on the development of many social structures. According to the US Energy Information Administration, the global energy demand is expected to rise 47% in the next 30 years, due to population and economic growth, especially in developing Asian countries. As the population and technologies are always expanding, the demand for renewable, efficient and less expensive energy sources is essential for the economic success of every nation [4].

1.2 Current energy sources

The energy resources are generally classified as nonrenewable and renewable. Fig. 1 shows various energy sources and their classification.

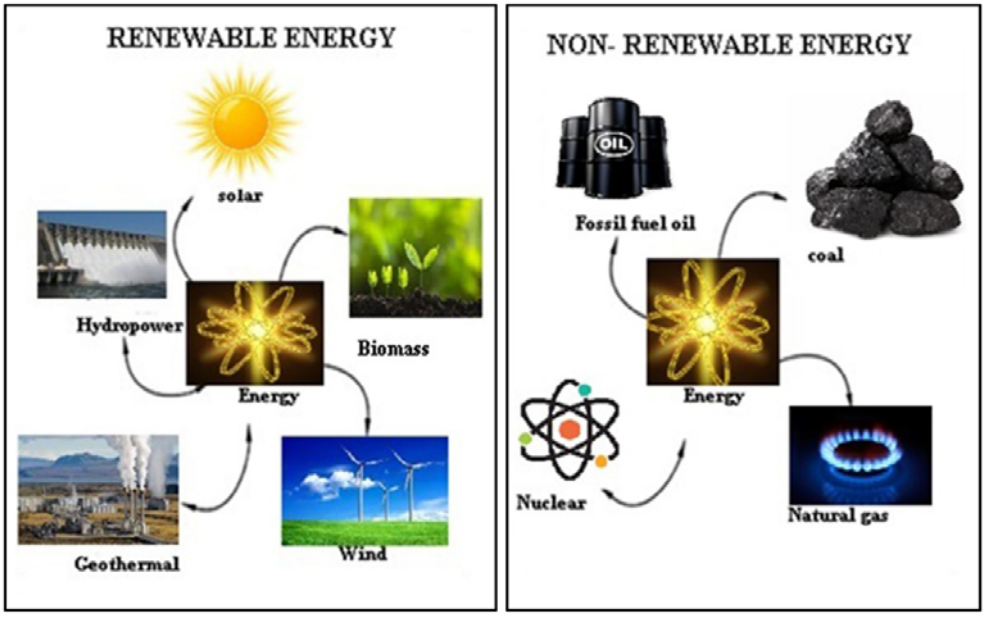

Fig. 1 Current energy sources.

1.2.1 Nonrenewable energy sources, advantages and limitations

Nonrenewable energy sources, such as crude oil, coal, natural gas and nuclear energy, take a long time to regenerate and hence they are limited and expensive. They will deplete in the near future, making them unsuitable for long-term use. Consumption of nonrenewable energy sources has been shown to inflict more damage on our environment than any other human activity over the last century [2,5].

1.2.1.1 Fossil fuels

Fuels such as coal, oil and natural gas are referred to as "fossil fuels". Their source (carbon and hydrogen) was discovered in the earth's crust, hence the word "fossil". Fossil fuels are the remains of animals and plants that lived millions of years ago. Electricity generated by coal and crude oil combustion has resulted in high levels of hazardous gases in the environment, including carbon dioxide, carbon monoxide,

sulphur dioxide, nitrogen monoxide and nitrogen dioxide. These hazardous gases pollute the air, which has detrimental consequences for human health and plant growth. Acid rain, which is mostly generated by sulphur dioxide and nitrogen oxide, causes soil, aquatic life and forests to deteriorate. Coal mining has resulted in the degradation of landscapes and habitats, as well as the barrenness of the terrain. Crops cannot be cultivated in such places due to the negative side effects. Global warming is mainly caused by carbon dioxide gas and the average temperature of the Earth's climate is rising as a result of it [3,6,7]. Because of the progressive warming of the Earth's surface, ice in the Arctic and Antarctica has constantly been melting, causing sea levels to rise. This process can cause devastating floods and has a significant impact on the environment. According to recent global carbon budgets, the concentration of carbon dioxide in the atmosphere has risen over time as a result of emerging economies and developing countries account for a bigger share of world emissions [8–10].

1.2.1.2 Nuclear energy

Nuclear energy is a portion of atomic nucleus energy that can be released through nuclear fission, fusion or radioactive decay. Nuclear reactors employ controlled fission to generate heat and energy. Nuclear waste from nuclear power plants produces thermal pollution, which can be harmful to the environment and hence the disposal of nuclear waste is a big issue [11]. There is also the risk of radioactivity being accidentally released. Natural disasters such as Tsunamis, earthquakes and other natural calamities have an impact on the working of nuclear reactors. For example, the Fukushima nuclear power plants disaster in 2011 and the Chernobyl disaster in 1986. In Fukushima, the tsunami caused by a massive

earthquake disrupted the power supply and cooling of three reactors in the plant, resulting in a nuclear disaster. In the first three days, all three cores melted to a great extent. As a precaution, 100,000 people were evacuated from their houses. The nonrenewable energy sources will run out one day, posing a danger to environmental balance and creating several ecological risks [12]. In this situation, industries must rely on renewable energy sources as soon as possible.

1.2.2 Renewable energy sources, advantages and limitations

Renewable energy sources, such as solar energy, wind energy, hydropower and biomass, are sources of energy that are abundant and almost endless. It is a non-polluting, non-depleting source of energy [2,13] and a more environmentally friendly alternative to traditional energy sources that rely on fossil fuels. India is lucky to have a lot of sunlight, water and biomass. The advantages of renewable energy sources are lower maintenance requirements, numerous environmental benefits and can create jobs more in the future [5]. The main disadvantages are its intermittent nature, limited storage capabilities and geographic limitations. Solar panels, wind turbines and hydroelectric dams, all generate electricity that is influenced by the weather, location and atmosphere [14]. The ministry of statistics and programme implementation, Government of India published a source-wise estimated potential of renewable power in India is shown in Fig. 2.

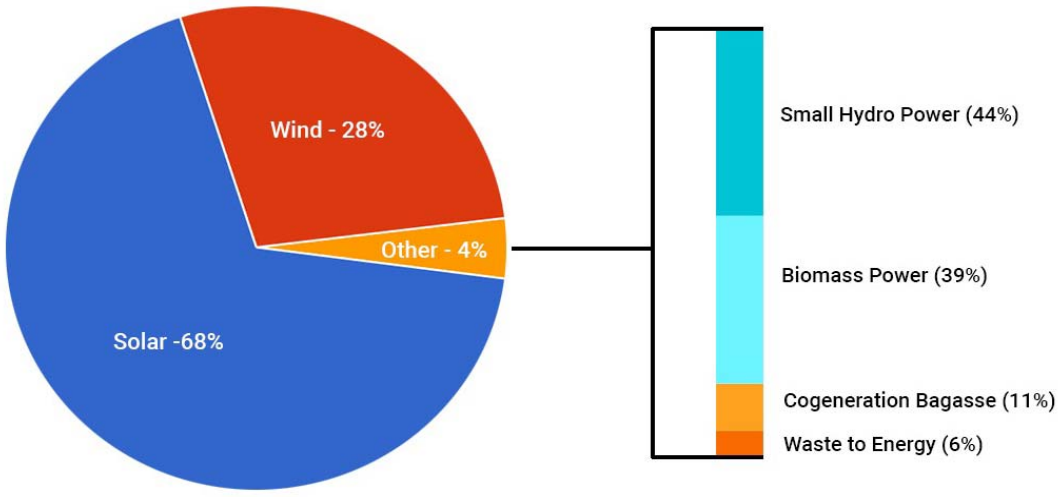

Fig. 2 A source-wise estimated potential of renewable power in India.

1.2.2.1 Solar energy

Solar energy is the energy from the sun, resulting from nuclear fusion at its core. The reaction releases energy that travels outward to the surface of the Sun. Along the way, to the surface, the energy transforms so that by the time it is released primarily as light. Solar energy is harnessed by catching the radiant energy of sunlight and converting it to heat and electricity. Solar energy may be used in a variety of ways in our daily lives, such as to generate power, cook meals and heat water. It has various benefits and the most significant advantage is that it is an infinite source of energy that can help to reduce the use of nonrenewable energy resources. It is also beneficial to the environment because no toxic gases are discharged into the atmosphere when it is utilized. If a small portion of solar energy is harnessed, we can meet the world's all energy needs [15].

1.2.2.2 Wind energy

Wind energy refers to the process of converting wind energy into electrical energy using wind turbines or other wind energy conversion devices. The uneven heating of the earth's surface by the sun produces wind and the kinetic energy created by airflow is used to generate electricity. When compared to coal, natural gas and fossil fuels, wind power is a cost-effective, clean and ecologically beneficial source of electricity. Wind energy can be found in a wide range of locations. The availability of sites with sufficient wind (at least 20 kilometers per hour) and the number of wind machines that the site can accommodate limit the widespread development of wind power [7,16].

1.2.2.3 Biomass Energy

Crops, waste wood and trees are examples of biomass, which is an organic material derived from plants and animals [17]. The chemical energy in biomass is transformed into heat, which can then be used to generate electricity via a steam turbine. Biomass is frequently referred to as a cleaner and greener renewable fuel that may be used to generate power instead of coal and other fossil fuels [18].

1.2.2.4 Geothermal Energy

The thermal energy created and stored in the Earth's crust is known as geothermal energy. This thermal energy comes from two sources: heat produced by gravitational collapse during the formation of the world and heat produced by the radioactive decay of certain isotopes. Geothermal energy is a low-cost, sustainable, long-term and environmentally beneficial source of energy. It is only found at the tectonic plate boundaries. Geothermal energy is renewable because of the reason that

Earth has retained a huge amount of the heat energy released during the formation of the planet. Furthermore, the decay of radioactive materials inside the Earth provides heat constantly. The total amount of heat lost through natural processes (such as volcanic movement and conduction/radiation to the environment) is far more than the total amount of heat lost by geothermal vitality generation [19–22].

1.2.2.5 Hydropower

The conversion of energy from falling or fast-moving water into electricity is known as hydropower or hydroelectricity. Water must be in motion to generate electricity and the kinetic energy of the flowing water is transferred to mechanical energy by turning blades in a turbine. The turbine subsequently spins the generator rotor, which converts mechanical energy into electrical energy [23,24].

1.3 The necessity of energy storage

In the future, renewable energy will play a bigger role as an energy source. The main disadvantage of wind and solar energy is that they are intermittent. As the amount of renewable energy produced grows, more energy storage systems will be required to compensate for the fluctuating power generated by wind and solar panels. This stored energy can then be released as needed, maintaining a continuous supply of clean energy at times of peak demand. Scalability, extended life-cycle cost, high efficiency and quick response time are the four primary characteristics of an effective energy storage system. Conventional rechargeable batteries offer a simple and efficient way to store electricity from renewable energy sources [24–29].

1.4 Battery as energy storage device

Batteries store chemical energy and generate electricity through an electrochemical redox reaction. The working of galvanic, fuel and flow cells are all based on redox reactions. A negative electrode, positive electrode, electrolyte (which conducts ions) and separator make a cell. Electrolytes provide the medium for the transfer of charges, which are in the form of ions, between the electrodes. The separator is a type of polymeric membrane that is placed between the anode and the cathode to prevent electrical short-circuiting. During charging of a cell, the electrode at which the oxidation occurs is called the anode and it has a positive voltage, while the electrode at which the reduction occurs is the cathode and has a negative voltage. While in discharging, the anode has a negative charge and the cathode a positive charge [30].

1.5 Types of batteries

Batteries are classified into two categories: primary and secondary batteries based on their capability of being electrically recharged. Fig. 3 represents the classification of various types of batteries.

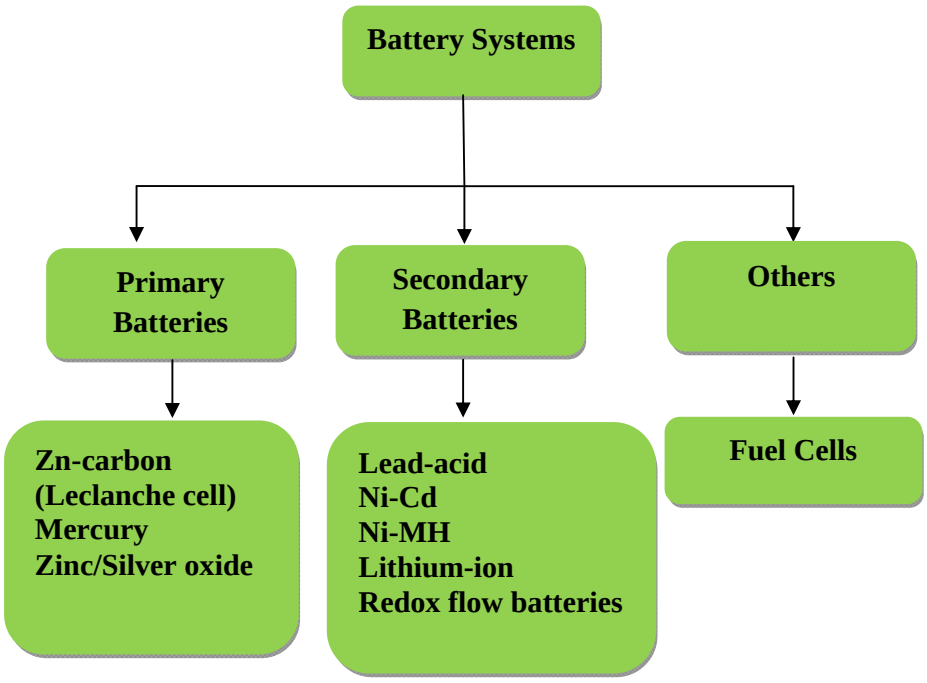

Fig. 3 Types of batteries [31].

1.5.1 Primary batteries

The chemical energy in primary batteries is transformed into electrical energy in a one-way process. It only transforms the chemicals into electricity once and then has to be thrown away after usage [32,33]. The primary batteries are used in remote controls, flashlights, clocks, transistor radios, etc. Leclanche cell, zinc-silver oxide, zinc-mercuric oxide and zinc-air are some examples and Table 1 explains the anode, cathode, electrolyte and cell reactions of these batteries [34].

Table 1 Examples of primary battery.

Battery	**Anode (material & reaction)**	**Cathode (material & reaction)**	**Electrolyte**	**Reaction Mechanism**	**Voltage (V)**
Zn-carbon (Leclanche cell)	Zn $Zn(s) \rightarrow Zn^{2+} + 2e^-$	MnO_2 $2MnO_2(s) + 2NH_4^+(aq) + 2e^- \rightarrow Mn_2O_3(s) + 2NH_3(aq) + 2H_2O$	Ammonium chloride and zinc chloride dissolved in water	$Zn + 2MnO_2 + 2NH_4^+ \rightarrow Zn^{2+} + Mn_2O_3 + 2NH_3 + 2H_2O$	1.5
Mercury	Zn (Hg) $Zn(Hg) + 2OH^- \rightarrow ZnO + H_2O + 2e^-$	HgO $HgO + H_2O + 2e^- \rightarrow Hg + 2OH^-$	KOH/NaOH	$Zn + HgO \rightarrow ZnO + Hg$	1.3
Zinc/Silver oxide	Zn $Zn + 2OH^- \rightarrow ZnO + H_2O + 2e^-$	Ag_2O $Ag_2O + H_2O + 2e^- \rightarrow 2Ag + 2OH^-$	KOH/NaOH	$Zn + Ag_2O \rightarrow ZnO + 2Ag$	1.6

1.5.2 Secondary batteries

A secondary battery converts chemical energy into electrical energy and can be recharged by passing a suitable current through the circuit in opposite direction. As a result, it is referred to as a storage or rechargeable battery because it can be recharged several times. Lead-acid, lithium-ion, Ni-Cd and Ni-MH batteries are all examples of secondary batteries [35,36]. Lead-acid battery is the oldest rechargeable battery with a life span of only 3 to 5 years. Lead and cadmium are very hazardous metals that can harm the environment if they are not properly disposed of after usage. Many applications that were previously served by lead and nickel-based batteries are

now being replaced by Li-ion batteries. The Li-ion battery requires a protection circuit for safety reasons and it costs more than other rechargeable batteries. Table 2 shows the anode, cathode, electrolyte and cell reactions of some of the secondary batteries [27].

Table 2 Examples of the secondary battery.

Battery	**Anode (material & reaction)**	**Cathode (material & reaction)**	**Electrolyte**	**Reaction Mechanism**	**Voltage (V)**
Lead-acid	Pb $Pb + H_2SO_4 \rightleftarrows PbSO_4 + 2H^+ + 2e^-$	PbO_2 $PbO_2 + H_2SO_4 + 2H^+ + 2e^- \rightleftarrows PbSO_4 + 2H_2O$	H_2SO_4	$Pb + PbO_2 + 2H_2SO_4 \rightleftarrows 2PbSO_4 + 2H_2O$	2.1
Ni-Cd	Cd $Cd + 2OH^- \rightleftharpoons Cd(OH)_2 + 2e^-$	Ni oxide $2NiOOH + 2H_2O + 2e^- \rightleftharpoons 2Ni(OH)_2 + 2OH^-$	KOH	$Cd + 2NiOOH + 2H_2O \rightleftharpoons 2Ni(OH)_2 + Cd(OH)_2$	1.35
Ni-MH	MH $MH + OH^- \rightleftharpoons M + H_2O + e^-$	Ni oxide $NiOOH + H_2O + e^- \rightleftharpoons Ni(OH)_2 + OH^-$	KOH	$MH + NiOOH \rightleftharpoons M + Ni(OH)_2$	1.2
Lithium-ion	Graphite/Carbon material $LiC_6 \rightleftharpoons C_6 + Li^+ + e^-$	$LiCoO_2/LiMn_2O_4$ $CoO_2 + Li^+ + e^- \rightleftharpoons LiCoO_2$	Lithium salts in organic solvents	$LiC_6 + CoO_2 \rightleftharpoons LiCoO_2 + C_6$	3.8

1.6 Redox flow batteries (RFBs)

Redox flow batteries (RFBs) are one of the most modern electrochemical systems and a highly promising solution for stationary energy storage applications [37]. RFBs are ideal electrical energy storage systems for the usage of renewable energy sources because of their high energy efficiency, low self-discharge, long discharge ability and cycle life. The decoupling of energy capacity and power density, which is not possible with other existing conventional systems, is a unique advantage of RFBs. In 1884, a French physicist named Charles Renard invented the first flow battery [38]. The reactive ingredients in the battery include zinc and chlorine and it was used to power an electric motor that drove the propeller of a warship. In the 1970s, NASA developed a flow battery based on the chemical reaction between iron and chromium as a new approach to store solar energy [39,40]. Different researchers and commercial organizations produced other flow batteries, such as the zinc-bromine redox flow battery [41] and the polysulfide-bromine flow battery [42], although their early development was hindered by numerous restrictions. These flow batteries contain hazardous chemicals and operate at high temperature and pressure. Since a variety of electrolytes were used in the negative and positive half-cells, a membrane failure or a small amount of molecular transfer through the membrane creates the cross-contamination of electrolytes in both half-cells after a few charge and discharge cycles [38]. These limitations prevented the widespread acceptance and commercial feasibility of redox flow batteries.

The conventional application of redox flow battery is load-leveling, which consists of storing energy during off-peak hours from a power plant and reliable it when the demand rights and this technology is often used with other renewable energy sources, such as photovoltaic cells and wind turbines [43]. Due to the rapid

progress of energy production from renewable energy increases, the development of more efficient, reliable and safer redox flow batteries are receiving more attention. Compared to other electrochemical energy storage systems, such as conventional batteries, redox flow batteries can store energy in the form of reduced and oxidized electroactive species in electrolyte, while conventional batteries store energy within the solid electrode materials. The electrolytes of the redox flow cell are stored externally and are consumed during the electrochemical reaction to release energy, while a H_2-O_2 fuel cell produces electricity using the chemical energy of hydrogen and oxygen [44,45]. The capacity of the redox flow battery can be increased by simply increasing the volume of electrolyte reservoirs [46], whereas the battery power depends on the number of electrochemical cells [27]. Redox flow batteries are mostly used in stationary applications for peak load and load balancing, as well as for uninterruptible power supply [47]. In comparison to batteries with a limited number of cycles, redox flow batteries are particularly versatile in daily use due to their limitless number of cycles throughout a lifespan of around 20 years. Table 3 shows the general comparison between batteries, fuel cells and redox flow cells.

Table 3 The comparison between battery, fuel cells and redox flow cells [48][43].

Energy storage Device	Reactants/products	Electrolytes	Separator
Battery	Active electrode material	Static and held within cell	Polymer separator (Microporous)
Fuel cell	Anode (gaseous or liquid fuel) and cathode (air)	Solid polymer or ceramic material acts as a solid electrolyte within the cell	Ion-exchange membrane
Redox flow Battery	Aqueous electrolytes in tanks	Electrolytes recirculate through the cell	Ion-exchange membrane or not necessary

1.7 Principle and characteristics of redox flow batteries

In redox flow batteries (RFBs), the electrolytes containing the active redox species are stored in external tanks and are circulated through bipolar stacks during charge and discharge [49]. The bipolar stack consists of several stack cells, each with a frame, a bipolar plate and a membrane. The power output depends on the number and size of the stack cells and the size of the tanks determine the capacity of a redox flow battery.

The following are the characteristics of redox flow batteries [50]:

- The basic principle of the battery reaction is the change in the valence of the metal ions in the electrolyte, resulting in a long charge/discharge cycle life.

- The cells and tanks are independent of each other and can be configured for application requirements.
- Individual cells are fed with the same electrolyte, making maintenance simple.
- Except in the cell portion, the electrolyte is held separately in the positive and negative tanks, preventing self-discharge during standby and stopping.
- The electrolytes are environmentally friendly and may be used permanently and can reuse.

1.8 Structure of a redox flow battery

Flow batteries are also known as redox flow batteries (RFBs) because, like conventional batteries and fuel cells, they also convert chemical energy in the electroactive materials stored in external tanks directly into electrical energy through an electrochemical redox reaction. A flow-type cell and electrolyte tanks are essential components of redox-flow batteries (one for the anolyte and another for the catholyte). An ion-exchange membrane separates two parallel electrodes in the electrochemical cell and all the electro-active components are dissolved in the liquid electrolyte and kept in separate tanks [51,52]. When the electrolytes are pumped from storage tanks to flow-through electrodes in a cell stack, electrochemical energy conversion occurs. The ion-exchange membrane prevents electro-active species from mixing or crossing over, which can lead to battery short-circuiting, while allowing charge-carrying ions to be transported to maintain electrical neutrality [53,54]. The electrodes have no active components and hence do not participate in the redox process. The cathode is the negative electrode during charging, while the anode is the

positive electrode. It is reversed during discharge. Fig. 4 shows a schematic illustration of a redox flow battery.

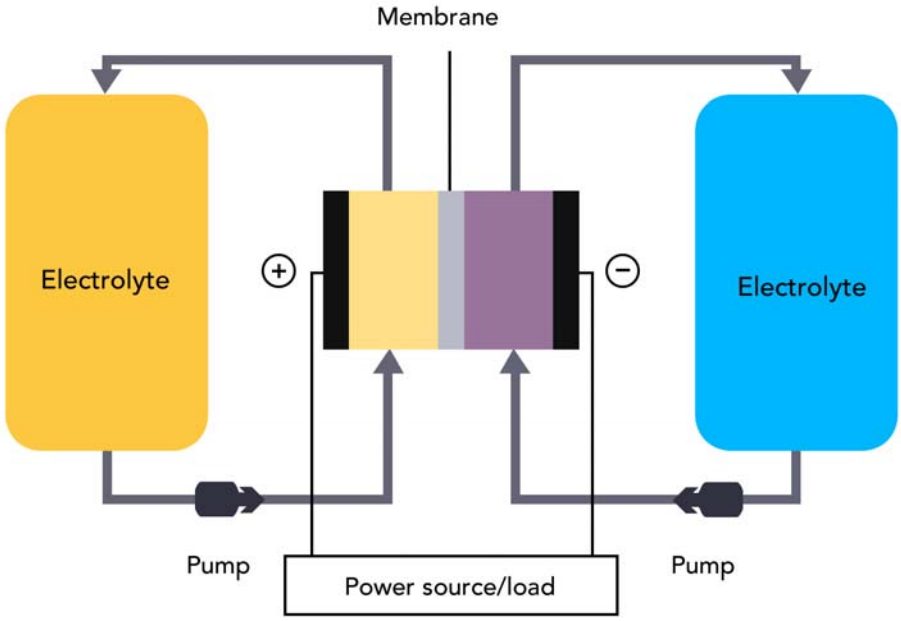

Fig. 4 Schematic of a redox flow battery.

1.9 Advantages and disadvantages of redox flow batteries

The following are the key advantages of redox flow batteries [35,38,48] :

- Long cycle life (~20 years)
- Quick response time
- Power and energy requirements are separated
- Deep charge and discharge cycles are possible without reducing cycle life
- Self-discharge lasts only a few minutes
- Operational flexibility and a quicker response to price changes
- Electricity stored in batteries can be used to fulfill unexpected demands

- The ability to buy or supply electricity at any time of day, whether it is peak or off-peak
- Excellent charging efficiency (70-90%)
- Operational flexibility
- The electrolytes are non-flammable and non-explosive

The following are the disadvantages of redox flow batteries [35,38,48]:

- Flow batteries are more complicated than standard batteries because they may require pumps, sensors, control units and secondary containment vessels
- Energy densities vary significantly but are low when compared to other battery systems
- Electrolytes and cell construction are major cost drivers
- Maintenance is difficult because the corrosive and toxic electrolyte needs thermal management, electrolyte management and careful storage and transportation
- Electrolyte crossover through the membrane
- Flow batteries are a relatively new technology

1.10 Design and components of redox flow batteries

The cell stack, external tanks and circulating pipes are the three primary components of a conventional RFB arrangement. Fig. 5 depicts a typical unit cell of a flow battery stack, which is made up of a positive and negative electrode separated by an ion-exchange membrane or separator. When the electrolytes are pumped through the electrodes, the chemical reactions take place in the cell stack. The oxidized and

reduced redox pairs on the electrode are recycled to external tanks, while charge balancing ions are transferred across the membrane.

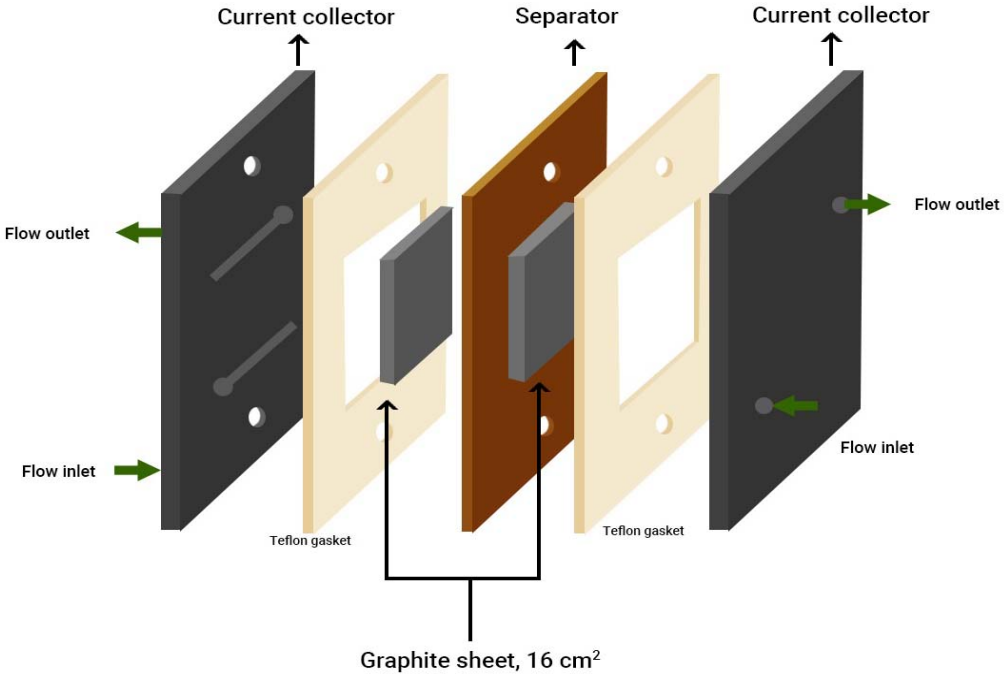

Fig. 5 Unit cell of a flow battery.

1.10.1 Electrode materials

In highly oxidizing conditions, a suitable electrode material should have high electrical conductivity, superior mechanical qualities and good chemical resistance, be economical and have a long cycle life. Carbon-based or inert metallic materials are commonly used as electrodes in redox flow batteries because they do not dissolve or produce oxide during chemical oxidation. In most metallic electrodes, metal ions can dissolve into the electrolyte due to corrosion causing a shift in redox potentials and disrupting the chemistry of redox flow batteries. Even though the precious metals like platinum and gold have great chemical stability and electrical conductivity, their high cost makes them unsuitable as electrodes for RFBs. Carbon felt, graphite felt and

porous graphite are some of the most commonly used carbon-based electrodes [43,55].

1.10.2 Electrolytes

Redox flow batteries performance is mainly influenced by redox electrolytes. High energy density can be achieved by redox-active species with high solubility and operating voltage [56]. One disadvantage of the redox flow battery system is the cross-contamination of active electrolytes by transport through the membrane. As a result, reactive species should be selected to minimize the impact of electrolyte cross-contamination. The selection of electrolytes is based on the following properties, which are generally desirable for the working of redox flow batteries [57]:

• High solubility of the electrolyte

• Fast kinetics at the electrode-electrolyte interface

• A relatively large open circuit potential

• Reasonable cost

1.10.3 Membranes as separators in RFBs

The membrane is a key component that determines the flow battery performance for practical applications. An ion-exchange membrane (IEM) prevents cross mixing of positive and negative electrolytes and transfers ions from the anode to the cathode to complete the circuit [43,48,53]. IEMs are classified into cation exchange membranes (CEMs) and anion exchange membranes (AEMs) based on the type of ionic functional groups attached to the membrane matrix. Anion exchange membranes contain positive functional groups such as quaternary ammonium groups which facilitate the passage of anions. Conversely, cation exchange membranes

contain negatively charged groups such as sulfonic acid anions, which facilitate the passage of cations [58]. The most commonly used membranes for redox flow batteries are Nafion, Daramic, Celgard or perfluorinated IEMs [59]. In recent years, much effort has been made to develop efficient AEMs for energy storage applications. A successful commercial AEM must have high anion conductivity, excellent chemical stability, improved mechanical strength and also be inexpensive. The ionic conductivity of the membranes must be high enough to support the passage of a large current through it. The conductivity can be improved by increasing the number of cationic groups in the membrane; however, it may cause a loss in mechanical properties by promoting excessive water uptake. Therefore, optimization of the membrane composition is necessary to improve the mechanical properties [60]. Hence, an ideal membrane should possess the following characteristics [58,59]:

a) High ionic conductivity:

AEMs conduct anions, such as OH^- and Cl^-, as they contain positively charged quaternary ammonium groups bound covalently to a polymer backbone. The membrane needs to assist the transport of ions carrying the charge to complete the current circuit while minimizing resistance and power loss.

b) High ion selectivity:

The membrane should be selective to the ions to provide high ionic conductivity while minimizing the permeation of active species through it, which reduces capacity and increases energy losses.

c) Chemical Stability:

The membrane should be highly stable for long-term battery cycling. It should not degrade or lose mechanical strength or produce impurities, which can affect the overall performance of the battery.

d) Mechanical stability:

The membrane has to tolerate harsh operational conditions and needs to retain shape after the charge/discharge cycles [58,59].

1.11 Thermodynamics

In a cell, the reduction reaction at the electrode can be represented as

$$aA + ne^- \rightleftharpoons cC \quad \text{..... (1.1)}$$

Where, 'a' molecules of A take up 'n' electrons to form 'c' molecules of C.

At the other electrode, the oxidation reaction can be represented as

$$bB \rightleftharpoons dD + ne^- \quad \text{.....(1.2)}$$

The overall reaction can be represented as

$$aA + bB \rightleftharpoons cC + dD \quad \text{..... (1.3)}$$

The reaction quotient Q for the above reaction can be written as

$$Q = \frac{C^c D^d}{A^a B^b} = \frac{[Red]}{[Ox]} \quad \text{..... (1.4)}$$

The standard free energy ΔG^0, is related to cell potential E^0 by the equation,

$$\Delta G^0 = -nFE^0_{cell} \quad \text{..... (1.5)}$$

Where, 'n' is the number of moles of electrons transferred in the reaction and 'F' is the Faraday constant (96,487 C/mol).

The change in the standard free energy ΔG^0 of a cell reaction is the driving force that enables a battery to deliver electric energy to an external circuit. For a

spontaneous cell reaction, the ΔG should be a negative value. The equation (1.5) indicates that E^0_{cell} should be positive to get a negative ΔG^0 value [33].

1.11.1 Nernst equation

When conditions are other than in the standard state, the voltage E of a cell is given by the Nernst equation [33].

We have learnt that, $\Delta G = \Delta G^0 + RT \ln Q$ .....(1.6)

Where, R is gas constant and T is absolute temperature.

The Gibbs free energy can be related to the cell emf as follows

$$\Delta G = -nFE_{cell} \text{ and } \Delta G^o = -nFE_{cell}^{\ o} \text{ .....(1.7)}$$

Substitute the values of ΔG, ΔG^o and Q in (1.6), we get

$$-nFE_{cell} = -nFE^o_{cell} + RT \ln \frac{C^c D^d}{A^a B^b} \text{ ……(1.8)}$$

$$-nFE_{cell} = -nFE^o_{cell} + RT \ln \frac{[Red]}{[Ox]} \text{ ……(1.9)}$$

Divide the above equation by (−nF)

$$E = E^0 - \frac{RT}{nF} \ln \frac{[Red]}{[Ox]} \text{ …… (1.10)}$$

$$E = E^0 - \frac{0.059}{n} \log \frac{[Red]}{[Ox]} \text{ ……. (1.11)}$$

1.11.2 Calculation of ΔG, ΔH and ΔS of cell reactions [61]

(i) Free energy change (ΔG)

The free energy change is given by

$$\Delta G = -nFE_{cell} \text{ ……. (1.12)}$$

(ii) Enthalpy change (ΔH)

According to the Gibbs-Helrnholtz equation, decrease in free energy, ΔG, of the cell reaction at constant pressure, is

$$\Delta G = \Delta H + T \left(\frac{\partial \Delta G}{\partial T}\right)_p \quad \text{.....(1.13)}$$

Substituting the equation (1.12) here,

$$nFE = -\Delta H + nFT \left(\frac{\partial E}{\partial T}\right)_p \quad \text{.....(1.14)}$$

$$\Delta H = nF[\, T\left(\frac{\partial E}{\partial T}\right)_p - E] \text{.....(1.15)}$$

(iii) Entropy change (ΔS)

The entropy change is related to enthalpy change and free energy change by the thermodynamic expression,

$$\Delta G = \Delta H - T\Delta S \text{ ..... (1.16)}$$

$$\Delta S = \frac{\Delta H - \Delta G}{T} \text{ ..... (1.17)}$$

1.12 Theory of redox reactions at the electrodes

To study a particular reaction, an electrochemical cell usually consists of three electrodes: working electrode, counter (auxiliary**)** electrode and reference electrode. The working electrode is the electrode on which the chemical reaction of interest is occurring, while the counter electrode is used to close the circuit with the electrolyte and the reference electrode is used to accurately measure the potential of the working electrode without passing a current through it. The cell voltage of an electrochemical reaction is the potential across the working and counter electrodes. A typical electron-transfer reaction in an aqueous solution can be represented as:

$$Ox + e^- \rightleftharpoons Red \quad \text{..... (1.18)}$$

Where, 'Ox' and 'Red' are the oxidized and reduced species respectively. Fig. 6 shows the general pathway of an electrode reaction that involves several stages [55,62], (1) mass transport (from the bulk to the electrode surface), (2) surface adsorption of reactant, (3) electron transfer at the electrode surface, (4) surface desorption and (5) the removal of product. An electrochemical reaction occurs by the transfer of charge across the interface between an electrode and an electrolyte. Generally, the electron transfer reaction requires the reactant species to be found within the molecular distances of the electrode surface. In addition to a charge-transfer, the overall reaction rates can be limited by the rates of reactant supply to the electrode surface and the removal of the product from that surface. This is known as a mass-transport process, which primarily comprises diffusion and convection processes. The diffusion process dominates within the Nernst's diffusion layer and an effective method to enhance the transport of material towards the electrode is forced convection, such as stirring or mechanical agitation [55].

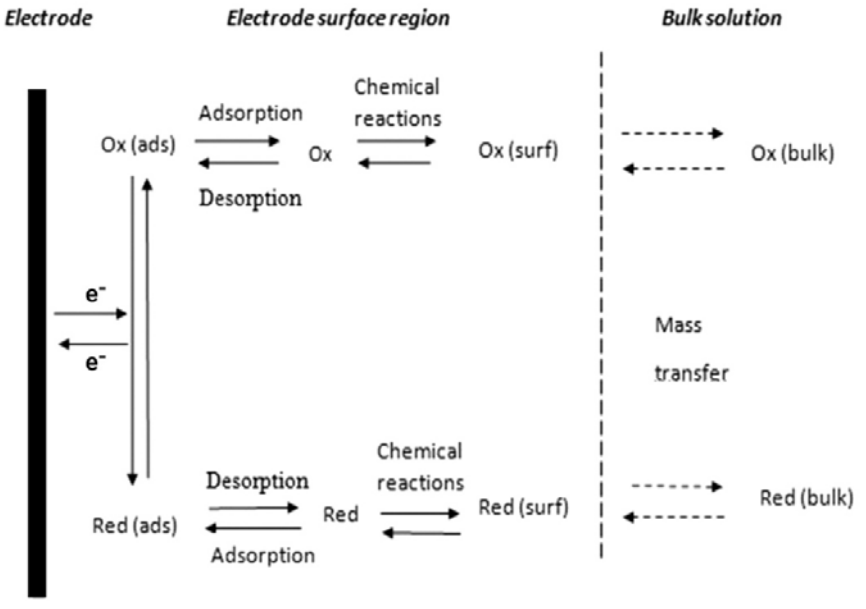

Fig. 6 Redox reactions at the electrodes [55,62].

1.13 Polarization losses in batteries

Polarization is a phenomenon that reduces battery performance. Fig. 7 shows a typical polarization curve that indicates losses in a battery setup. Due to irreversible losses in the system caused by current flow, the potential of a cell decreases from its open-circuit value. These losses result in a drop in voltage and a reduction in power density. The total cell voltage can be calculated as follows:

Total cell voltage = Open circuit voltage – Losses

Three main reasons for the drop in power density and cell performance are: Activation, ohmic, and concentration polarization [63].

1.13.1 Activation polarization

At lower current densities, activation polarization is the main cause of cell internal loss [37]. Activation polarization is a result of sluggish charge transfer reactions at the electrode and electrolyte interface and is directly influenced by the rate of electrochemical reactions [64]. It can be reduced or eliminated with the use of electrocatalysts.

1.13.2 Ohmic polarization

The ohmic resistance of a cell is due to the resistance of the electrolyte (electrolyte solution and the separator), electrodes and the contact resistance between cell components [64,65].

1.13.3 Concentration polarization

This arises due to the difference in concentration of the reactants and products at the surface of electrodes and in the bulk as a result of mass transfer [33]. When

mass transport of reactants limits the current density of a cell, concentration polarization dominates [64].

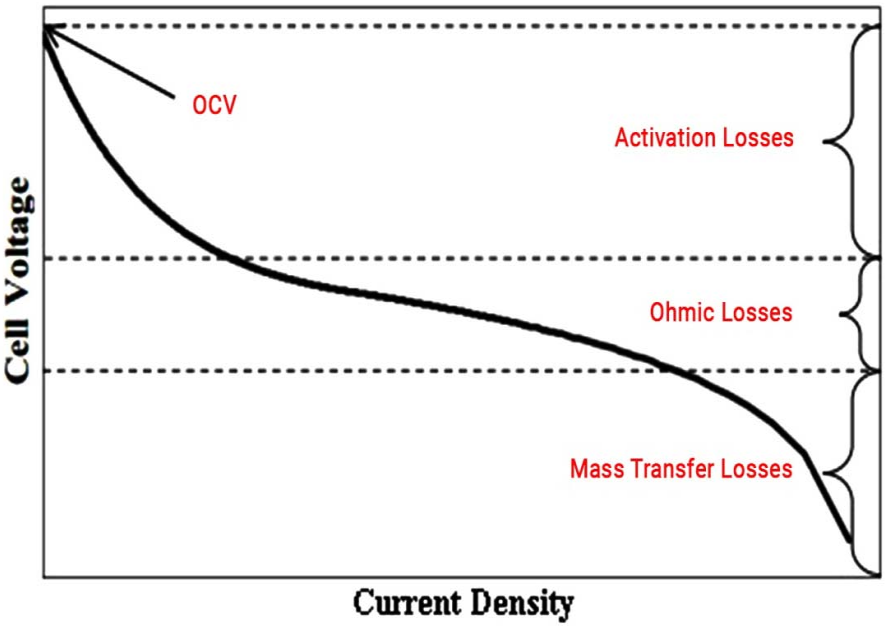

Fig. 7 Potential losses in a battery [33,37,64].

1.14 Types of redox flow batteries

Redox flow batteries can be divided into two categories: True/classical and hybrid redox flow batteries [66]. The positive and negative half cells of these flow cells have the same design but use different electrolytes. Fig. 8 shows the classification of RFBs and their examples.

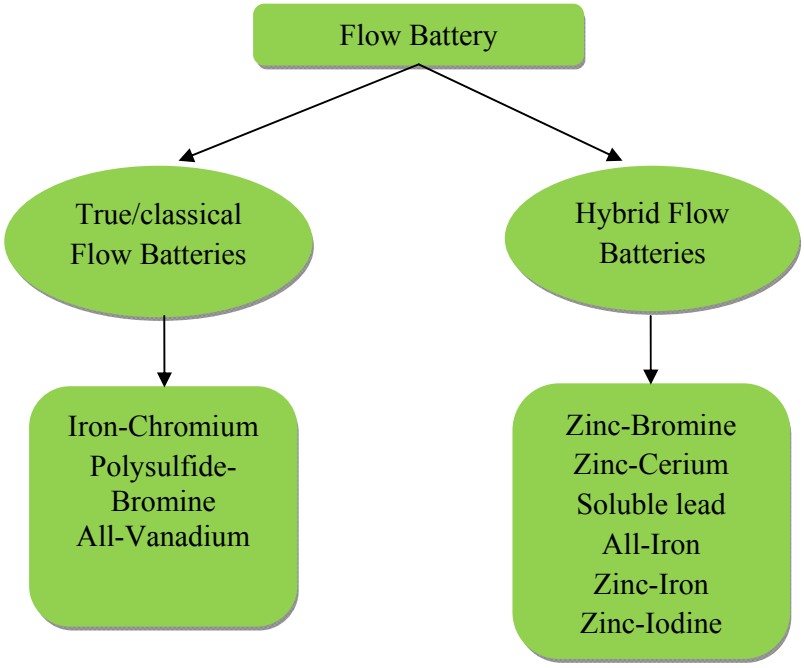

Fig. 8 Classification of RFBs.

1.14.1 True/classical redox flow batteries

In a true/classical redox flow battery, the reactive species in both the reacted and non reacted state were soluble in the electrolyte solution. In these batteries, the electrode serves only as a surface for which the electrochemical reaction takes place, and hence there is no electrodeposition or plating upon the electrode surface [66].

1.14.1.1 Iron-Chromium redox flow battery (ICRFB)

The Fe-Cr flow battery was invented by Thaller, which was later modified by NASA in the 1980s. The Fe^{2+}/Fe^{3+} and Cr^{2+}/Cr^{3+} redox couples in hydrochloric acid are the positive and negative electrolytes, respectively [27]. Fig. 9 illustrates a schematic diagram of the cell.

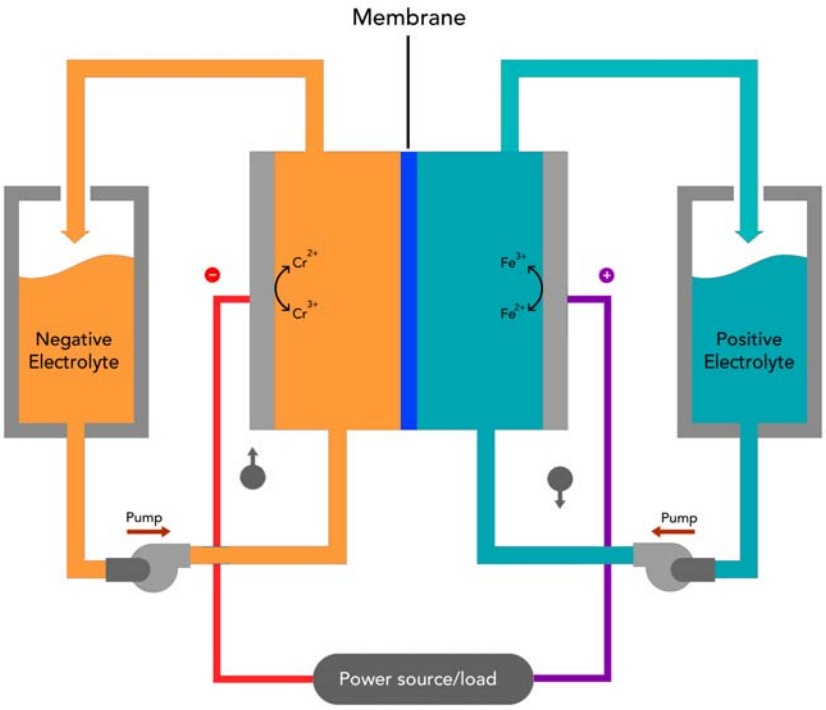

Fig. 9 Schematic of an iron-chromium redox flow battery.

The electrochemical reactions during the charge-discharge process are as follows:

During discharge,

At negative electrode: $Cr^{2+} \rightleftharpoons Cr^{3+} + e^{-}$ $E^0 = -0.424$ V …..(1.19)

At positive electrode: $Fe^{3+} + e^{-} \rightleftharpoons Fe^{2+}$ $E^0 = 0.77$ V …… (1.20)

The overall reaction: $Cr^{2+} + Fe^{3+} \rightleftharpoons Cr^{3+} + Fe^{2+}$ $E^0 = 1.2$ V …..(1.21)

During discharging, Cr^{2+} is oxidized to Cr^{3+} at the negative electrode, while Fe^{3+} is reduced to Fe^{2+} at the positive electrode. The process is reversed during the charge. The iron-chromium redox flow battery offers a standard cell voltage of 1.2 V. The battery uses a proton or anion exchange membrane and the electrode material is usually carbon fiber, carbon felt or graphite. Only protons and chloride anions pass through the ion-selective membrane and the battery exhibits an efficiency of 95%.

The Fe^{3+}/Fe^{2+} redox couple has good reversibility and fast kinetics, but the Cr^{3+}/ Cr^{2+} redox couple has sluggish kinetics, which necessitates the creation of redox catalysts and an elevated operating temperature, both of which add to the cost. Meanwhile, the Cr^{3+}/Cr^{2+} couple has a low redox potential that might lead to H_2 evolution and hence may reduce coulombic efficiency and cycle life [43,53,67–69].

1.14.1.2 Polysulfide-Bromine redox flow battery (PBB)

Remick was the first to report about the polysulfide-bromine battery [42] in which the positive electrolyte is sodium bromide and the negative electrolyte is sodium polysulfide. A perfluorinated sulfonic membrane such as DuPont's Nafion is often used in PBBs. Na_2S_2 is changed to Na_2S_4 at the negative electrode and Br_3^- is transformed to $3Br^-$ at the positive electrode during the discharge process, and excess Na^+ ions at the anode move through the membrane to the cathode side to maintain electrical neutrality [70]. The charge and discharge reactions are as follows [26]:

During discharge,

At negative electrode: $2S_2^{2-} \rightleftharpoons S_4^{2-} + 2e^- \quad E^0 = -0.265\ V$ ….. (1.22)

At positive electrode: $Br_3^- + 2e^- \rightleftharpoons 3Br^- \quad E^0 = 1.087\ V$ …..(1.23)

The overall reaction: $2S_2^{2-} + Br_3^- \rightleftharpoons S_4^{2-} + 3Br^- \quad E^0 = 1.35\ V$ …..(1.24)

Polysulfide-bromine redox flow batteries have a standard cell voltage of 1.35 V. Although this technique is safe for the environment, there is concern that if there is an accident, hazardous bromine vapor may be released [42,43]. Fig. 10 shows a schematic diagram of the cell.

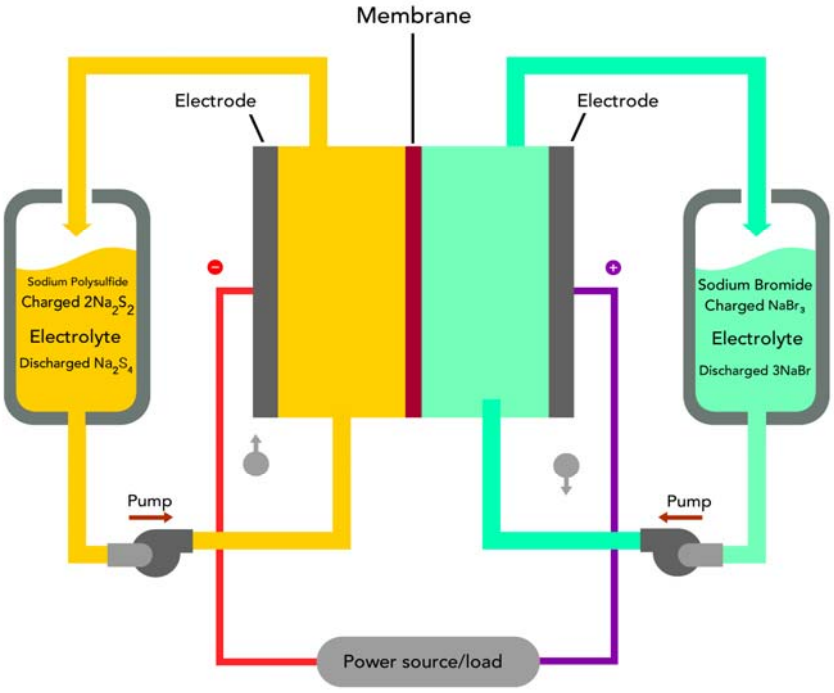

Fig. 10 Schematic of a polysulfide-bromine redox flow battery.

1.14.1.3 All-Vanadium redox flow battery (VRB)

Skyllas-Kazacos and colleagues at the University of New South Wales in Australia invented the vanadium redox flow battery (VRB) in the 1980s. Vanadium has four valence states in VRFB and this fact is used to create a battery with only one electroactive element instead of two. It uses two vanadium redox couples, V^{3+}/V^{2+} and VO^{2+}/VO_2^{+} as negative and positive electrolytes in H_2SO_4 solution [71,72]. The use of the same element avoids any cross-contamination, allowing the electrolyte life to be extended indefinite. During discharge, oxidation of V^{2+} to V^{3+} occurs at the negative electrode and the reduction of V^{5+} to V^{4+} occurs at the positive electrode. The following are the charge and discharge reactions in the VRFB [67,68]:

During discharging,

At positive electrode: $VO_2^+ + 2H^+ + e^- \rightleftharpoons VO^{2+} + H_2O \quad E^0 = 1.0\ V$ …..(1.25)

At negative electrode: $V^{2+} \rightleftharpoons V^{3+} + e^- \quad E^0 = -0.255\ V$ …..(1.26)

The overall reaction: $VO_2^+ + V^{2+} \rightleftharpoons VO^{2+} + V^{3+} \quad E^0 = 1.26\ V$ …..(1.27)

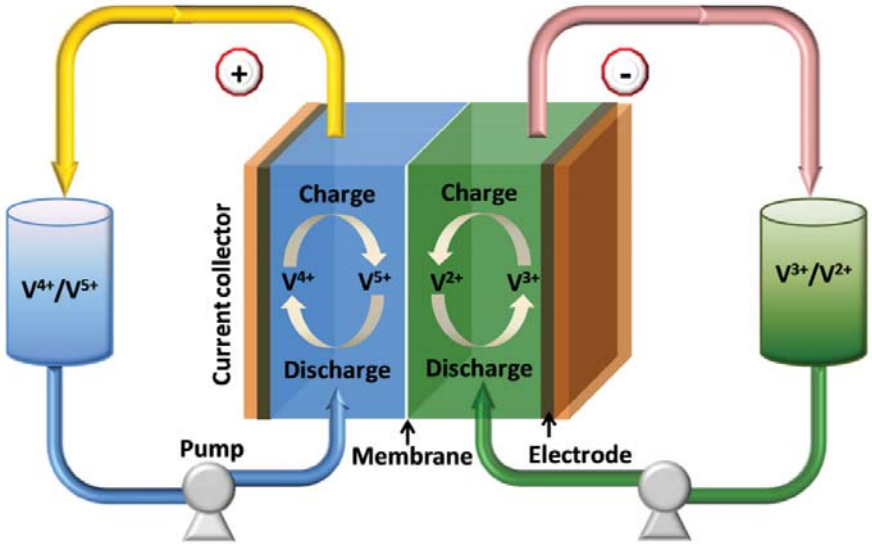

Fig. 11 Schematic representation of all-vanadium redox flow battery [73].

VRFB flow batteries have a cell voltage of 1.26 V, making them ideal for large stationary storage applications. Fig. 11 is a schematic illustration of the cell. VRFB is divided into two half-cells by an ion-permeable membrane. Electrochemical reactions occur on inert electrodes such as carbon felt or graphite sheets in the half-cells, from which the current is collected. According to Skyllas-Kazacos and colleagues, commercially available membranes break down in the highly oxidizing V^{5+} electrolyte and are unable to give a long cycle life. Only a few membranes were discovered to be chemically stable in the V^{5+} solution, such as the New Selemion anion exchange membrane and the Nafion cation exchange membrane. The strong oxidation activity of V^{5+} limits the positive electrode material to graphite or carbon

felt. The general acceptance of these batteries has also been hindered by the high cost of membranes, the toxicity of soluble vanadium, the strong corrosive strength of VO^{2+}/VO_2^+ and poor V^{5+} solubility. However, the VRFBs have made great progress in recent years due to the advancements in electrode and membrane materials [39,43].

1.14.2 Hybrid flow battery

A hybrid-flow battery (HFB) is a type of flow battery in which one or more electro-active components are deposited as a solid layer during the charging process. The electrode surface area limits the amount of energy that can be stored in this type of battery [74]. During charging, the active material is electroplated on an electrode and then dissolves back into the electrolyte during successive discharges [75]. Zinc-bromine, zinc-cerium, zinc-iron, zinc-iodine, soluble lead-acid and all-iron are examples of hybrid flow batteries. Zinc is widely used as a negative electrode in many hybrid redox flow batteries because of its significant negative electrode potential in both acidic (−0.76 V vs. SHE) and alkaline (−1.22 V vs. SHE) conditions [43].

1.14.2.1 Zinc-Bromine redox flow battery (ZBB)

The ZBB was developed by Exxon and Gould in the early 1970s. The zinc bromide salt dissolved in water is used as the electrolyte. Zinc is electroplated on the negative electrode during the charging process, while bromine is created on the positive electrode and forms a bromine complex that sinks to the bottom of the positive electrolyte tank. At the negative electrode, zinc deposits are dissolved to create zinc ions, while bromide ions are formed at the positive electrode during the discharge process. Fig. 12 shows a schematic diagram of the battery. As indicated in figure, a third pump is necessary to circulate the bromine complex [38,76,77]. The

overall efficiency of the zinc-bromine battery is between 60% and 75%. Dendrite production, hydrogen evolution reaction and battery safety are the three key issues with zinc-bromine batteries [67]. The following are the charge and discharge reactions [68]. During discharging,

At negative electrode: $Zn \rightleftharpoons Zn^{2+} + 2e^{-}$ $E^0 = -0.76$ V ……. (1.28)

At positive electrode: $Br_2 + 2e^{-} \rightleftharpoons 2Br^{-}$ $E^0 = 1.09$ V ……. (1.29)

The overall cell reaction: $Zn + Br_2 \rightleftharpoons Zn^{2+} + 2Br^{-}$ $E^0 = 1.85$ V …… (1.30)

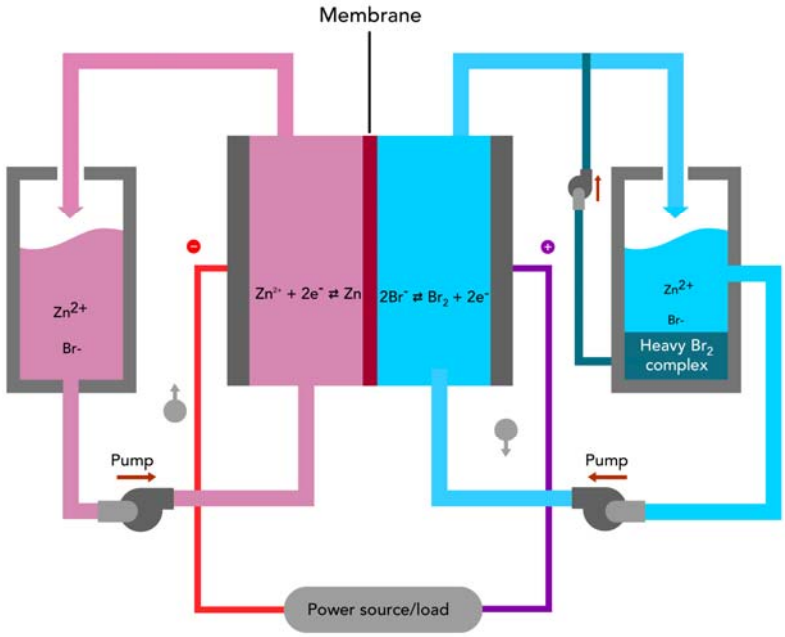

Fig. 12 Schematic diagram of zinc-bromine flow battery.

1.14.2.2 Zinc-Cerium redox flow battery (ZCRFB)

Plurion [37,50] developed the first zinc-cerium system. The materials of zinc and cerium are good for energy storage because of their high standard reduction potentials. Platinum or titanium is used as the electrodes separated by a proton

exchange membrane and Zn(II) and Ce(III) methanesulfonate solutions as the electrolytes. The reaction of discharging is [78]:

At negative electrode: $Zn \rightleftharpoons Zn^{2+} + 2e^-$ $E^0 = -0.76$ V vs. SHE …..(1.31)

At positive electrode: $2Ce^{4+} + 2e^- \rightleftharpoons 2Ce^{3+}$ E^0 = between 1.28 and 1.72 V vs. SHE depending on the supporting electrolyte …… (1.32)

The overall cell reaction: $Zn + 2Ce^{4+} \rightleftharpoons Zn^{2+} + 2Ce^{3+}$ $E^0 = \sim 2.5$ V …… (1.33)

Compared to other redox systems, the cell voltage of the Zn-Ce system is approximately 2.5 V [79] during the charge cycle and falls below 2 V during the discharge cycle. The total efficiency of the battery ranges between 75% and 90% [48,80]. The high cost of Pt/Ti electrodes and electrolyte cross-mixing are the main drawbacks of the Zn-Ce RFB [76]. Fig. 13 shows the schematic representation of a Zn-Ce RFB.

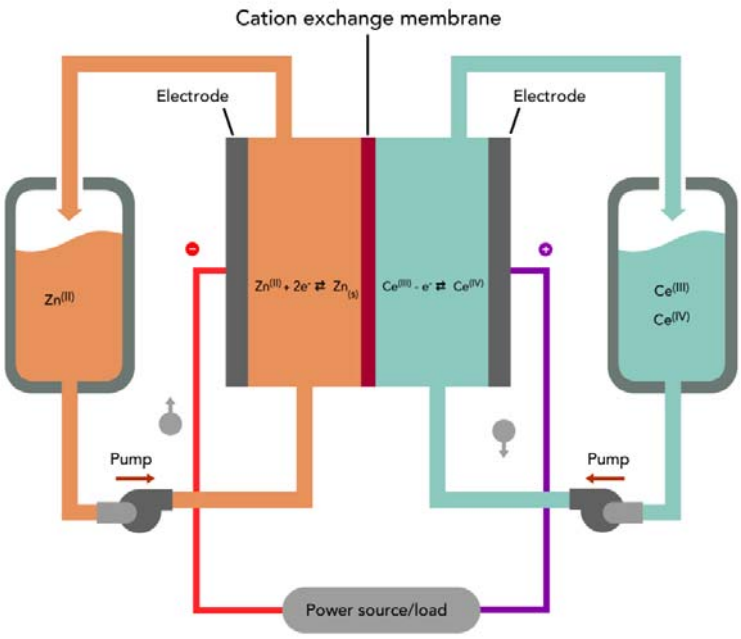

Fig. 13 Schematic representation of a zinc-cerium redox flow battery.

1.14.2.3 Soluble lead redox flow battery (SLRFB)

SLRFB differs from ordinary lead-acid batteries as it uses a highly soluble Pb(II) ions in methanesulfonic acid solution for both negative and positive half-cells [81]. There is no need for a separator or membrane because it uses a single electrolyte and includes the deposition of solid Pb and PbO_2 at the negative and positive electrodes during charging. This lowers the cost of the batteries and simplifies their design. During discharging cycles, the deposited Pb and PbO_2 are converted to soluble species. The following are the charge and discharge reactions [67,82]:

During discharging,

At negative electrode: $Pb \rightleftharpoons Pb^{2+} + 2e^- \quad E^0 = -0.13\ V$ …..(1.34)

At positive electrode: $PbO_2 + 4H^+ + 2e^- \rightleftharpoons Pb^{2+} + 2H_2O \quad E^0 = 1.49\ V$ …. (1.35)

Overall cell reaction: $Pb + PbO_2 + 4H^+ \rightleftharpoons 2Pb^{2+} + 2H_2O \quad E^0 = 1.62\ V$ ….(1.36)

If metal develops across the inter-electrode gap and short circuits the battery, it may reduce the overall performance of the battery. Hydrogen evolution is detected throughout the charge cycle at a high state-of-charge, as in the case with traditional lead-acid batteries, it lowers the storage capacity [39]. Fig. 14 shows the schematic representation of a soluble lead RFB.

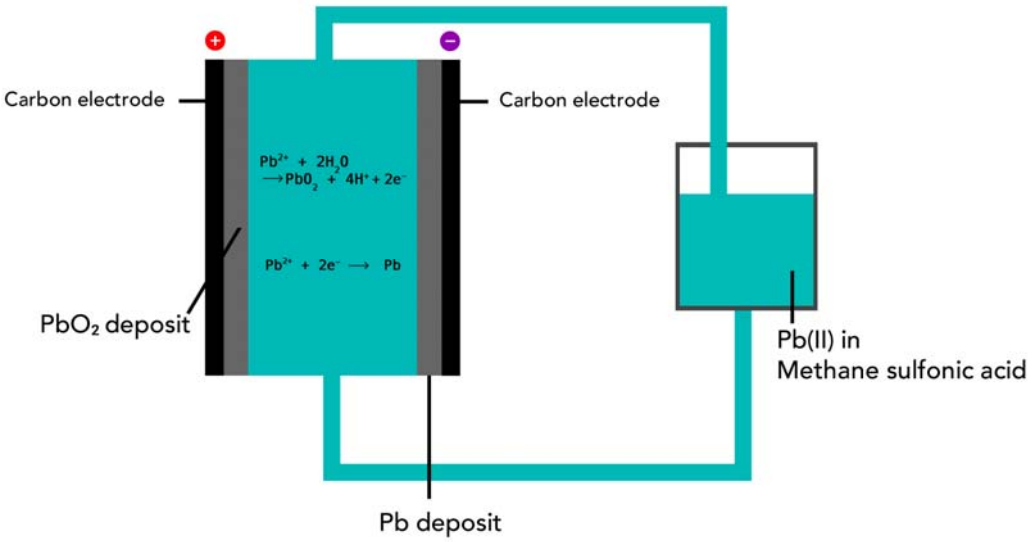

Fig. 14 Schematic representation of a soluble lead redox flow battery.

1.14.2.4 Zinc-Iron redox flow battery

Scientists at Lockheed Missiles and Space Company (LMSC) introduced the 'zinc-ferricyanide' battery, an early zinc-iron hybrid flow battery based on alkaline electrolytes [77]. ViZn Inc. is now marketing this technology for grid-scale applications [76,83,84]. The zinc and iron are among the most abundant metals in the earth's crust and hence are cheap [85]. In alkaline electrolytes, ferricyanide/ferrocyanide redox couple is known to be extremely reversible. The chloride-based zinc-iron systems have recently been introduced in addition to alkaline systems. The half-cell electrode reactions during discharge are as follows [84]:

At negative electrode: $Zn \rightleftharpoons Zn^{2+} + 2e^-$ $E^0 = -0.76$ V …….. (1.37)

At positive electrode: $2Fe^{3+} + 2e^- \rightleftharpoons 2Fe^{2+}$ $E^0 = +0.77$ V ……. (1.38)

The overall reaction: $Zn + 2Fe^{3+} \rightleftharpoons Zn^{2+} + 2Fe^{2+}$ $E^0 = 1.53$ V …..(1.39)

The Fe(III) ions at the positive electrode changed to Fe(II) ions during the discharging process; at negative electrode, the zinc deposit is dissolved to create zinc ions. Fig. 15 shows the schematic of a zinc-iron redox flow battery. The formation of zinc dendrites during the charging process reduces the efficiency, capacity and lifetime of the cell. As a result, inhibiting the formation of zinc dendrites is essential for the successful commercialization of zinc-iron RFBs.

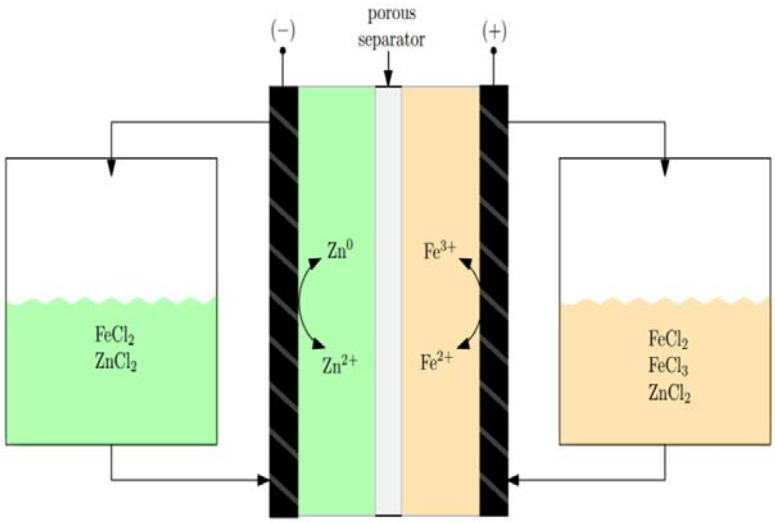

Fig. 15 Schematic of a zinc-iron redox flow battery [84].

1.14.2.5 Zinc-Iodine redox flow battery (ZIFB)

Zinc-iodine redox flow batteries (ZIFBs) have attracted interest as the next-generation RFBs due to their outstanding energy density and use of less oxidative chemistries to extend membrane durability. Fig. 16 shows a schematic representation of the zinc-iodide system reported by Wang et al., in which the zinc iodide solutions are pumped between two graphite felt electrodes separated by a Nafion membrane. During discharge, the following reactions are takes place [86,87].

At negative electrode: $Zn \rightleftharpoons Zn^{2+} + 2e^-$ $E^0 = -0.76$ V …… (1.40)

At positive electrode: $I_3^- + 2e^- \rightleftharpoons 3I^-$ $E^0 = 0.54$ V …… (1.41)

The overall reaction: $Zn + I_3^- \rightleftharpoons Zn^{2+} + 3I^-$ $E^0 = 1.3$ V …... (1.42)

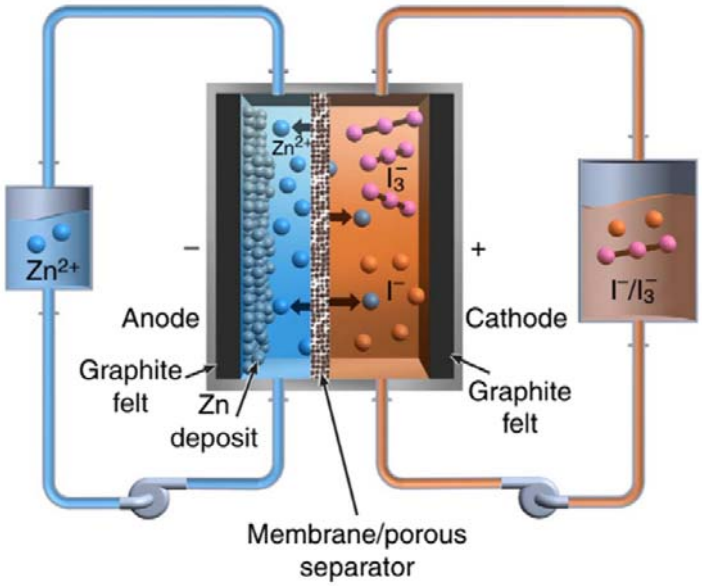

Fig. 16 Schematic of the zinc-iodide system [86].

During discharge, at the negative electrode, the zinc deposit undergoes oxidation and forms zinc ions, while triiodide (I_3^-) is reduced to iodide (I^-) at the positive electrode. With the redox process in the below equations, the cell offers an OCV of 1.3 V. The high energy density (167 WhL^{-1}) [76,88], use of weaker acids as supporting electrolytes and use of environmentally benign components are all reasons why ZIFBs are among the most viable candidates for future commercial RFBs. However, expanding the battery capacity, voltage and cycle life to their full potential is a difficult for ZIFBs. Modifying electrolyte design with complex-forming ions like bromide [89,90] and altering the pH of the anolyte [88] are two techniques that potentially overcome some of these issues. Wei Wang and co-workers claim that ethanol was found to inhibit dendritic formation during the battery operation [76]. The

development of electrolytes and membranes could open a new window to the commercialization of ZIFBs.

1.14.2.6 All-Iron redox flow battery (all-Fe RFB)

Savinell and Hrushka introduced the all-Fe battery system in 1981. The Fe(III)/Fe(II) couple at the positive electrode and the Fe/Fe(II) couple at the negative electrode constitute the redox chemistry of the all-iron redox flow battery. Iron(III) chloride is converted to iron(II) chloride at the positive electrode during the battery discharge. Metallic iron is dissolved as iron(II) chloride in the electrolyte at the negative electrode. During battery charging, these processes are reversed [91]. For large-scale applications, an aqueous all-iron redox flow battery with a cell voltage of 1.21 V and theoretical specific energy of 170 Wh/ kg is one of the low cost, durable and environmentally benign energy storage device. The electrochemical reactions are shown below [92].

During discharge,

At negative electrode: $Fe \rightleftharpoons Fe^{2+} + 2e^{-}$ $E^0 = -0.44$ V ……... (1.43)

At positive electrode: $2Fe^{3+} + 2e^{-} \rightleftharpoons 2Fe^{2+}$ $E^0 = 0.77$ V ……. (1.44)

Overall reaction: $2Fe^{3+} + Fe \rightleftharpoons 3Fe^{2+}$ $E^0 = 1.21$ V …… (1.45)

The competitive hydrogen evolution reaction (HER) at the negative electrode during the charging process is now the biggest barrier to the commercialization of all-Fe RFB technology [93]. Due to changes in electrolyte composition, HER affects the round-trip coulombic efficiency and causes capacity to diminish. The impact of pH, electrolyte additives, secondary metal co-deposition, charging current density and temperature on the performance of the battery was investigated in order to improve the coulombic efficiency and the researchers believe that the all-iron redox flow

battery based on iron chloride will continue to be an attractive pathway for large-scale electrical energy storage in the future. Fig. 17 shows the schematic of the all-iron redox flow battery.

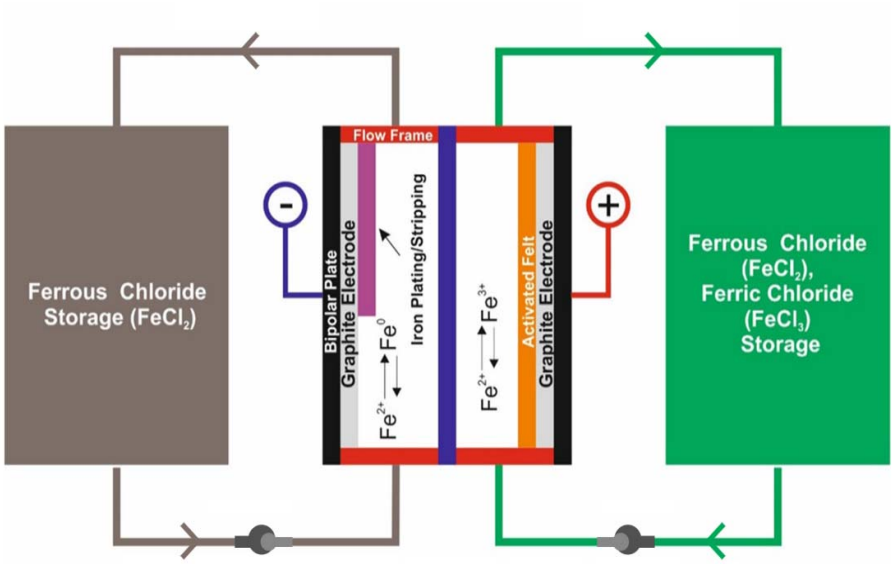

Fig. 17 The schematic of all-iron redox flow battery [94].

1.15 Limitations of hybrid redox flow batteries

The Zn/Zn(II) redox pair has recently attracted a lot of attention as a negative electrode in a number of RFBs for renewable energy storage. The use of this redox couple has several advantages, including a negative standard electrode potential, the high solubility of Zn(II) ions, fast kinetics, low cost, abundance and recyclability of zinc compounds [95]. However zinc-based systems are often less durable due to issues with uneven metal deposition during battery charging, the so-called dendrite deposits, which occur particularly under mass transport limited conditions due to non-uniform concentration gradients. Dendrite deposit causes battery failure due to dendrite penetration through the separator and cell short-circuit. Furthermore, zinc dendrites can easily fall from anodes, reducing efficiency and capacity. Nucleation

initiates the zinc deposition, which continues with growth. As demonstrated in Fig. 18a, the energy barrier for zinc nucleation is significantly larger than for zinc growth on the nucleus. As a result, zinc nucleation has a higher overpotential than zinc growth on the nucleus (Fig. 18b) [96,97].

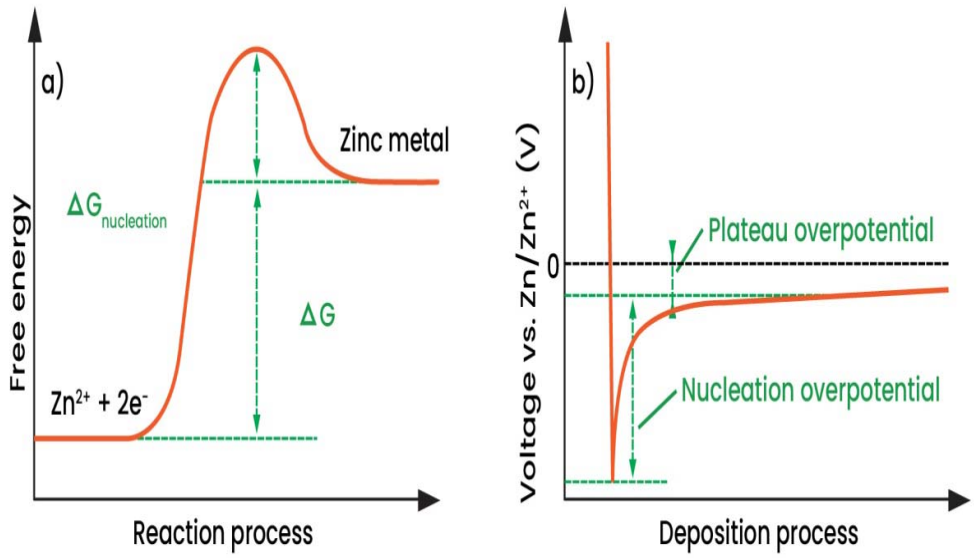

Fig. 18 a) The energy barrier at the zinc nucleation process
b) The voltage profile during zinc deposition [96,98].

This suggests that zinc ions prefer to deposit on a zinc nucleus rather than produce a new nucleus once it has formed. Since the small nuclei have high surface energy, they tend to cluster into larger particles thermodynamically. As a result, obtaining homogeneous zinc nuclei on the anode is extremely challenging [98]. Optimized operational regimes and the application of organic or inorganic electrolyte additions can increase the uniformity of the deposited layer (levelers, brighteners, etc.) [77]. As a result, preventing the formation of zinc dendrites is critical for the continued development of zinc-based flow batteries. Fig. 19 shows the schematic representation of nucleation and growth of zinc dendrites. Researchers have recently

focused their efforts on modifying the electrolyte, anodes, electric field and zinc ion transport to solve zinc dendrite development.

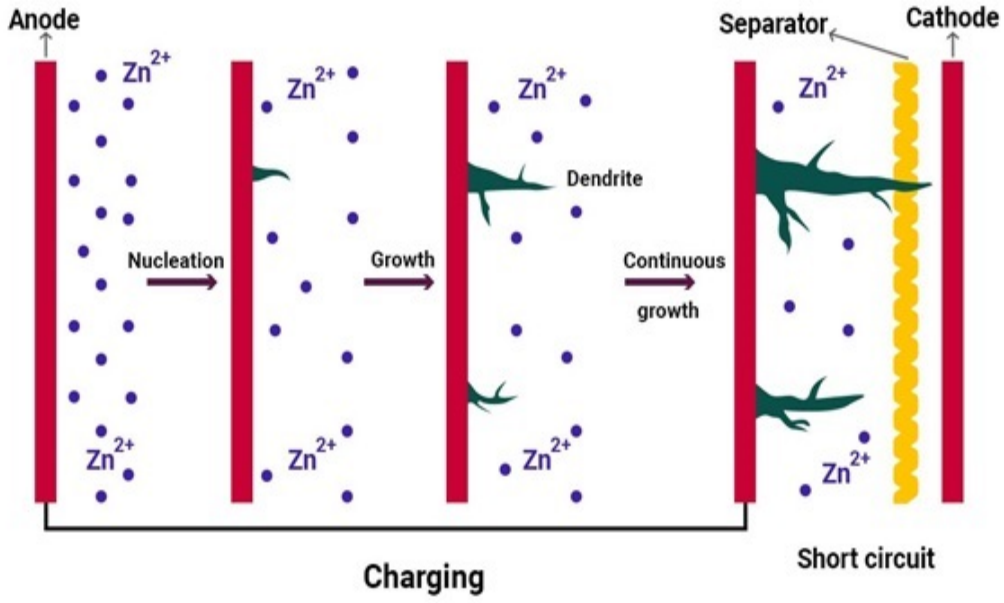

Fig. 19 Schematic representation of the nucleation and growth mechanism of zinc dendrites [96].

All-iron redox flow batteries are an attractive solution for large-scale energy storage because of the low cost and environmental friendliness of iron-based materials [99]. The parasitic evolution of hydrogen at the iron electrode during battery charging is a fundamental barrier to achieving a continuously functioning battery. Most crucially, the hydrogen evolution affects the repetitive cycling of the flow cell by rapidly changing the electrolyte composition. The pH of the solution rises when protons are changed to hydrogen and the concentration of hydroxide ions rises. The imbalance of hydroxide ions on the positive and negative sides of the cell causes hydroxide ions to diffuse from the positive to the negative side of the cell through the anion exchange membrane. As a result of hydrogen evolution, the pH of both the

negative and positive sides will continue to rise, eventually resulting in the formation of iron hydroxides [91].

Another barrier to the widespread use of RFBs originates from the fact that almost all RFBs depend on a single ion-exchange membrane (IEM). The crossover of redox species is another problem caused by the imperfect selectivity of ion-exchange membranes. The IEM also contributes to a major portion of the internal resistance. To solve this problem, researchers are still doing a lot of efforts in developing a membrane with improved selectivity and reduced internal resistance [100].

1.16 Objectives of the present work

The objectives of the present study are

1) To develop a zinc-iron redox flow battery with no zinc dendrite formation on the zinc electrode during battery charging
2) To develop an all-iron redox flow battery with low parasitic hydrogen evolution reaction and high efficiency
3) To demonstrate a novel chloride-based copper-cerium redox flow battery containing Cu/Cu(II) and Ce(IV)/Ce(III) redox couples
4) To study the effectiveness of a self-made anion exchange membrane as separator in the above three redox flow batteries.

1.17 Thesis structure

Development of redox flow batteries has been a subject of extensive research in the last decade due to its potential applications in the field of energy conversion and storage. Many works have been reported in the literature on the development of various redox flow batteries. There are still several challenges to be overcome for the

commercialization of RFBs. Here, the contents of this thesis are arranged in six chapters and Fig. 20 depicts the general framework of the thesis.

- Chapter 1 introduces the electrochemistry and performance of various energy storage systems, such as redox flow batteries.
- Chapter 2 describes the experimental methodologies and techniques used to characterize the redox flow batteries developed in this study.
- Chapter 3 describes a zinc-iron redox flow battery with no zinc dendrite formation on the zinc electrode during battery charging. The Zn/Zn(II) and Fe(III)/Fe(II) redox couples were separated by a self-made anion exchange membrane.
- Chapter 4 deals with an all-iron RFB containing Fe/Fe(II) and Fe(III)/Fe(II) redox couples separated by a self-made anion exchange membrane. The chapter also includes a study on the improvement in the performance of Fe/Fe^{2+} electrode by the addition of Zn^{2+} ions.
- Chapter 5 presents the development of a new chloride-based copper-cerium redox flow battery and the measurement of its electrochemical performances.
- Chapter 6 includes summary and conclusions of the present work.
- Finally, chapter 7 presents the recommendations for future studies.

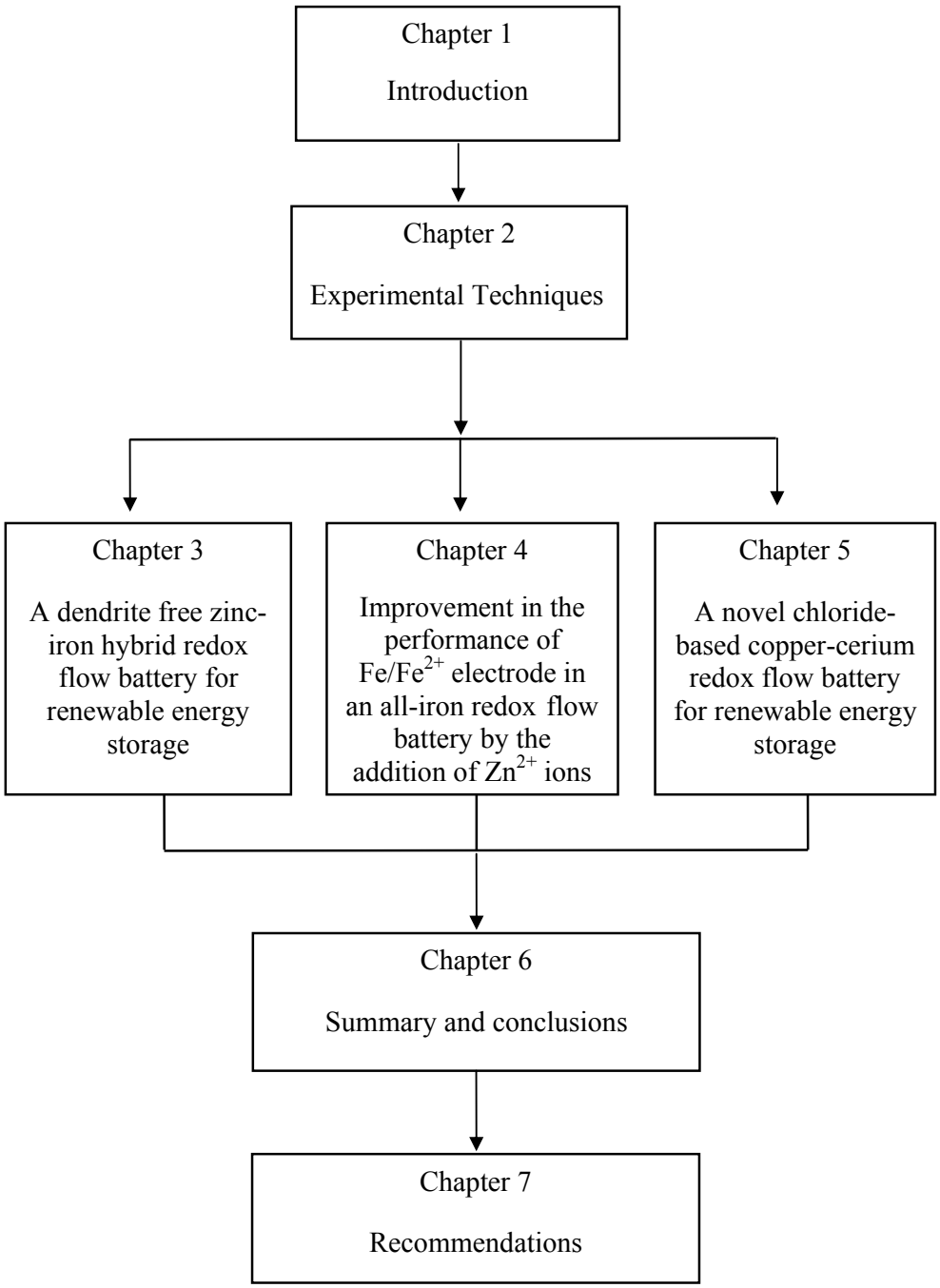

Fig. 20 Thesis layout

1.18 References

[1] Z. Asghar, Energy-GDP Relationship: A Causal Analysis for the Five Countries of South Asia, Appl. Econom. Int. Dev. 8 (2008) 167–180. http://www.usc.es/econo met/reviews/aeid8114.pdf.

[2] S. Ali, S. Anwar, S. Nasreen, Renewable and Non-Renewable Energy and its Impact on Environmental Quality in South Asian Countries, in: Econ. Pakistan Oppor. Vulnerabilities, 2018, 1-19. doi:10.32368/FJES.20170009.

[3] G.E. Halkos, Reviewing Usage, Potentials, and Limitations of Renewable Energy Sources, Energies. 13 (2020) 1-19 . doi:10.3390/en13112906.

[4] S. Chinnammai, A Study on Energy Crisis and Social Benefit of Solar Energy, Int. J. Environ. Sci. Dev. 5 (2014) 404–411. doi:10.7763/IJESD.2014.V5.518.

[5] I. Khan, L. Han, H. Khan, L. Thi, K. Oanh, Analyzing Renewable and Nonrenewable Energy Sources for Environmental Quality : Dynamic Investigation in Developing Countries, Math. Probl. Eng. 2021 (2021) 1-12. doi:org/10.1155/2021/3399049.

[6] U. Shahzad, The Need For Renewable Energy Sources, Int. J. Inf. Technol. Electr. Eng. (2017) 16-18. https://www.researchgate.net/publication/316691176.

[7] D. Pimentel, M. Herz, M. Glickstein, M. Zimmerman, R. Allen, K. Becker, J. Evans, B. Hussain, R. Sarsfeld, A. Grosfeld, T. Seidel, Renewable Energy : Current and Potential Issues, Bioscience. 52 (2002) 1111–1120. doi:org/10.1641/0006-3568(2002)052.

[8] P. Friedlingstein, M.W. Jones, M.O. Sullivan, R.M. Andrew, J. Hauck, G.P. Peters, W. Peters, J. Pongratz, S. Sitch, C. Le Quéré, Global Carbon Budget 2019, Earth Syst. Sci. Data. 11 (2019) 1783–1838. doi:org/10.5194/essd-11-1783-2019.

[9] P. Friedlingstein, M.O. Sullivan, M.W. Jones, R.M. Andrew, J. Hauck, Global Carbon Budget 2020, Earth Syst. Sci. Data. 12 (2020) 3269–3340. doi:org/10.5194/essd-12-3269-2020.

[10] C. Le Quéré, R.M. Andrew, P. Friedlingstein, S. Sitch, J. Hauck, J. Pongratz, P.A. Pickers, J.I. Korsbakken, G.P. Peters, J.G. Canadell, Global Carbon Budget 2018, Earth Syst. Sci. Data. 10 (2018) 2141–2194. doi:org/10.5194/essd-10-2141-2018.

[11] M.A. Rosen, I. Dincer, Nuclear energy as a component of sustainable energy systems, Int. J. Low Carbon Technol. (2000) 4–6. https://academic.oup.com.

[12] N. Abas, A. Kalair, N. Khan, Review of fossil fuels and future energy technologies, Futures. 69 (2017) 31–49. doi:10.1016/j.futures.2015.03.003.

[13] P.A. Owusu, S. Asumadu-sarkodie, A review of renewable energy sources, sustainability issues and climate change mitigation, Cogent Eng. 3 (2016) 1–14. doi:10.1080/23311916.2016.1167990.

[14] T. Shibata, T. Kumamoto, Y. Nagaoka, K. Kawase, Redox Flow Batteries for the Stable Supply of Renewable Energy, SEI Tech. Rev. 76 (2009) 14–22. https://global-sei.com/technology/tr/bn76/pdf/76-03.pdf.

[15] N. Keskar Vinaya, Electricity Generation Using Solar Power, Int. J. Eng. Res. Technol. 2 (2013) 1-5. https://www.ijert.org.

[16] S. Abolhosseini, A. Heshmati, J. Altmann, A Review of Renewable Energy Supply and Energy Efficiency Technologies, IZA Discuss. Pap. No. 8145. (2014) 1-36. doi:org/10.2139/ssrn.2432429.

[17] A. Kumar, N. Kumar, P. Baredar, A. Shukla, A review on biomass energy resources, potential, conversion and policy in India, Renew. Sustain. Energy Rev. 45 (2015) 530–539. doi:10.1016/j.rser.2015.02.007.

[18] P. Mckendry, Energy production from biomass (part 1): overview of biomass, Bioresour. Technol. 83 (2002) 37–46. doi:org/10.1016/S0960-8524(01)00118-3.

[19] C.F. Kutscher, The Status and Future of Geothermal Electric Power, in: Am. Sol. Energy Soc. Conf., (2000) 1-5. https://www.nrel.gov.

[20] J.E. Mock, J.W. Tester, P.M. Wright, Geothermal energy from the earth : Its Potential Impact as an Environmentally Sustainable Resource, Annu. Rev. Energy Environ. 22 (1997) 305–356. doi:org/10.1146/annurev.energy.22.1.305.

[21] B. Dursun, C. Gokcol, The role of geothermal energy in sustainable development of Turkey, Energy Explor. Exploit. 30 (2012) 207–222. doi:10.1260/0144-5987.30.2.207.

[22] I.B. Fridleifsson, Status of geothermal energy amongst the world's energy sources, Geothermics. 32 (2003) 379–388. doi:10.1016/j.geothermics.2003.07.004.

[23] C.S. Kaunda, C.Z. Kimambo, T.K. Nielsen, Hydropower in the Context of Sustainable Energy Supply : A Review of Technologies and Challenges, 2012 (2012) 1-15. doi:10.5402/2012/730631.

[24] A. Zayed, A.L. Shaqsi, K. Sopian, A. Al-hinai, Review of energy storage services, applications, limitations and benefits, Energy Reports. 6 (2020) 288–306. doi:10.1016/j.egyr.2020.07.028.

[25] S.R. Narayanan, G.K.S. Prakash, A. Manohar, B. Yang, S. Malkhandi, A. Kindler, Materials challenges and technical approaches for realizing inexpensive and robust iron–air batteries for large-scale energy storage, Solid State Ionics. 216 (2012) 105–109. doi:10.1016/j.ssi.2011.12.002.

[26] A.Z. Weber, M.M. Mench, J.P. Meyers, P.N. Ross, J.T. Gostick, Q. Liu, Redox flow batteries: A review, J. Appl. Electrochem. 41 (2011) 1137–1164. doi:10.1007/s10800-011-0348-2.

[27] G.L. Soloveichik, Battery Technologies for Large-Scale Stationary Energy Storage, Batter. Station. Energy Storage 505. (2011) 503-527. doi:10.1146/annurev-chembioeng-061010-114116.

[28] X. Li, H. Zhang, Z. Mai, H. Zhang, I. Vankelecom, Ion exchange membranes for vanadium redox flow battery (VRB) applications, Energy Environ. Sci. 4 (2011) 1147-1160. doi:10.1039/c0ee00770f.

[29] T. Nyugen, R.F. Savinell, Flow Batteries, Electrochem. Soc. Interface. (2010) 54–56. https://iopscience.iop.org/article/10.1149/2.F06103if.

[30] K. Schmidt-rohr, How Batteries Store and Release Energy: Explaining Basic Electrochemistry, J. Chem. Educ. (2018). doi:10.1021/acs.jchemed.8b00479.

[31] P. Modiba, Electrolytes for redox flow battery, Doctoral dissertation, University of Stellenbosch, 2010.

[32] N. Singamsetti, S. Tosunoglu, A Review of Rechargeable Battery Technologies, in: 8th Int. Symp. Manag. Eng. Informatics, MEI 2012, 16th World Multi-Conference Syst. Cybern. Informatics, WMSCI 2012, 2012, 1-6. https://www.semanticscholar.org.

[33] D. Linden, T.B. Reddy, Handbook of batteries, Third edit, McGraw-Hill education-Europe, 2001, 4-5.

[34] J. Hunter, G. Blomgren, Batteries, Primary cells, 2000, 434-471. doi:10.1002/0471238961.1618091302121513.a01.

[35] A. D. Bank, Handbook on Battery Energy Storage System, 2018, 1-94. doi:org/10.22617/TCS189791-2.

[36] J.L Walkins, D.M. Bush, J.L. Chamberlin, R.P. Clark, Handbook of Secondary Storage Batteries and Charge Regulators in Photovoltaic Systems Final Report, Prepared by Exide Management and Technology Company,Pennsylvania, 2002, 1-180. https://www.azsolarcenter.org.

[37] P. Alotto, M. Guarnieri, F. Moro, Redox flow batteries for the storage of renewable energy: A review, Renew. Sustain. Energy Rev. 29 (2014) 325–335. doi:10.1016/j.rser.2013.08.001.

[38] D. Dumancic, F. Wallin, Flow Batteries Status and Potential, Doctoral dissertation, Mälardalen University, 2011.

[39] M. Skyllas-Kazacos, M.H. Chakrabarti, S.A. Hajimolana, F.S. Mjalli, M. Saleem, Progress in Flow Battery Research and Development, J. Electrochem. Soc. 158, 8 (2011), 55-79, doi:10.1149/1.3599565.

[40] W. Wang, S. Kim, B. Chen, Z. Nie, J. Zhang, Guan-Guang Xia, L. Li, Y. Zhenguo, A new redox flow battery using Fe/V redox couples in chloride supporting electrolyte, Energy Environ. Sci. (2011) 4068–4073. doi:10.1039/c0ee00765j.

[41] G.P. Rajarathnam, A.M. Vassallo, Description of the Zn/Br RFB System, in: Springer Briefs in Energy, 2016, 11–28. doi:10.1007/978-981-287-646-1.

[42] S. Zhang, W. Guo, F. Yang, P. Zheng, R. Qiao, Recent Progress in Polysulfide Redox-Flow Batteries, Batter. Supercaps. (2019) 627–637. doi:10.1002/batt.201900056.

[43] P. Leung, X. Li, P. De Leo, L. Berlouis, C. T. John, F. C. Walsh, Progress in redox flow batteries, remaining challenges and their applications in energy storage, RSC Adv. 2 (2012) 10125–10156. doi:10.1039/c2ra21342g.

[44] W. Winkler, Fuel cells and flow batteries-chances and challenges for sustainable energy supply, in: 7th Int. Green Energy Conf. 1st DNL Conf. Clean Energy, 2012, 1-11. https://www.researchgate.net.

[45] K. Maheshwari, S. Sharma, A. Sharma, S. Verma, Fuel Cell and Its Applications : A

Review, Int. J. Eng. Res. Technol. 7 (2018) 6–9. http://www.ijert.org.

[46] M. Moghaddam, S. Sepp, C. Wiberg, A. Bertei, A. Rucci, Thermodynamics, Charge Transfer and Practical Considerations of Solid Boosters in Redox Flow Batteries, Molecules. 26 (2021) 1–19. doi:10.3390/molecules26082111.

[47] A. Clemente, R. Costa-castelló, Redox flow batteries : A literature review oriented to automatic control, Energies. (2020) 1–32. doi:10.3390/en13174514.

[48] C.P. De Le, F.C. Walsh, Redox flow cells for energy conversion, J. Power Sources. 160 (2006) 716–732. doi:10.1016/j.jpowsour.2006.02.095.

[49] P.K. Pathak, Battery Energy Storage System, in: 4th Int. Conf. Comput. Intell. Commun. Technol. (CICT 2018), IEEE, 2018, 1–9. doi:10.1109/CIACT.2018.8480377.

[50] T. Shigematsu, Redox Flow Battery for Energy Storage, SEI Tech. Rev. number 73(2011), 4-11. https://global-sei.com.

[51] X. Ke, J.M. Prahl, J.I.D. Alexander, J.S. Wainright, A. Zawodzinski, R.F. Savinell, Rechargeable redox flow batteries: flow fields, stacks and design considerations, Chem.Soc.Rev., 47 (2018) 8721–8743. doi:10.1039/c8cs00072g.

[52] J. Girschik, L. Kopietz, M. Joemann, A. Greve, C. Doetsch, Redox Flow Batteries : Stationary Energy Storages with Potential, Chemie Ing. Tech. 93 (2021) 523–533. doi:10.1002/cite.202100001.

[53] W. Wang, Q. Luo, B. Li, X. Wei, L. Li, Z. Yang, Recent progress in redox flow battery research and development, Adv. Funct. Mater. 23 (2013) 970–986. doi:10.1002/adfm.201200694.

[54] T. Van Nguyen, R.F. Savinell, Flow Batteries, Electrochem. Soc. Interface. 19 (2010) 54–56. doi:10.1021/ac200156s.

[55] P. Leung, Development of a zinc-cerium redox flow battery, Doctoral dissertation, University of Southamption, 2011.

[56] Z. Huang, Organic Redox-Active Flow Batteries Enabled by Aqueous Ionic Liquid Electrolytes, Doctoral dissertation, Universität des Saarlandes and Korea Institute of Science of Technology (KIST) Europe., 2020.

[57] M.H. Chakrabarti, R.A.W. Dryfe, E.P.L. Roberts, Evaluation of electrolytes for redox flow battery applications, Electrochim. Acta. 52 (2007) 2189–2195. doi:10.1016/j.electacta.2006.08.052.

[58] H. Prifti, A. Parasuraman, S. Winardi, T.M. Lim, M. Skyllas-kazacos, Membranes for Redox Flow Battery Applications, Membranes (Basel). 2 (2012) 275–306. doi:10.3390/membranes2020275.

[59] T. Janoschka, N. Martin, U. Martin, C. Friebe, S. Morgenstern, H. Hiller, M.D. Hager, U.S. Schubert, An aqueous, polymer-based redox-flow battery using non-corrosive, safe, and low-cost materials, Nature. 527 (2015) 78–81. doi:10.1038/nature15746.

[60] G. Merle, M. Wessling, K. Nijmeijer, Anion exchange membranes for alkaline fuel cells : A review, J. Memb. Sci. 377 (2011) 1–35. doi:10.1016/j.memsci.2011.04.043.

[61] P. Puri, Sharma, Principles of Physical Chemistry, Vishal publishing Co., Jalandhar, India, 2013.

[62] A. Mallik, B.C. Ray, Evolution of Principle and Practice of Electrodeposited Thin Film : A Review on Effect of Temperature and Sonication, Int. J. Electrochem. 2011 (2011) 1-17. doi:10.4061/2011/568023.

[63] S. Yadav, Fabrication and Characterization of Novel Flow Battery Electrodes using Electrospinning, postgraduate dissertation, University of Waterloo, 2018.

[64] D. Aaron, Z. Tang, Polarization curve analysis of all-vanadium redox flow batteries, J. Appl Ied Electrochem. 41 (2011) 1175–1182. doi:10.1007/s10800-011-0335-7.

[65] K.J. Yoon, S. Gopalan, U.B. Pal, Effect of Fuel Composition on Performance of Single-Step, J. Electrochem. Soc. 154 (2007) 1080–1087. doi:10.1149/1.2769826.

[66] M.V. Holland-Cunz, F. Cording, J. Friedl, U. Stimming, Redox flow batteries-Concepts and chemistries for cost- effective energy storage, Front. Energy. (2018) 1–27. doi:org/10.1007/s11708-018-0552-4.

[67] M.K. Ravikumar, S. Rathod, N. Jaiswal, S. Patil, A. Shukla, The renaissance in redox flow batteries, J. Solid State Electrochem. (2016) 1-22. doi:10.1007/s10008-016-3472-4.

[68] T. Van Nguyen, R.F. Savinell, Flow Batteries, Electrochem. Soc. Interface. 19 (2010) 54–56. doi:10.1021/ac200156s.

[69] M. Bartolozzi, Development of redox flow batteries. a historical bibliography, J. Power Sources. 27 (1989) 219–234. doi:org/10.1016/0378-7753(89)80037-0.

[70] H. Zhang, Polysulfide-bromine flow batteries (PBBs) for medium and large-scale energy storage, Elsevier Ltd., 2015, 1-11. doi:10.1016/B978-1-78242-013-2.00009-1.

[71] M. Skyllas-kazacos, G. Kazacos, G. Poon, H. Verseema, Recent advances with UNSW vanadium-based redox flow batteries, Int. J. Energy Res. 34 (2010) 182–189. doi:10.1002/er.1658.

[72] D.J. Park, K.S. Jeon, C.H. Ryu, G.J. Hwang, Performance of the all-vanadium redox flow battery stack, J. Ind. Eng. Chem. 45 (2017) 387–390. doi:10.1016/j.jiec.2016.10.007.

[73] M. Ulaganathan, V. Aravindan, Q. Yan, S. Madhavi, M. Skyllas-kazacos, T.M. Lim, Recent Advancements in All-Vanadium Redox Flow Batteries, Adv. Mater. Interfaces. 3 (2016) 1–22. doi:10.1002/admi.201500309.

[74] S. Badwal, S.S. Giddey, C. Munnings, A.I. Bhatt, A.F. Hollenkamp, Emerging electrochemical energy conversion and storage technologies, Front. Chem. 2 (2014) 1–28. doi:10.3389/fchem.2014.00079.

[75] J. Winsberg, T. Hagemann, T. Janoschka, M.D. Hager, U.S. Schubert, Redox-Flow Batteries : From Metals to Organic Redox- Active Materials, Angew. Chemie Int. Ed. 55 (2016) 2–28. doi:10.1002/anie.201604925.

[76] L.F. Arenas, A. Loh, D.P. Trudgeon, X. Li, C. Ponce, D. León, F.C. Walsh, The

characteristics and performance of hybrid redox flow batteries with zinc negative electrodes for energy storage, Renew. Sustain. Energy Rev. 90 (2018) 992–1016. doi:10.1016/j.rser.2018.03.016.

[77] E. Ventosa, M. Guarnieri, A. Trov, C. Flox, R. Marcilla, F. Soavi, P. Mazur, E. Aranzabe, R. Ferret, Redox flow batteries : Status and perspective towards sustainable stationary energy storage, 481 (2021) 1-23. doi:10.1016/j.jpowsour.2020.228804.

[78] Z. Xie, Q. Liu, Z. Chang, X. Zhang, The developments and challenges of cerium half-cell in zinc-cerium redox flow battery for energy storage, Electrochim. Acta. 90 (2013) 695–704. doi:10.1016/j.electacta.2012.12.066.

[79] Z. Xie, Y. Bin, D. Cai, Y. Liang, Hierarchical porous carbon toward effective cathode in advanced zinc-cerium redox flow battery, J. Rare Earths. 32 (2014) 973–978. doi:10.1016/S1002-0721(14)60171-X.

[80] P.K. Leung, C.P. De León, F.C. Walsh, An undivided zinc–cerium redox flow battery operating at room temperature (295 K), Electrochem. Commun. 13 (2011) 770–773. doi:10.1016/j.elecom.2011.04.011.

[81] C.P. Zhang, S.M. Sharkh, X. Li, F.C. Walsh, C.N. Zhang, J.C. Jiang, The performance of a soluble lead-acid flow battery and its comparison to a static lead-acid battery, Energy Convers. Manag. 52 (2011) 3391–3398. doi:10.1016/j.enconman.2011.07.006.

[82] R. Suman, M.K. Ravikumar, J. Nandini, P. Satish, A.K. Shukla, Extending cycle life of the soluble lead redox flow battery with an auxiliary gas-diffusion electrode : a proof of concept study, Ionics (Kiel). 27 (2021) 3403–3414. doi:10.1007/s11581-021-04127-5.

[83] G.L. Soloveichik, Flow Batteries : Current Status and Trends, Chem. Rev. 115 (2014) 11533–11558. doi:10.1021/cr500720t.

[84] S. Selverston, R.F. Savinell, J.S. Wainright, Zinc-Iron Flow Batteries with Common Electrolyte, J. Electrochem. Soc. 164 (2017) 1069–1075. doi:10.1149/2.0591706jes.

[85] K. Gong, X. Ma, K.M. Conforti, K.J. Kuttler, J.B. Grunewald, K.L. Yeager, M.Z. Bazant, S. Gu, Y. Yan, A zinc–iron redox-flow battery under $100 per kW h of system capital cost, Energy Environ. Sci. 8 (2015) 2941–2945. doi:10.1039/C5EE02315G.

[86] B. Li, Z. Nie, M. Vijayakumar, G. Li, J. Liu, V. Sprenkle, W. Wang, Ambipolar zinc-polyiodide electrolyte for a high-energy density aqueous redox flow battery, Nat. Commun. 6 (2015) 1–8. doi:10.1038/ncomms7303.

[87] M. Mousavi, G. Jiang, J. Zhang, A.G. Kashkooli, Decoupled low-cost ammonium-based electrolyte design for highly stable zinc–iodine redox flow batteries, Energy Storage Mater. (2020) 1-49. doi:10.1016/j.ensm.2020.06.031.

[88] J. Zhang, G. Jiang, P. Xu, A. G. Kashkooli, M. Mousavi, A. Yu, Z. Chen, An All-Aqueous Redox Flow Battery with Unprecedented Energy Density, Energy Environ. Sci. (2018) 2010–2015. doi:10.1039/C8EE00686E.

[89] W. Guo-Ming, Z. Li, G. Cong, Y. Zhou, L. Yi-Chun, Unlocking the capacity of iodide for high-energy-density zinc/polyiodide and lithium/polyiodide redox flow batteries, Energy Environ. Sci. 10 (2017) 735–741. doi:10.1039/C6EE03554J.

[90] C. Xie, H. Zhang, W. Xu, W. Wang, X. Li, A Long Cycle Life Self-Healing Zinc-Iodine Flow Battery with High Power Density, Angew. Chemie Int. Ed. 57 (2018) 1-7. doi:10.1002/anie.201803122.

[91] B.S. Jayathilake, E.J. Plichta, M.A. Hendrickson, S.R. Narayanan, Improvements to the Coulombic Efficiency of the Iron Electrode for an All-Iron Redox-Flow Battery, J. Electrochem. Soc. 165 (2018) 1630–1638. doi:10.1149/2.0451809jes.

[92] M.C. Tucker, A. Phillips, A.Z. Weber, All-Iron Redox Flow Battery Tailored for Off-Grid Portable Applications, (2015) 3996–4004. doi:10.1002/cssc.201500845.

[93] K. Gong, F. Xu, J.B. Grunewald, X. Ma, Y. Zhao, S. Gu, Y. Yan, All-Soluble All-Iron Aqueous Redox-Flow Battery, ACS Energy Lett. (2016) 89–93. doi:10.1021/acsenergylett.6b00049.

[94] A. Dinesh, S. Olivera, K. Venkatesh, M. Sridhar, S. Murugesan, G. Priya, Iron‐based flow batteries to store renewable energies, Environ. Chem. Lett. (2018) 1-12. doi:10.1007/s10311-018-0709-8.

[95] L.F. Arenas, A. Loh, D.P. Trudgeon, X. Li, C. Ponce, D. León, F.C. Walsh, The characteristics and performance of hybrid redox flow batteries with zinc negative electrodes for energy storage, Renew. Sustain. Energy Rev. 90 (2018) 992–1016. doi:10.1016/j.rser.2018.03.016.

[96] L. Guo, H. Guo, H. Huang, S. Tao, Y. Cheng, Inhibition of Zinc Dendrites in Zinc-Based Flow Batteries, Front. Chem. 8 (2020) 1–8. doi:10.3389/fchem.2020.00557.

[97] J. Zheng, Q. Zhao, T. Tang, J. Yin, C.D. Quilty, G.D. Renderos, X. Liu, Y. Deng, L. Wang, D.C. Bock, C. Jaye, D. Zhang, E.S. Takeuchi, K.J. Takeuchi, A.C. Marschilok, L.A. Archer, Reversible epitaxial electrodeposition of metals in battery anodes, 648 (2019) 645–648. doi:10.1126/science.aax6873.

[98] Q. Zhang, J. Luan, Y. Tang, X. Ji and H. Wang, Interfacial design of dendrite-free zinc anodes for aqueous zinc-ion batteries, Angew. Chemie Int. Ed. (2020) 1-13. doi:10.1002/anie.202000162.

[99] H. Zhang, C. Sun, Cost-effective iron-based aqueous redox flow batteries for large-scale energy storage application : A review, J. Power Sources. 493 (2021) 1-20, 229445. doi:10.1016/j.jpowsour.2020.229445.

[100] K. Gong, Study of novel redox flow batteries based on double-membrane, single-membrane, and membrane-less cell configurations, Doctoral dissertation, University of Delaware, 2016.

CHAPTER 2

Experimental Techniques

Physical electrochemistry deals mainly with the broad area of fundamental electrochemistry. This includes theoretical and experimental aspects of the kinetics and thermodynamics of heterogeneous electron transfer at electrode-electrolyte interfaces and the application of spectroscopic and other techniques to the study of the electrochemical interface and processes [1]. In this chapter the analytical techniques that were used such as cyclic voltammetry, constant-current charge-discharge, electrochemical impedance spectroscopy and scanning electron microscopy for the characterization of the redox flow batteries developed in the present work were described.

2.1 Cyclic voltammetry

Cyclic voltammetry is one of the most extensively used potentiodynamic electrochemical measurement for the characterization of redox systems [2]. In a cyclic voltammetry experiment, the potential of a stationary working electrode is linearly scanned at a given speed using a triangle potential waveform. When the predetermined potential is reached in the experiment, the potential of working electrode is ramped in the opposite direction to return to the initial potential. Single or several cycles might be employed depending on the information desired. The potentiostat monitors the current generated by the applied potential throughout the potential sweep and the resulting plot of current vs. potential is known as a cyclic

voltammogram. CV is commonly used to investigate aqueous redox processes, surface deposition and adsorption.

A three-electrode setup comprising a reference electrode, working electrode and counter electrode is used in a typical CV experiment and Fig. 21 shows a schematic of an electrochemical cell. The current flow between the working and counter electrodes, and the reference electrode is used to measure the potential applied in relation to a stable reference response. The working electrode is the one where the current is measured and the potential is controlled. This is the electrode where the electrochemical reactions (reduction or oxidation) take place. The working electrode acts as a surface for the electrochemical reaction to occur on. Common working electrode materials include mercury, glassy carbon, platinum, gold, graphite and carbon paste.

The reference electrode establishes a well-defined potential against which the working electrode potential is measured. Two common and accurate secondary reference electrodes for aqueous solutions are saturated calomel electrode (SCE) and silver/silver chloride electrode (Ag/AgCl).

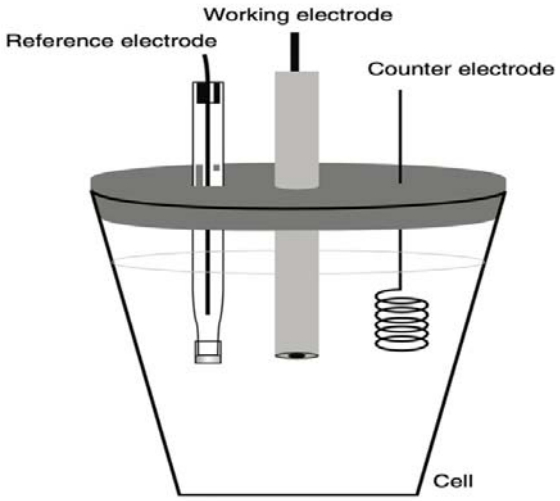

Fig. 21 An electrochemical cell for CV experiment [3].

The counter or auxiliary electrode functions as an electron source or sink, allowing current to flow from the external circuit through the cell. The current that enters the solution through the working electrode, leaves through the counter electrode. A non-reactive, high surface area electrode, such as platinum or carbon, should be used as the counter electrode [3–5].

The electrode-mediated oxidation and reduction reactions of electroactive species in solution are the principal reaction in most CV experiments. The electroactive substance must diffuse from the bulk solution to the electrode-solution interface in order to react. Migration, diffusion and convection are three types of mass transport reactions that are responsible for transferring of electroactive species from bulk solution to the interface. The movement of an electroactive species under the influence of an electric field is known as migration. Diffusion is the movement of an electroactive species caused by a chemical potential gradient, such as a concentration gradient. Convection is a form of transport that involves the movement of electroactive species due to density gradients, laminar flow, turbulent flow and agitation [6,7]. A potentiostat is one of the most widely used equipment for CV analysis. The Autolab PGSTAT (Model No. 204 with NOVA 1.11 software) instrument in Fig. 22 connected to a PC was used to perform the CV experiments in this study.

Fig. 22 An Autolab PGSTAT instrument (Model No. 204).

When the three electrodes are connected to the potentiostat, it is possible to control the working electrode potential with respect to the reference (silver/silver chloride), which is equivalent to controlling the energy of the electrons within the working electrode. When the working electrode potential is scanned toward negative values by applying negative potentials, the energy of the electrons is increased as the potential becomes more negative. When the applied negative potential is sufficient and the electrodes were placed in the solution, the electrons will reach a level that is high enough to transfer into vacant electronic states on electroactive species in the solution. Thus, the electrons flow from the working electrode to electroactive species in solution and a reduction current is obtained. At the same time, electroactive species in solution are reduced at the electrode-electrolyte interface. In an analogous manner, when the energy of the electron is lowered by applying a sufficiently positive potential, the electrons flow from electroactive species in solution to the working

electrode and an oxidation current is obtained. In this case, electroactive species in solution undergo oxidation at the electrode-electrolyte interface.

Fig. 23 shows a typical cyclic voltammogram with an initial forward scan from 0.0 V to 1.0 V and the cathodic current is indicated by i_{pc} and the cathodic peak potential for reduction is indicated by E_{pc}. E_{pa} determines the anodic peak potential [8]. The Randles Sevcik in equation 2.1, determines the magnitude of the peak current i_p [4].

$$i_p = (2.69 \times 10^5)\, n^{3/2} A C D^{1/2} v^{1/2} \quad \text{……..(2.1)}$$

Where i_p is peak current (μA), n is the number of electrons transferred, A is electrode surface area (cm^2), C is analyte concentration (mol/cm^3), D is analyte diffusion coefficient in solution (cm^2/s) and v is scan rate (V/s).

If the redox couple is reversible, the oxidation peak has a shape similar to that of reduction peak. However, if the redox pair is irreversible, the oxidation peak current may be lower than the reduction peak current or there may be no oxidation peak during the reverse scan, due to the chemical reaction that occurs after the electron transfer process. As a result, cyclic voltammetry can identify the reversibility of electron transfer as well as the stability of the electro generated product. For an irreversible process, the half-wave potential $E_{1/2}$ is the average value of E_{pc} and E_{pa} as seen in equation 2.2.

$$E_{1/2} = \frac{Epa + Epc}{2} \quad \text{…….. (2.2)}$$

According to Nernst Equation, the ΔE_p for a reversible processes should be $\frac{59}{n}$ mV at 25 ^oC. Thus, the number of electron transferred during the redox process can be determined [8].

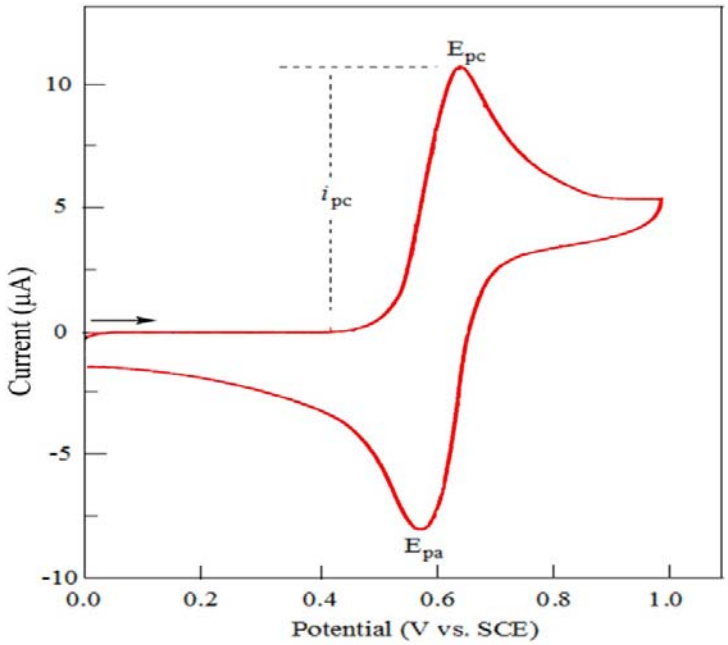

Fig. 23 Cyclic voltammogram [8].

2.2 Charge-discharge performance

An electrochemical cell is a chemical device that uses electricity to generate or store energy. It is made up of two electrodes, one positive and the other negative, separated by an electrolyte. Fig. 24 shows the schematic diagram of the operation of an electrochemical cell. The electrolyte can carry ions between the two electrodes, but it is an electronic insulator by itself. The reactive compounds are stored within the electrodes, but sometimes also in the electrolyte and the positive and negative electrodes are immersed in the electrolyte. At the two electrodes, chemical reactions associated with energy conversion occur. The negative electrode contains the substance that is oxidized (i.e. releases electrons) during discharge (Fig. 24a), whereas the positive electrode contains the substance that is reduced (i.e. accepts electrons). The electrons flow through the external load and do useful work. This process is

reversed when the battery is charged and an equivalent quantity of energy must be provided to the cell from an external source (Fig. 24b).

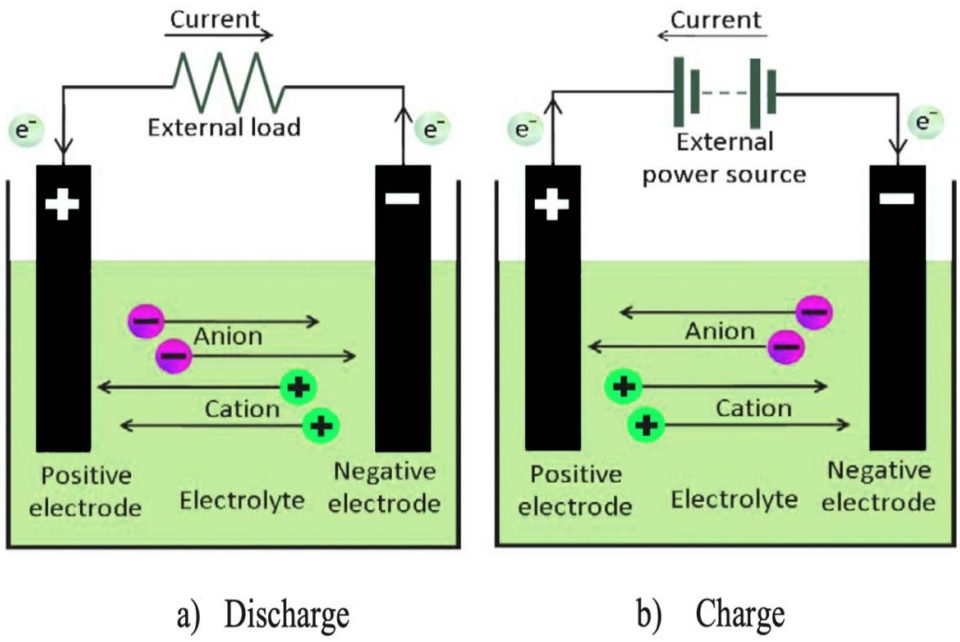

Fig. 24 Schematic diagram of the operation of an electrochemical cell [9].

The transport of electrons from one electrode to the other generates current in the battery. The difference between the potentials of the positive and negative electrodes gives the open-circuit voltage (OCV) of the cell, when there is no current flowing through it. However, when current flows, mass transport is required to transfer the reacting chemicals to or away from the electrode surface. As a result, the voltage under current flow differs from the OCV and the difference comprises with (i) an overvoltage at the electrodes due to electrochemical reactions and concentration deviations due to transport phenomena and (ii) ohmic voltage drops due to electronic and ionic current flows in the conducting parts, such as the electrolyte, current-collectors and active masses. The sum of both causes a decreased cell voltage

during discharge and an increased cell voltage during charge, which is referred to as polarization [9].

The chronopotentiometry (galvanostatic cycling) is the most popular technique for evaluating the performance of a flow cell. The Autolab PGSTAT 204 instrument in Fig. 22 is also used for charge-discharge measurement of the battery. The galvanostat uses a three electrode configuration, in which a current is applied between the working and counter electrodes and the potential of the working electrode (measured with respect to the reference electrode) is monitored. When a cell is charged and discharged at a steady current, the voltage of the cell is monitored over time. A typical charge-discharge measurement would show a progressive increase in cell voltage during charging and a gradual reduction in cell voltage during discharge. The electrochemical cell test enables users to choose the number of cycles to be repeated as well as the voltage limit and applied current for each charge-discharge cycle. For security reasons, when measuring voltage range, the current limit has to be set to prevent the occurrence of extreme voltages or currents [1]. The three generally used performance measures of a flow cell that are obtained from the resultant charge-discharge reaction are coulombic, voltaic and energy efficiency.

2.2.1 Coulombic Efficiency (CE)

Coulombic efficiency is the ratio of the charge released during discharge to the amount of charge used during the charging process [10].

$$CE = \frac{t_d}{t_c} X\ 100\% \qquad \text{…….. (2.3)}$$

Here, t_d represents the discharge time and t_c the charge time.

Low CE value indicates the crossover of reactive species between half-cells causing self-discharge or the side reactions that consume the active species as a reactant during battery operation. Hence, the membrane should have high ion selectivity to prevent the cross-mixing of reactive species between the electrode compartments [11,12].

2.2.2 Voltage Efficiency (VE)

The voltage efficiency (VE) of the cell is given by the ratio of the discharge voltage to the theoretical cell voltage [10].

$$VE = \frac{V_d}{V_c} X\ 100\% \qquad \ldots\ldots (2.4)$$

Here, V_d is the average discharge voltage and V_c the average charge voltage.

The reduction potential of the redox process in each half-cell and the total overpotential of the RFB determine the discharge and charge potentials. If the total overpotentials of the system are negligible in the cell, a 100% VE can be obtained. A reduction in VE is mainly due to ohmic, activation and concentration overpotentials usually observed in battery systems [11,12].

2.2.3 Energy Efficiency (EE)

EE is simply the product of coulombic efficiency (CE) and voltage efficiency (VE) [10]. Overall, EE is affected by the factors that can affect CE and VE as discussed above. EE indicates how much of the energy provided to the battery while charging may be extracted when the battery is discharged [11,12].

$$EE = VE\ X\ CE \ldots\ldots\ldots (2.5)$$

2.3 Electrochemical impedance spectroscopy (EIS)

Electrochemical impedance spectroscopy (EIS) is an important electrochemical technique, in which the impedance in a circuit is measured in ohms. The EIS measurement was used to determine the ionic conductivity of the membrane using the Autolab PGSTAT 204 instrument shown in Fig. 22. In the conductivity cell, a fully hydrated membrane was inserted between two platinum electrodes and 1 M NaOH was added. The cell was thermostated at 25 ± 0.1°C for at least 20 minutes to ensure thermal equilibrium [13]. An alternating potential of amplitude 10 mV was used to measure the frequency range of 100 Hz to 1000 kHz. The resistance of the membrane and solution (R_{total}) was obtained from the Nyquist plot by extrapolating to the high frequencies. Using the same method, the resistance of the solution ($R_{solution}$) was also measured without the membrane. The difference between the observed resistances ($R_{total} - R_{solution}$) was used to calculate membrane resistance (R_{mem}) [14,15]. A digital micrometer was used to measure the thickness of the membrane, which was placed between two glass slides to provide a planar surface and minimum compression. The membrane resistance was then used to calculate the membrane conductivity (σ) by the equation:

$$\sigma = \frac{L}{R_{mem}\, A} \text{ mS cm}^{-1} \quad \ldots\ldots\ldots (2.6)$$

Where R_{mem} is the membrane resistance (in Ω), L is the thickness of the membrane (in cm) and A is the cross sectional area of membrane samples (cm^2) [13].

2.4 Scanning electron microscopy (SEM)

Scanning electron microscopy was used to investigate the surface morphology of the samples [16]. When the finely focused electron beam interacts with the sample surface, there are three main phenomena occur (i) the emission of secondary electrons (SE) (ii) back-scattering of electrons (BSE) and (iii) the transmission of electrons. These three major phenomena and some other important phenomena [17,18] are shown in Fig. 25. The samples were kept in a vacuum oven at 30 °C overnight and were coated with a thin layer of gold by ion sputtering method before the microscopic examination. The energy dispersive analyzer was used for the elemental detection of the samples.

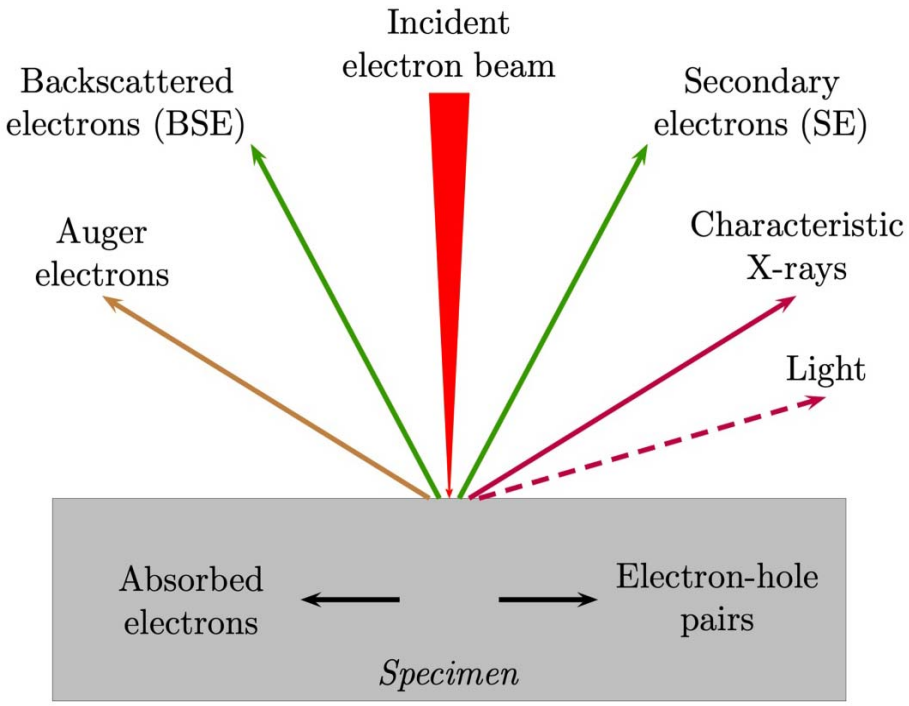

Fig. 25 Types of interactions between electrons and a sample [19].

A source of electrons, electromagnetic lenses to focus electrons, electron detectors, sample chambers, computers and monitors to view the images are the primary components of the SEM (Fig. 26) [20]. In SEM technique, the electron from a finely focused electron beam gets restored across the surface of the sample. The reflected electrons by the surface of the sample and the emitted secondary electrons give an image of the surface topography of the sample. SEM analysis is very useful for determining the particle size, crystal morphology, magnetic domains and surface defects, etc. A wide range of magnification methods can be used, in which the best feasible resolution is being about 2 nm. In the present study, we have used SEM analysis (using Jeol 6390 LA/OXFORD XMX N instrument) to find out the particle size and to see the surface morphology.

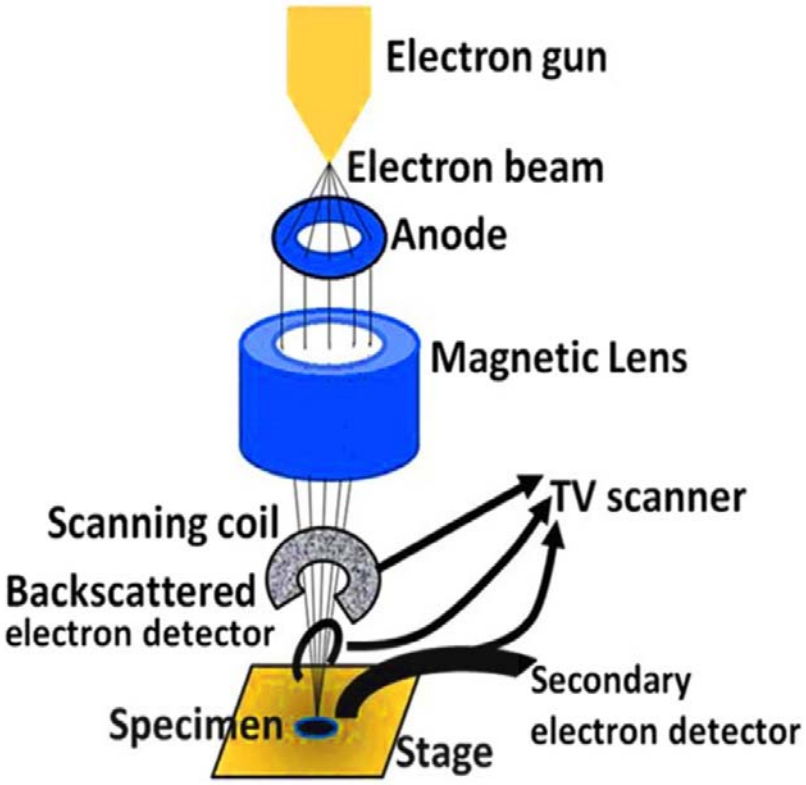

Fig. 26 Components of scanning electron microscopy [20].

2.5 References

[1] P. Modiba, Electrolytes for redox flow battery, Doctoral dissertation, Stellenbosch, 2010.

[2] Z. Huang, Organic Redox-Active Flow Batteries Enabled by Aqueous Ionic Liquid Electrolytes, Doctoral dissertation, Universität des Saarlandes and Korea Institute of Science of Technology (KIST) Europe., 2020.

[3] L. Khalafi, Cyclic voltammetry, in: E.J. Zerong Wang, Uta Wille, Authors: (Eds.), Encycl. Phys. Org. Chem., Wiley, 2017, 3437–3478. doi:10.1002/9781118468586.epoc4036/abstract.

[4] P.S. Joshi, D.S. Sutrave, A brief study of cyclic voltammetry and electrochemical analysis, Int. J. Chemtech Res. 11 (2018) 77–88. doi:10.1021/ac60180a004.

[5] K.J. Rountree, B.D. Mccarthy, E.S. Rountree, T.T. Eisenhart, J.L. Dempsey, A Practical Beginner's Guide to Cyclic Voltammetry, J. Chem. Educ. 95 (2017) 197–206. doi:10.1021/acs.jchemed.7b00361.

[6] F. Scholz, Voltammetric techniques of analysis : the essentials, ChemTexts. 1 (2015) 1–24. doi:10.1007/s40828-015-0016-y.

[7] D. Andrienko, Cyclic Voltammetry, in: Cycl. Voltammetry, 2008, 1–12. https://www2.mpip-mainz.mpg.de.

[8] L. Zeng, Electrochemical and spectroelectrochemical studies on bis-porphyrins, porphyrins with charged substituents and water-soluble porphyrazines,Postgraduate dissertation, University of Houston, 2015.

[9] S. Li, Study of Battery Modeling using Mathematical and Circuit Oriented Approaches, IEEE Power Energy Soc. Gen. Meet. (2011) 1–8. doi:10.1109/PES.2011.6039230.

[10] Y.K. Zeng, T.S. Zhao, X.L. Zhou, L. Wei, Y.X. Ren, A novel iron-lead redox flow battery for large-scale energy storage, J. Power Sources. 346 (2017) 97–102. doi:10.1016/j.jpowsour.2017.02.018.

[11] I.L.E. Gancia, Fundamental and flow battery studies for non-aqueous redox systems,Doctoral dissertation, Case Western Reserve University, 2015.

[12] M.V. Holland-Cunz, F. Cording, J. Friedl, Redox flow batteries-Concepts and chemistries for cost- effective energy storage, Front. Energy.(2018) 1–27. doi:org/10.1007/s11708-018-0552-4.

[13] J.A. Vega, C. Chartier, W.E. Mustain, Effect of hydroxide and carbonate alkaline media on anion exchange membranes, J. Power Sources. 195 (2010) 7176–7180. doi:10.1016/j.jpowsour.2010.05.030.

[14] P.M. Gomadam, J.W. Weidner, Analysis of electrochemical impedance spectroscopy in proton exchange membrane fuel cells, Int. J. Energy Res. 29 (2005) 1133–1151. doi:10.1002/er.1144.

[15] G. Sowmya, M.R. Prabhu, Different approaches in sulfonated poly (ether ether ketone) conductivity measurements, in: IOP Conf. Ser. Mater. Sci. Eng., 2019, 1-5. doi:10.1088/1757-899X/503/1/012030.

[16] B.J. Inkson, Scanning electron microscopy (SEM) and transmission electron microscopy (TEM); for materials characterization, Elsevier Ltd, 2016, 17-43. doi:10.1016/B978-0-08-100040-3.00002-X.

[17] W.E. Pretorius, An introduction to electron microscopy and X-ray, (2002) 1-32. http://natural-sciences.nwu.ac.za.

[18] J. Beauvaisa, D. Drouinb, SEM techniques for materials characterization, Mater. Charact. Opt. Probe Tech. A Crit. Rev. 10291 (2017) 175-199. doi:10.1117/12.279839.

[19] I.Z. Jenei, Scanning electron microscopy (SEM) analysis of tribofilms enhanced by fullerene-like nanoparticles,Thesis for the degree of Licentiate in Physics, Stockholm University,Sweden, 2012.

[20] A.K. Singh, Experimental Methodologies for the Characterization of Nanoparticles, in: Eng. Nanoparticles, 2016, 125–170. doi:10.1016/B978-0-12-801406-6.00004-2.

CHAPTER 3

A Dendrite Free Zinc-Iron Hybrid Redox Flow Battery for Renewable Energy Storage

3.1 Introduction

The redox flow batteries (RFBs) are attractive electrochemical systems which store energy in two electrolyte solutions comprising of different redox couples separated by an ion-exchange membrane (IEM) [1–5]. Among various traditional flow battery systems, the hybrid flow batteries involve the deposition of a metal coating on at least one of the electrodes [4][6]. The main advantages of RFBs over other battery systems are their safety, moderate cost, modularity, transportability and flexibility in charge-discharge cycles [7–9]. Unfortunately, the inadequate ionic selectivity of the existing IEMs leads to undesired crossover of redox species between negative and positive electrolytes through the membrane. This result a permanent lose in both coulombic efficiency (CE) and battery capacity and will lead to overall performance loss of RFBs [5,10–13].

Zinc-based redox flow batteries are generally more attractive due to favorable electrochemical properties of zinc such as its low cost, fast electrode kinetics, negative electrode potential (E^0 = −0.76 vs. SHE) and high overpotential for the hydrogen evolution reaction (HER) [14–16]. A Zn-Fe flow battery system reported by S. Selverston et al. used mixed zinc-iron electrolytes and porous separator in place of expensive ion-exchange membranes [15]. Ke Gong et al. reported a zinc-iron RFB

based on double-membrane triple electrolyte design [17]. Zhizhang Yuan et al. reported a battery that employs $Zn(OH)_4^{2-}/Zn$ and $Fe(CN)_6^{3-}/Fe(CN)_6^{4-}$ as the negative and positive redox couples, respectively, while a self-made, cost-effective polybenzimidazole (PBI) membrane was used as a separator. Zhipeng Xie et al. reported an energy efficiency of 71.1% over 50 cycles for a zinc-ferrum redox flow battery (Zn/Fe RFB) employing an ion-exchange membrane as a separator [18]. Qixing Wu et al. developed a chloride acid-based tin-iron hybrid flow battery with good rate and cycle performance [19,20]. Wang and co-workers developed a zinc-polyiodide flow battery and reported high energy density [21].

During the charging process of Zn based flow batteries, zinc dendrites form and ultimately pierce the separator, causing a short circuit and battery failure [22–25]. Additionally, the zinc dendrites can easily fall from anodes, reducing efficiency, capacity and life time of the cell [26]. As a result, inhibiting the formation of zinc dendrites is essential for the successful commercialization of zinc based RFBs. Researchers have recently focused their efforts on modifying the electrolyte, anodes, electric field and rate of zinc ion transfer to solve zinc dendrite formation [22–24]. To prevent negative effects of zinc dendrites on the performance and lifetime of zinc-based batteries, the separator should also have good mechanical stability to prevent the direct contact of the anode and cathode [27]. Thus, developing a highly efficient dendrite free zinc based electrical energy storage system having negligible crossover of the electroactive materials between the anode and cathode compartments is an important goal towards the wide spread use of renewable energy sources.

Herein we report a novel zinc-iron hybrid redox flow battery (Zn/Fe hybrid RFB), in which Zn/Zn(II) and Fe(III)/Fe(II) couples act as negative and positive redox

materials and the two redox couples are separated by a self-made anion exchange membrane. Both zinc and iron are the two advantageous elements for energy storage due to their low cost and high abundance [17]. The ferric/ferrous chloride redox pair, which has been used in a variety of flow battery systems, is promising as an active material on the positive side due to its rapid kinetics [28]. A schematic representation of the Zn-Fe hybrid redox flow battery is shown in Fig. 27. The electrochemical reaction through which Zn-Fe RFB stores and releases electricity can be expressed by following reactions:

At negative electrode: $Zn^{2+} + 2e^{-} \rightleftharpoons Zn$ $E^0 = -0.76$ V ……. (3.1)

At positive electrode: $2Fe^{2+} \rightleftharpoons 2Fe^{3+} + 2e^{-}$ $E^0 = +0.77$ V ……(3.2)

The overall reaction is: $Zn^{2+} + 2\,Fe^{2+} \rightleftharpoons Zn + 2Fe^{3+}$ $E^0 = 1.53$ V …..(3.3)

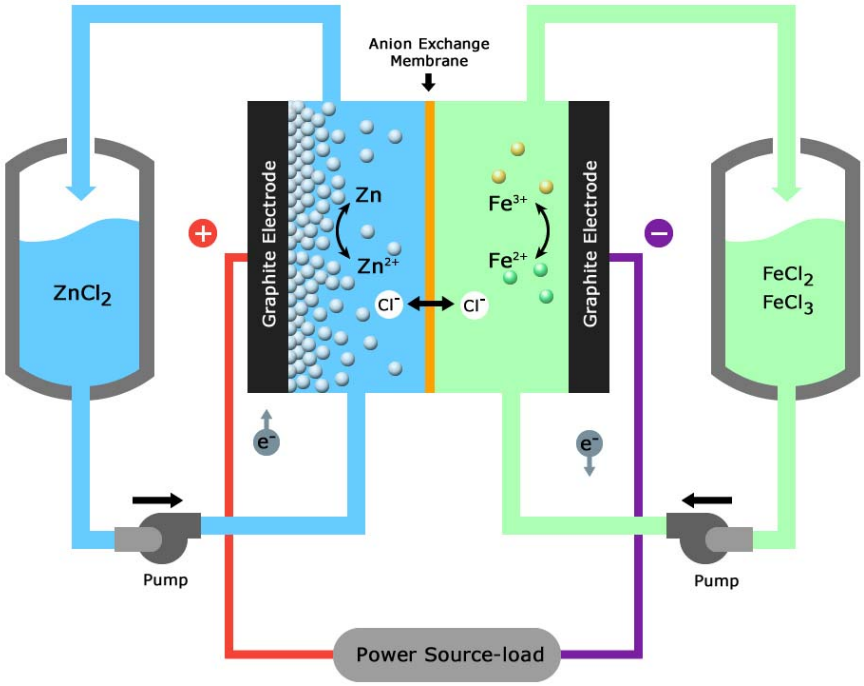

Fig. 27 Schematic of a Zn-Fe flow battery.

During the charging process, the Fe(II) ions at the positive electrode release the electrons, and get oxidized to Fe(III) ions; the Zn(II) ions at the negative electrode acquire these electrons from the external circuit and electrodeposits onto the electrode as metallic Zn. The chloride ions move through the anion exchange membrane from zinc compartment to the iron compartment, to maintain charge neutrality. During the discharge, the above electrochemical processes are reversed. At the positive electrode, the Fe(II)/Fe(III) redox couple have good solubility in acidic media and exhibits facile kinetics [17]. At the negative electrode, the Zn/Zn(II) redox couple also exhibit fast kinetics and has high overpotential for hydrogen evolution reaction [29].

3.2 Experimental

3.2.1 Chemicals

All chemicals were of reagent grade and the electrolytes were prepared with deionized water. Zinc chloride anhydrous ($ZnCl_2$), iron(II) chloride tetrahydrate ($FeCl_2$. $4H_2O$), iron(III) chloride anhydrous ($FeCl_3$), ammonium chloride (NH_4Cl) and formaldehyde solution (37%) were obtained from Merck India. Guanidine carbonate salt (CH_5N_3. 0.5 CH_2O_3) and melamine ($C_3H_6N_6$) were obtained from Sigma-Aldrich.

3.2.2 Preparation of electrolytes

1 M Zn/Zn(II) electrolyte is prepared by dissolving Zn(II) chloride in deionised water (pH = 5.8). The positive electrolyte is a mixture of 0.5 M $FeCl_2$ and 0.5 M $FeCl_3$ with 2 M NH_4Cl in deionised water (pH = 1.7). The NH_4Cl was added to the positive electrolyte as a supporting electrolyte in order to improve conductivity of the solution.

3.2.3 Preparation of anion exchange membrane

The anion exchange membrane was prepared by condensing guanidine carbonate with formaldehyde followed by cross-condensation with melamine. The dried powder was mixed with a polymer powder as a binder and made into a homogeneous suspension and converted into the membrane by solvent casting method. The prepared membranes were highly flexible and had a thickness of ~120 μm. The membrane resistance was examined by an electrochemical impedance spectroscopy measurement using the Autolab PGSTAT instrument.

3.2.4 Cyclic voltammetry

Cyclic voltammetry (CV) experiments were conducted in a three-electrode cell as shown in Fig. 28, using a potentiostat/galvanostat (Autolab PGSTAT) instrument. A graphite sheet, platinum sheet and an Ag/AgCl electrode were used as working, counter and reference electrodes, respectively. The CV was measured from −1.6 to −0.2 V versus Ag/AgCl reference electrode using 0.085 M $ZnCl_2$ as the electrolyte at a scan rate of 50 mV/s. The measurement was performed at room temperature.

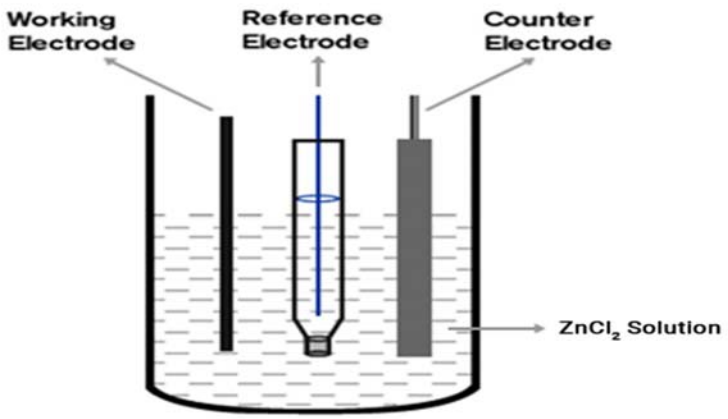

Fig. 28 The electrochemical set-up of a three-electrode cell.

3.2.5 Battery performance

The redox flow battery consists of a reaction chamber (cell) and two reservoirs to store electrolytes externally. The cell was made of acrylic sheet and the positive and negative electrodes were densified graphite sheets with an area of 16 cm^2 and thickness of 2 mm. The negative and positive electrodes were separated by the self-made anion exchange membrane. The total volume of each compartment of the cell is 3 cm × 3 cm × 1 cm. The negative electrolyte of this zinc-iron flow cell consisted of 1 M $ZnCl_2$ and the positive electrolyte is a mixture of 0.5 M $FeCl_2$ and 0.5 M $FeCl_3$ with 2 M NH_4Cl. The electrolytes were stored in two external reservoirs (each of 75 ml). Both positive and negative electrolytes were circulated through the cell using two peristaltic pumps. The cell performance was measured under a constant-current charge-discharge measurement using an Autolab PGSTAT instrument connected to a PC. The charge-discharge measurements were carried out using a standard two-electrode setup as shown in Fig. 29, in which the graphite sheets act as both working electrode and counter electrode respectively.

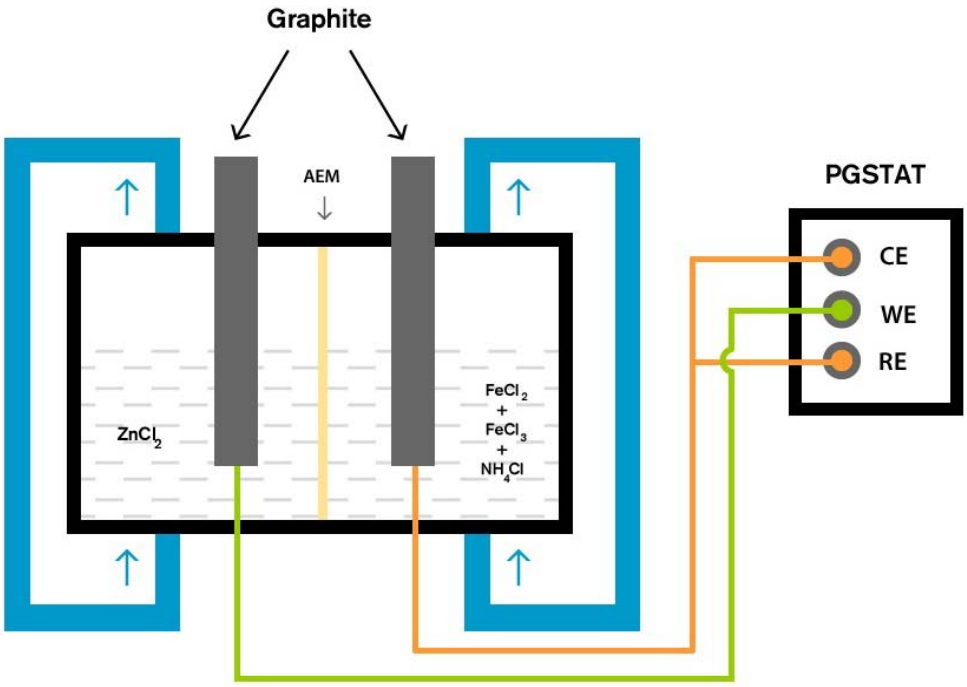

Fig. 29 The standard two-electrode setup for charge-discharge measurements.

The charge-discharge experiment of the zinc-iron redox flow cell is performed by charging the cell at a constant current of 25 mA cm^{-2} for 1800 seconds followed by discharge at the same current, until the cell reached a voltage of 0.0 V to completely strip off any deposited zinc. The cell parameters like coulombic efficiency (CE), voltage efficiency (VE) and energy efficiency (EE) of the battery are calculated using the equations described in chapter 2.

3.2.6 Scanning electron microscopy

Surface morphology of the membrane and zinc electrodeposits were analyzed using scanning electron microscope (Jeol 6390 LA/OXFORD XMX N).

3.3 Results and discussion

3.3.1 Electrochemical impedance spectra

Fig. 30 shows the Nyquist plots of the conductivity cell with membrane and without membrane. From the figure, the membrane resistance (R_{mem}) was calculated ($R_{mem} = R_{total} - R_{solution}$) and the value obtained is 0.5 Ω. From the membrane resistance, the conductivity was calculated and the membrane exhibited a hydroxide ion conductivity of around 80 mS^{-1} (at room temperature). Fig. 31 shows a photograph of the membrane prepared.

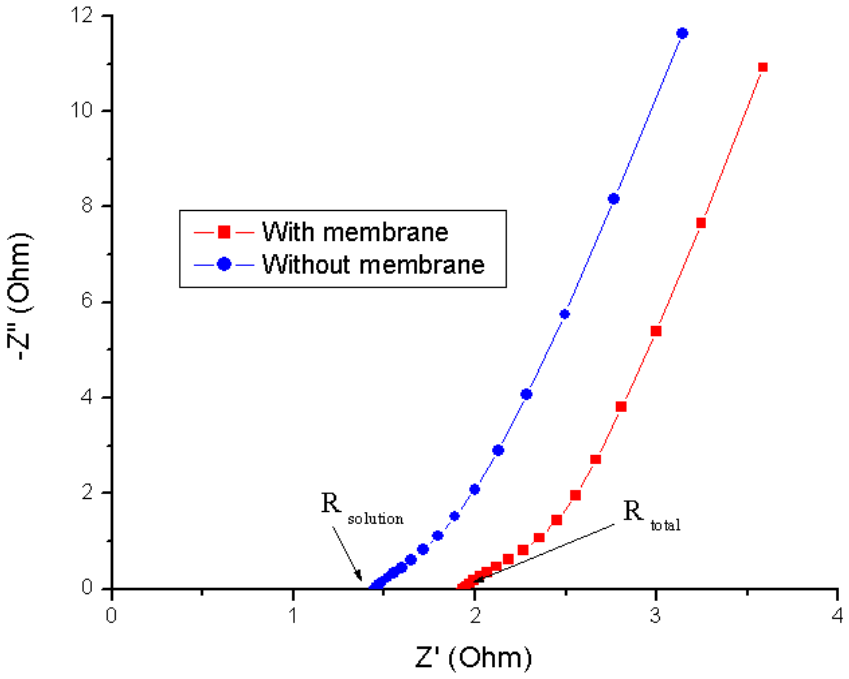

Fig. 30 Nyquist plot with membrane and without membrane.

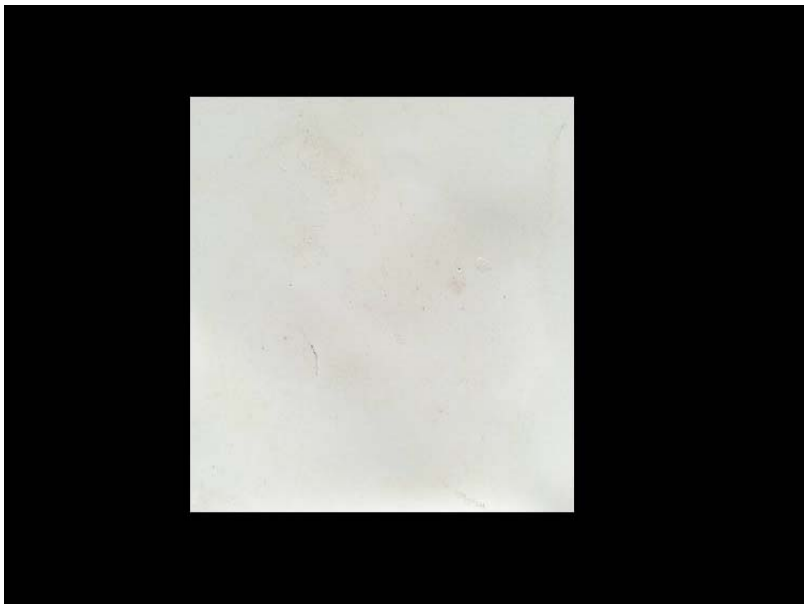

Fig. 31 Photograph of the membrane.

3.3.2 Cyclic voltammogram

A cyclic voltammogram of 0.085 M $ZnCl_2$ on a graphite sheet working electrode in the range of −1.6 to −0.2 V (versus Ag/AgCl) at the scan rate of 50 mV s^{-1} is shown in Fig. 32. From figure, it is clear that the cathodic peak at −1.28 V corresponds to the electrodeposition of zinc and the anodic peak at −0.74 V corresponds to the dissolution of zinc to the solution.

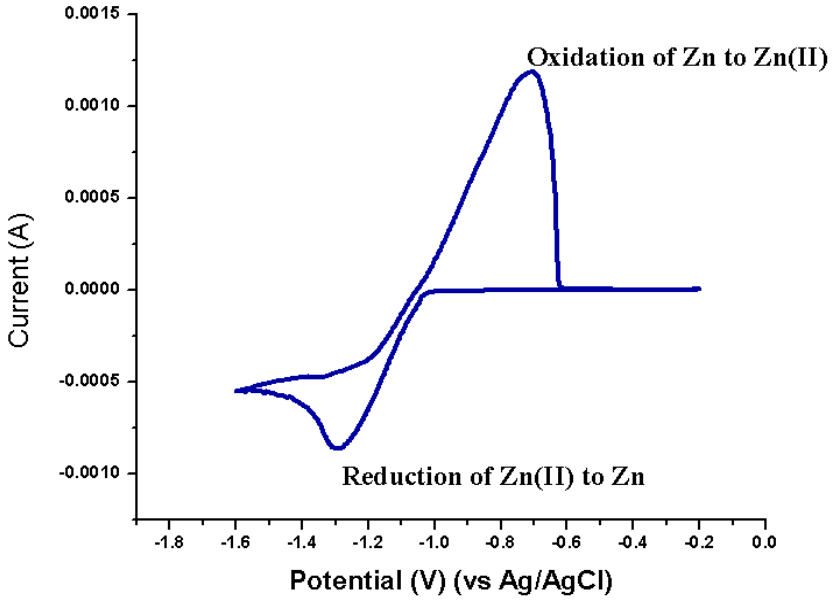

Fig. 32 CV of 0.085 M $ZnCl_2$ on a graphite electrode at the scan rate of 50 mV s^{-1}.

3.3.3 Charge-discharge cycle performance

The performance of a Zn-Fe RFB employing 1 M Zn(II) chloride aqueous solution as negative active species and 0.5 M $FeCl_2$ and 0.5 M $FeCl_3$ with 2 M NH_4Cl aqueous solution as positive species was evaluated with constant-current charge-discharge measurements. The charge-discharge measurements were repeated over 30 cycles and are shown in Fig. 33. Fig. 34 represents the characteristic charge/discharge curves for 15th cycle at 25 mA cm^{-2}. These curves were obtained from 30 minutes of charging followed by 30 minutes of discharging under a current density of 25 mA cm^{-2} using graphite electrodes. It shows a relatively flat voltage profile for charge and discharge process. The cycling studies at 25 mA cm^{-2} revealed good stability of the battery, without any evidence of degradation. The curves are identical with a charge voltage of approximately 1.59 V and a discharge voltage of 1.34 V.

Any crossover of Fe^{2+}/Fe^{3+} through the membrane to the anodic compartment will result in a gradual fading of coulombic efficiency on repeating the charge-discharge cycles [15,18]. However, this phenomenon is not observed in our redox flow system indicating that the crossover of Fe^{2+}/Fe^{3+} does not occur appreciably. This may be due to the good cation-blocking ability of the anion exchange membrane. In this case, during charging, excess chloride ions left in the anode compartment move towards cathode compartment through the membrane for electrical neutrality. During discharge process, opposite changes take place. When we repeated the experiments with a porous PVC membrane instead of an AEM, dendrite formation was observed on zinc electrodes even on first charging step, before any appreciable mixing of the two electrolytes happened. Fig. 35 shows the photograph of zinc deposit formation using PVC membrane and AEM. When an AEM is used, only chloride ions can diffuse from anode compartment to the cathode compartments through the AEM, during charging. From the above observations, it is clear that the selective migration of chloride ions has a strong influence on uniform deposition of zinc. Similar results of suppression of dendrite formation in zinc RFBs with different kinds of membranes have been reported by many other groups [30–32].

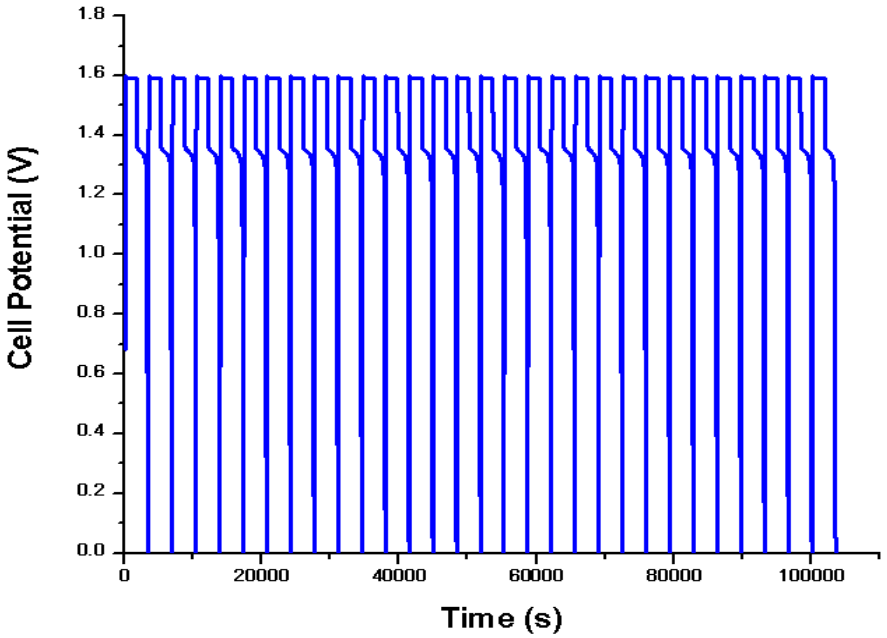

Fig. 33 Cell potential vs. time response for 30 cycles of Zn-Fe RFB at 25 mA cm^{-2}.

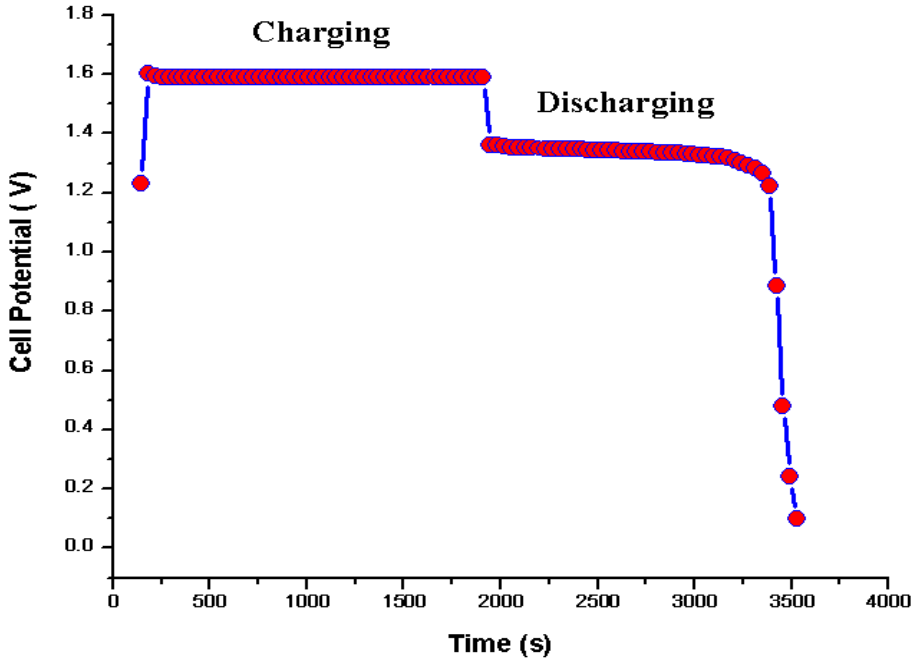

Fig. 34 Cell potential vs. time response for 15th charge-discharge cycle at 25 mA cm^{-2}.

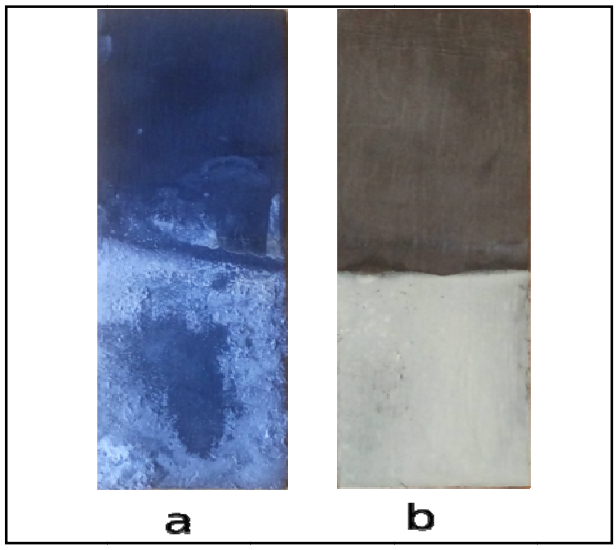

Fig. 35 The photograph of zinc deposit formation using (a) PVC membrane and (b) AEM.

The dependences of cell performance on concentration and current density were also investigated by performing the galvanostatic charge-discharge measurement at different $ZnCl_2$ concentrations (1 M, 3 M and 5 M) and at different current densities (15, 25 and 50 mA cm^{-2}) for 1 M $ZnCl_2$. The results are tabulated in Table 4 and 5.

Table 4 The Zn-Fe RFB performance as a function of $ZnCl_2$ concentration, at a current density of 25 mA cm^{-2}.

$ZnCl_2$ (M)	**OCV (V)**	**Avg. charge voltage (V)**	**Avg. discharge voltage (V)**	**CE (%)**	**VE (%)**	**EE (%)**
1 M	1.44	1.59	1.343	92	85	78.2
3 M	1.31	1.65	1.138	92	68.9	63.38
5 M	1.09	1.7	1.01	90	59.4	53.46

Table 5 The electrochemical performances for Zn-Fe cell with 1 M $ZnCl_2$ run at different charge/discharge current densities.

Current density (mA cm^{-2})	**OCV (V)**	**Avg. charge voltage (V)**	**Avg. discharge voltage (V)**	**CE (%)**	**VE (%)**	**EE (%)**
15	1.52	1.55	1.4	90	90	81
25	1.44	1.58	1.343	92	85	78.2
50	1.38	1.71	1.27	92	74	68.08

From Table 4, it is found that the average discharge voltage decreases from 1.34 V to 1.01 V on increasing concentration of $ZnCl_2$ from 1 M to 5 M, while the coulombic efficiency remains nearly constant at ~90-92% which indicates the high anion selectivity of the membrane. A higher CE compared to that of the cells reported by other researchers is mainly due to the negligible crossover of Fe^{3+} ions through AEM used in our redox flow battery. This result also confirms the high anion selectivity of our anion exchange membrane when used as a separator in Zn-Fe redox flow battery. The decrease in energy efficiency values from 78.2% to 53.46% with increasing electrolyte concentration is mostly related to a reduction in voltage efficiency from 85% to 59.4% due to increased electrolyte resistance [21,33].

The electrochemical performance of the Zn-Fe system with 1 M $ZnCl_2$ at different current densities (such as 15, 25 and 50 mA cm^{-2}) is shown in Table 5. The coulombic efficiency remained nearly constant at 90-92% when current densities were increased from 15 to 50 mA cm^{-2}. However, the voltage efficiency and energy

efficiency reduced from 90% to 74% and 81% to 68% respectively. The coulombic efficiency is mainly influenced by three key factors: temperature, current and state-of-charge. The relationship between charge or discharge currents and coulomb efficiency can be expressed by the Peukert equation [33]. This states that the overall battery capacity or the total energy supplied by the battery, decreases disproportionately as the discharge current rises.

$$\eta_c = \frac{Q_d}{Q_N} = \left(\frac{I_d}{I_N}\right)^{1-n} \quad \text{..... (3.4)}$$

Where I_d is discharge current, I_N is base current, Q_d is the capacity discharged by I_d and Q_N is the capacity discharged by base current I_N. The equation relating internal resistance, discharge current and energy efficiency can be written as

$$\eta_w = \eta_c \eta_v = \left(\frac{I_d}{I_N}\right)^{1-n} \frac{V_B - R_i I_d}{V_B + R_i I_c} \quad \text{..... (3.5)}$$

From the equations 3.4 and 3.5, it is clear that the internal resistance and discharge current values are obviously two key factors that reduce energy efficiency. Reducing internal resistance and maintaining an optimum charge and discharge current will help to increase the energy efficiency.

From charge-discharge plot, the coulombic, voltage and energy efficiencies were calculated and plotted vs. cycle number in Fig. 36. From the figure, it is clear that the Zn-Fe RFB shows no decrease for coulomb efficiency (92%), voltage efficiency (85%) and energy efficiency (78.2%) on 30 repeated charge-discharge cycles at 25 mA cm^{-2}. The average coulombic efficiency of about 92% in all the cycles indicates that the products formed during battery discharge return almost completely to their initial conditions on charging. Low coulombic efficiency in

aqueous electrolytes is generally attributed to the side reactions due to water electrolysis [5]. The standard reduction potential of zinc in acid media is −0.76 V vs. the standard hydrogen electrode (SHE). During the charge process, proton or water reduction leading to H_2 evolution is the preferred reaction thermodynamically. However zinc is a relatively poor electrocatalyst for the H_2 evolution and hence increase the overall cell efficiency by suppressing hydrogen evolution reaction [14]. After repeated charge-discharge cycles, no appreciable changes in pH were observed. Hydrogen evolution reaction ($2H^+ + 2e^- \rightarrow H_{2(g)}$) is a side reaction that decrease the efficiency of many redox flow batteries. This will also increase the pH of the anolyte. Higher coulombic efficiency and near consistency of the pH values after many charge-discharge cycles indicates that the hydrogen evolution on the anode is negligible in the present system. No zinc dendrite formation was observed on increasing the current densities to 15, 25, 50,100 and 150 mA cm^{-2}.

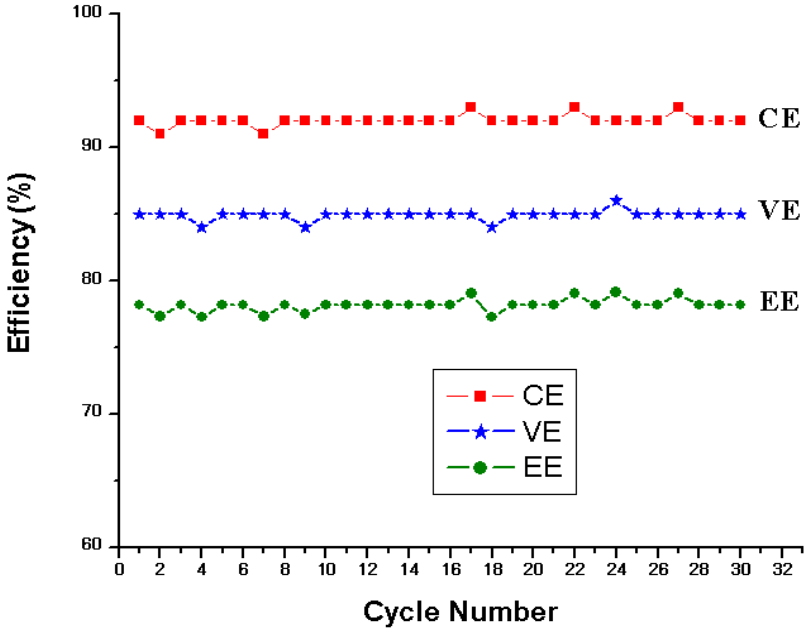

Fig. 36 Efficiency of the cell with 1 M $ZnCl_2$ under the current density of 25 mA cm^{-2}.

3.3.4 SEM Analysis

Fig. 37 shows the SEM images of surface and cross-section of the anion exchange membrane prepared. The smooth and uniform surface of the membrane indicated its dense nature, which was further confirmed by a cross-section image.

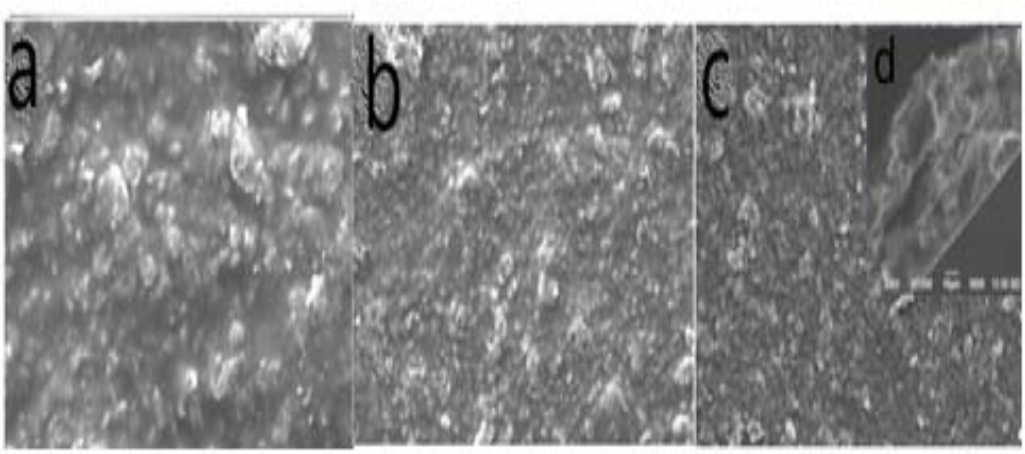

Fig. 37 (a-c) shows the SEM images of the membrane and (d) cross-sectional image of membrane.

The deposition of a uniform, thick zinc layer onto an inert current collector has become a necessity in all zinc-based redox flow batteries. Fig. 38 shows SEM micrograph of zinc electrodeposit obtained during the charging phase of the zinc half-cell under a current density of 25 mA cm^{-2}. Visually, all the electrodeposited Zn coatings were homogeneous metallic grey. It is pertinent to note that no dendrite growth occurs on the zinc electrode which was a severe drawback of previously reported zinc based rechargeable batteries. Absence of dendrite growth might be due to the fact that, only the chloride ions shuttles between two electrolyte solutions through AEM and has some influence on preventing the dendrite growth.

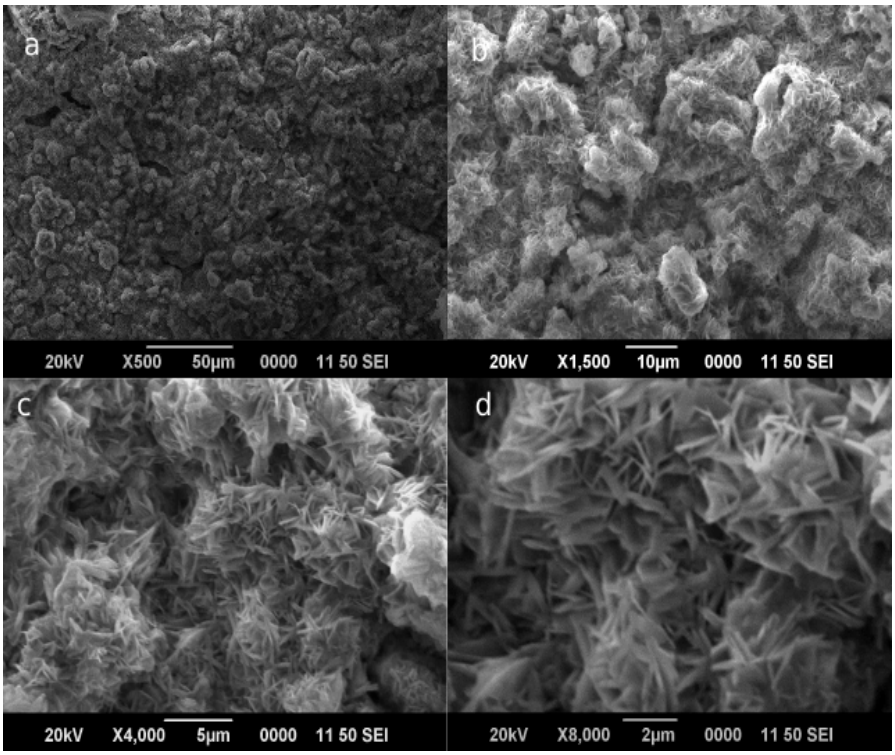

Fig. 38 (a-d) SEM images of zinc deposition at various magnifications.

3.4 Conclusions

In conclusion, the feasibility of a Zn-Fe RFB system utilizing Zn/Zn(II) and Fe(III)/Fe(II) redox couples separated by a self-made anion exchange membrane has been demonstrated. The anion exchange membrane exhibits a thickness of ~120 µm, resistance of 0.5 Ω and hydroxide ion conductivity of around 80 mS^{-1}. Densified graphite sheets were used both as positive and negative electrode current collectors and the performance of the test cell was evaluated with repeated constant-current charge-discharge experiments. The cell delivered an average discharge voltage of ~1.34V at 25 mA cm^{-2}, with a high average coulombic efficiency of 92%, voltage efficiency of 85% and energy efficiency of 78.2% over 30 cycles at 298 K. During charge-discharge cycles, only chloride ions shuttle between anode and cathode

compartments through AEM, which eliminates the issue of cross contamination of electroactive materials and thus increase the performance of the battery. From SEM images, it was clear that the Zn coatings were homogeneous and dendrite-free.

The dependence of cell performance on concentration and current density was also investigated by performing the galvanostatic charge-discharge measurements at different electrolyte concentrations (1 M, 3 M and 5 M) and at different current densities (15, 25 and 50 mA cm^{-2}). The results show that the average discharge voltage decreases from 1.34 to 1.01 V on increasing concentration of $ZnCl_2$ from 1 M to 5 M, while the coulombic efficiency (CE) remains nearly constant (90-92%). Higher coulombic efficiency confirms negligible hydrogen evolution side reaction and high anion selectivity of AEM. The energy efficiency values, however, decrease from 78.2 to 53.46% with increase in electrolyte concentration and this is mainly due to the decreasing voltage efficiency arising from the increased electrolyte resistance. On increasing the current densities to 15 to 50 mA cm^{-2} the coulombic efficiency remained almost same (90-92%). However, voltage efficiency decreased from ~ 90% to 74% and energy efficiency decreased from ~81% to 68%. The results show that the operating conditions are crucial impact factors for the cell performance and the Zn-Fe RFB can exhibit good performance at low concentration (1 M) and at low current density (15 mA cm^{-2}). Thus, we have successfully demonstrated the working of a high efficiency and stable Zn-Fe hybrid redox flow battery with no dendrite growth during zinc deposition by optimizing charge-discharge conditions and employing an anion exchange membrane as separator.

3.5 References

[1] M. Bartolozzi, Development of redox flow batteries. a historical bibliography, J. Power Sources. 27 (1989) 219–234. doi:org/10.1016/0378-7753(89)80037-0.

[2] J. Noack, N. Roznyatovskaya, T. Herr, P. Fischer, The Chemistry of Redox-Flow Batteries Angewandte, 54 (2015) 9776–9809. doi:10.1002/anie.201410823.

[3] M. Skyllas-kazacos, G. Kazacos, G. Poon, H. Verseema, Recent advances with UNSW vanadium-based redox flow batteries, Int. J. Energy Res. 34 (2010) 182–189. doi:10.1002/er.1658.

[4] P. Leung, X. Li, P. De Leo, L. Berlouis, C.T. John, F.C. Walsh, Progress in redox flow batteries, remaining challenges and their applications in energy storage, RSC Adv. 2 (2012) 10125–10156. doi:10.1039/c2ra21342g.

[5] G.L. Soloveichik, Flow Batteries : Current Status and Trends, Chem. Rev. 115 (2014) 11533–11558. doi:10.1021/cr500720t.

[6] T. Van Nguyen, R.F. Savinell, Flow Batteries, Electrochem. Soc. Interface. 19 (2010) 54–56. doi:10.1021/ac200156s.

[7] R. Chen, S. Kim, Z.Chang, Redox Flow Flow Batteries : Fundamentals and Applications, in: Redox-Principles Adv. Appl., (2017) 103–118. doi:10.5772/intechopen.68752.

[8] C.P. De Le, F.C. Walsh, Redox flow cells for energy conversion, J. Power Sources. 160 (2006) 716–732. doi:10.1016/j.jpowsour.2006.02.095.

[9] T. Shigematsu, Recent Development Trends of Redox Flow Batteries, SEI Tech. Rev. (2019) 5–11. https://sumitomoelectric.com.

[10] C. Zhang, L. Zhang, Progress and prospects of next-generation redox flow batteries, Energy Storage Mater. 15 (2018) 324–350. doi:10.1016/j.ensm.2018.06.008.

[11] L.J. Small, J.E. Soc, L.J. Small, H.D.P. Iii, T.M. Anderson, Crossover in Membranes for Aqueous Soluble Organic Redox Flow Batteries, J. Electrochem. Soc. 166 (2019) A2436–A2542. doi:10.1149/2.0681912jes.

[12] H. Prifti, A. Parasuraman, S. Winardi, T.M. Lim, M. Skyllas-kazacos, Membranes for Redox Flow Battery Applications, Membranes (Basel). 2 (2012) 275–306. doi:10.3390/membranes2020275.

[13] A.Z. Weber, M.M. Mench, J.P. Meyers, P.N. Ross, J.T. Gostick, Q. Liu, Redox flow batteries: A review, J. Appl. Electrochem. 41 (2011) 1137–1164. doi:10.1007/s10800-011-0348-2.

[14] X. Li, C.P. De Le, Zinc-based flow batteries for medium and large-scale energy storage, (2015). doi:10.1016/B978-1-78242-013-2.00008-X.

[15] S. Selverston, R.F. Savinell, J.S. Wainright, Zinc-Iron Flow Batteries with Common Electrolyte, J. Electrochem. Soc. 164 (2017) 1069–1075. doi:10.1149/2.0591706jes.

[16] L.F. Arenas, A. Loh, D.P. Trudgeon, X. Li, C. Ponce, D. León, F.C. Walsh, The characteristics and performance of hybrid redox flow batteries with zinc negative electrodes for energy storage, Renew. Sustain. Energy Rev. 90 (2018) 992–1016. doi:10.1016/j.rser.2018.03.016.

[17] K. Gong, X. Ma, K.M. Conforti, K.J. Kuttler, J.B. Grunewald, K.L. Yeager, M.Z. Bazant, S. Gu, Y. Yan, A zinc–iron redox-flow battery under $100 per kW h of system capital cost, Energy Environ. Sci. 8 (2015) 2941–2945. doi:10.1039/C5EE02315G.

[18] Z. Xie, Q. Su, A. Shi, B. Yang, B. Liu, J. Chen, X. Zhou, High performance of zinc-ferrum redox flow battery with Ac − / HAc buffer solution, J. Energy Chem. 0 (2016) 1–5. doi:10.1016/j.jechem.2016.02.009.

[19] X. Zhou, L. Lin, L. Yunhui, X. Zhang, L. Fan, Q. Wu, Elucidating effects of component materials and flow fields on Sn–Fe hybrid flow battery performance, J. Power Sources. 450 (2020) 227613, 1-9. doi:10.1016/j.jpowsour.2019.227613.

[20] X. Zhou, L. Lin, L. Yunhui, X. Zhang, Q. Wu, A Sn-Fe flow battery with excellent rate and cycle performance, J. Power Sources. 404 (2018) 89–95. doi:10.1016/j.jpowsour.2018.10.011.

[21] B. Li, Z. Nie, M. Vijayakumar, G. Li, J. Liu, V. Sprenkle, W. Wang, Ambipolar zinc-polyiodide electrolyte for a high-energy density aqueous redox flow battery, Nat. Commun. 6 (2015) 1–8. doi:10.1038/ncomms7303.

[22] C. Xie, H. Zhang, X. Li, Zinc dendrites Inhibition for Zinc-based Battery, ChemSusChem. 11 (2018) 1-12. doi:10.1002/cssc.201801657.

[23] K. Wang, P. Pei, Z. Ma, H. Chen, H. Xu, D. Chen, X. Wang, Dendrite growth in the recharging process of zinc–air batteries, J. Mater. Chem. A. (2015), 1-8. doi:10.1039/C5TA06366C.

[24] L. Guo, H. Guo, H. Huang, S. Tao, Y. Cheng, Inhibition of Zinc Dendrites in Zinc-Based Flow Batteries, Front. Chem. 8 (2020) 1–8. doi:10.3389/fchem.2020.00557.

[25] C. Li, X. Zhang, W. He, G. Xu, R. Sun, Cathode materials for rechargeable zinc-ion batteries : From synthesis to mechanism and applications, J. Power Sources. 449 (2020) 227596, 1-18. doi:10.1016/j.jpowsour.2019.227596.

[26] Y. Cheng, Q. Lai, X. Li, X. Xi, Q. Zheng, Zinc-nickel single flow batteries with improved cycling stability by eliminating zinc accumulation on the negative electrode, Electrochimica Acta, 145 (2014) 109–111. org/10.1016/j.electacta.2014.08.090

[27] Q. Li, Dendrites issues and advances in Zn anode for aqueous rechargeable Zn-based batteries, (2020) 1–14. doi:10.1002/eom2.12035.

[28] A.K. Manohar, K.M. Kim, E. Plichta, M. Hendrickson, S. Rawlings, S.R. Narayanan, A High Efficiency Iron-Chloride Redox Flow Battery for Large-Scale Energy Storage, J. Electrochem. Soc. 163 (2016) A5118–A5125. doi:10.1149/2.0161601jes.

[29] F.C. Walsh, P. De Løon, L. Berlouis, G. Nikiforidis, The Development of Zn-Ce Hybrid Redox Flow Batteries for Energy Storage and Their Continuing Challenges, Chempluschem. (2014) 1–25. doi:10.1002/cplu.201402103.

[30] Z. Yuan, X. Liu, W. Xu, Y. Duan, H. Zhang, X. Li, Negatively charged nanoporous membrane for a dendrite-free alkaline zinc-based flow battery with long cycle life, Nat. Commun. 9 (2018) 1–11. doi:10.1038/s41467-018-06209-x.

[31] B. Lee, S. Cui, X. Xing, H. Liu, V. Petrova, H. Lim, R. Chen, P. Liu, Energy , Environmental, and Catalysis Applications Dendrite Suppression Membranes for Rechargeable Zinc Batteries Dendrite Suppression Membranes for Rechargeable Zinc Batteries, (2018), 1-25. doi:10.1021/acsami.8b14022.

[32] X. Hao, J. Hu, Z. Zhang, Y. Luo, H. Hou, G. Zou, X. Ji, Interfacial regulation of dendrite-free zinc anodes through a dynamic hydrophobic molecular, (2021) 14265–14269. doi:10.1039/d1ta01697k.

[33] R. Lu, A. Yang, Y. Xue, L. Xu, C. Zhu, Analysis of the key factors affecting the energy efficiency of batteries in electric vehicle, World Electr. Veh. J. 4 (2010) 9–13. ISSN 2032-6653.

CHAPTER 4

Improvement in the Performance of Fe/Fe^{2+} Electrode in an All-Iron Redox Flow Battery by the addition of Zn^{2+} ions

4.1 Introduction

The imperfect ionic selectivity of existing ion-exchange membranes used as separators in redox flow batteries (RFBs) leads to the crossover of reactants between negative and positive electrolytes and cause permanent losses in both battery capacity and coulombic efficiency (CE). The electrolyte contamination associated with the crossover problem can be mitigated to a certain extent by using two redox couples of the same metal as both negative and positive electrolytes. The RFBs having same redox-active elements at different valence states are all-vanadium (all-V) [1,2], all-chromium (all-Cr) [3], all-lead (all-Pb) [4–6], all-copper (all-Cu) [7,8], all-iron (all-Fe) [9–11], etc. All-iron RFBs, in particular, have benefits such as low chemical toxicity and low material cost [12]. The first all-Fe RFB reported in 1981 by L.W. Hruska and R. Savinell consists of Fe/Fe(II) and Fe(II)/Fe(III) redox pairs, in negative electrolyte and positive electrolytes separated by commercially available anion exchange membranes [12,13]. The cell had a round trip current efficiency of 90%, energy efficiency of 50% and a power density of 50 mW/cm^2. The largest voltage losses were found to occur at the Fe/Fe^{2+} electrode. The major technical challenges that slowed down the successful commercialization of all-iron redox flow batteries were low charging efficiency of the negative electrode, self-discharge by electrolyte

cross-over through the membrane and poor cycle-life. The low charging efficiency of the negative electrode is mainly due to the hydrogen evolution reaction (HER) [14]. The standard redox potential of Fe^{2+}/Fe is 440 mV more negative than that of hydrogen evolution reaction at pH = 0 and HER creates a serious challenge to all-iron RFB [12,15].

$$Fe^{2+} + 2e^{-} \rightleftharpoons Fe \qquad E^0 = -0.44\ V \quad \ldots\ldots (4.1)$$

Hydrogen evolution that occurs during charging can be represented as

$$2H^{+} + 2e^{-} \rightleftharpoons H_2 \qquad E^0 = 0.0\ V \quad \ldots\ldots (4.2)$$

Suppression of hydrogen evolution is essential for the better performance of all-iron systems. Several methods have been attempted by researchers for solving the hydrogen evolution reaction at the negative electrode like pH control, co-deposition of secondary metals and increasing the overpotential for hydrogen evolution by electrolyte additives. Metals such as platinum and nickel facilitate hydrogen evolution because of the improved chemisorption of hydrogen due to the partially filled d-bands of the metal. In contrast, elements like cadmium, zinc, lead, bismuth and mercury with filled d-bands do not support hydrogen evolution readily [16,17]. The second metal will continue to restrict hydrogen evolution by remaining on the surface throughout the electrodeposition process [18,19]. The zinc metal has a higher hydrogen evolution overpotential than iron [20,21] and alloying iron with a small amount of zinc inhibits the hydrogen evolution at the Fe/Fe(II) electrode.

In the present work, we studied the performance of an all-iron redox flow battery containing Fe/Fe(II) and Fe(III)/Fe(II) redox couples in the negative and positive half-cells separated by a self-made anion exchange membrane [22]. The

details of the membrane were given in chapter 3. The charge-discharge performance of the cell was evaluated at a constant current density of 25 mA cm^{-2}. We also studied the influence of adding 0.03 M $ZnCl_2$ in the anode compartment, on the electrode performance of the Fe/Fe(II) redox couple. The anion exchange membrane, being permeable to only negative ions, allows the transfer of chloride ions between the positive and negative sides of the cell and thus the self-discharge resulting from the transfer of Fe(III) ions across the membrane could be avoided. A schematic diagram of the operation of the battery system is shown in Fig. 39.

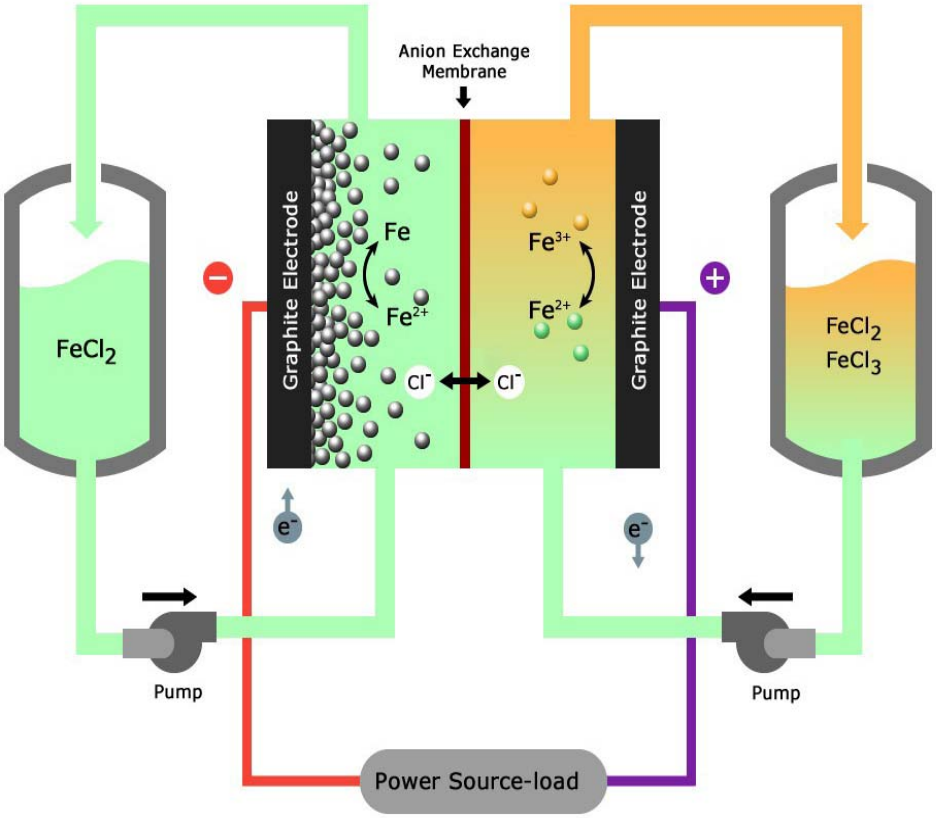

Fig. 39 Schematic of an all-Fe RFB.

The working principle that the all-Fe RFB stores and releases electricity can be expressed as follows [23]: During charging:

At negative electrode: $Fe^{2+} + 2e^- \rightleftharpoons Fe$ $E^0 = -0.44$ V …… (4.3)

At positive electrode: $2Fe^{2+} \rightleftharpoons 2Fe^{3+} + 2e^-$ $E^0 = 0.77$ V ..… (4.4)

Overall reaction: $3Fe^{2+} \rightleftharpoons 2Fe^{3+} + Fe$ $E^0_{cell} = 1.21$ V …… (4.5)

During the charging process, the Fe(II) ions at the positive electrode release the electrons and get oxidized as Fe(III) ions. At the same time, the Fe(II) ions at the negative electrode acquire these electrons and get electrodeposited as metallic Fe. To maintain charge neutrality, chloride ions move from the negative electrolyte to the positive electrolyte, through the anion exchange membrane. These processes are reversed during battery discharging.

4.2 Experimental

4.2.1 Chemicals

Iron(II) chloride tetrahydrate ($FeCl_2.\ 4H_2O$), iron(III) chloride anhydrous ($FeCl_3$), ammonium chloride (NH_4Cl) and zinc chloride ($ZnCl_2$) were obtained from Merck India.

4.2.2 Electrolyte preparation

All the electrolytes are prepared using deionized water.

(i) Preparation of negative electrolyte solution without zinc additive

The negative electrolyte consists of 1 M Fe(II) chloride and 2 M NH_4Cl.

(ii) Preparation of negative electrolyte solution with zinc additive

The negative electrolyte consists of 1 M $FeCl_2$, 0.03 M $ZnCl_2$ and 2 M NH_4Cl.

(iii) Preparation of positive electrolyte solution

The positive electrolyte consists of 0.5 M of $FeCl_2$, 0.5 M of $FeCl_3$ and 2 M NH_4Cl. The NH_4Cl was added as a supporting electrolyte to eliminate the IR drop by increasing the solution conductivity and suppressing the migration current.

4.2.3 Cyclic voltammetry

CV analysis was performed by employing the same working, counter and reference electrodes as indicated in chapter 3 section 3.2.4 and Fig. 40 depicts the schematic representation of a three-electrode cell. The solutions used for CV consists of 1 M $FeCl_2$ in 2 M NH_4Cl and a mixture of 1 M $FeCl_2$ and 0.03 M $ZnCl_2$ in 2 M NH_4Cl.

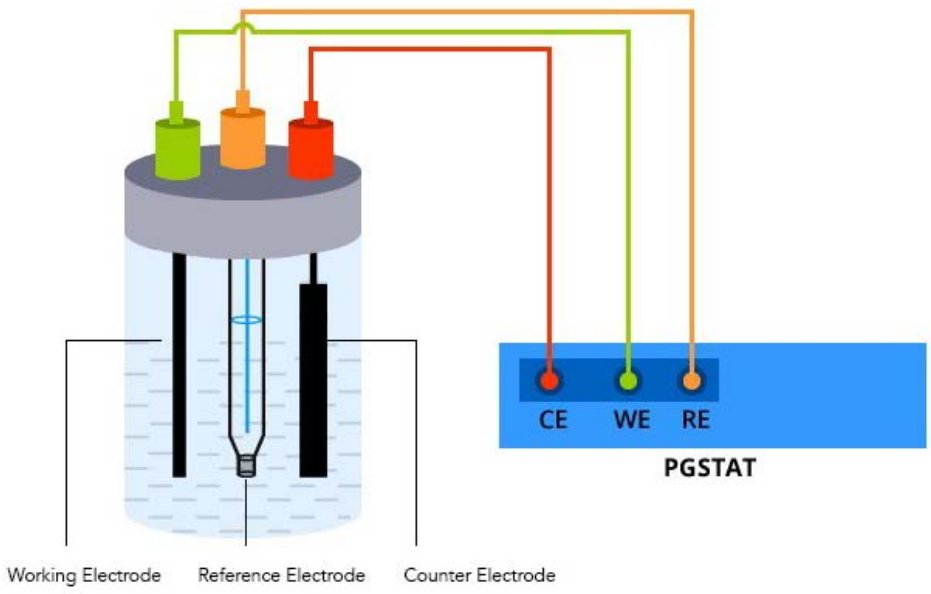

Fig. 40 The electrochemical set-up of a three-electrode cell.

4.2.4 Battery performance

The performances of the two all-iron redox flow cells (A & B) were evaluated with constant-current charge-discharge measurements. Compositions of the two cells are as follows:

(i) Cell A (without $ZnCl_2$): The negative electrolyte consisting of 1 M Fe(II) chloride and 2 M NH_4Cl and a positive electrolyte consisting of 0.5 M Fe(II) chloride, 0.5 M Fe(III) chloride and 2 M NH_4Cl.

(ii) Cell B (with $ZnCl_2$): The negative electrolyte consisting of 1 M Fe(II) chloride, 0.03 M $ZnCl_2$ and 2 M NH_4Cl and positive electrolyte consisting 0.5 M Fe(II) chloride, 0.5 M Fe(III) chloride and 2 M NH_4Cl.

The electrochemical cell set-up for charge-discharge measurement is same as described in chapter 3 section 3.2.5 and Fig. 41 shows the schematic representation of the standard two-electrode configuration used for the study. The effect of $ZnCl_2$ additive on the potential of negative electrode during cell charging and discharging was measured using a three-electrode configuration. For this setup, the Fe/Fe^{2+}, Ag/AgCl and Fe^{3+}/Fe^{2+} electrodes were used as working, reference and counter electrodes respectively.

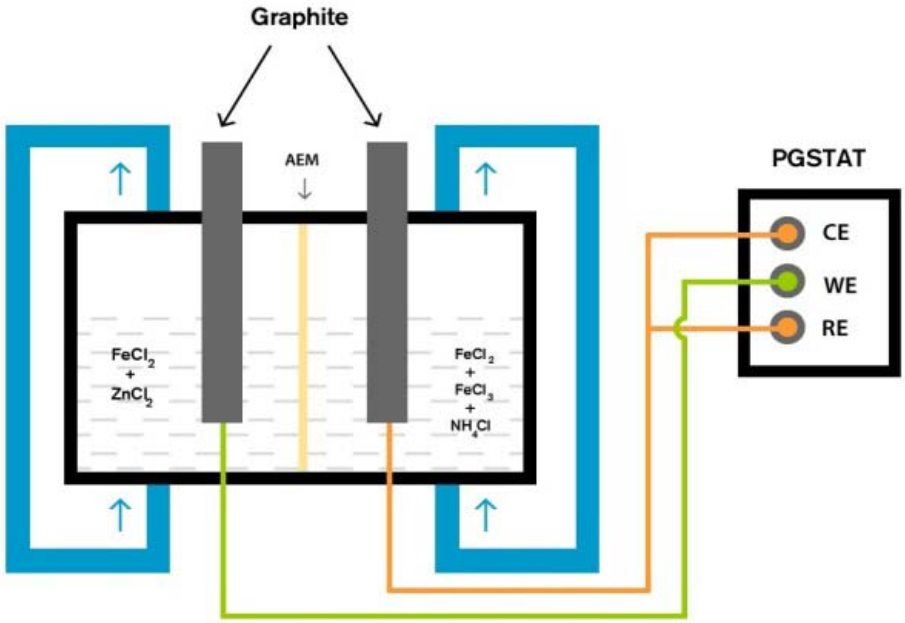

Fig. 41 The standard two-electrode setup for charge-discharge measurements.

The charging and discharging of the cells were carried out at a current density of ± 25 mA cm^{-2}. Battery charging is carried out for 1800 seconds followed by the stripping of iron deposit until the discharge voltage reaches a cut-off 0.6 V. The coulombic efficiency (CE), voltage efficiency (VE) and energy efficiency (EE) of the cells were also calculated.

4.3 Results and discussion

4.3.1 Cyclic voltammograms

Fig. 42 shows the cyclic voltammogram of 1 M $FeCl_2$ and 2 M NH_4Cl at the scan rate of 50 mV s^{-1}. A cathodic peak at −0.98 V is due to the electrodeposition of Fe and the anodic peak at −0.26 V could be ascribed to the anodic dissolution of the

deposited iron. Robert F. Savinell et al. reported that the peak corresponding to the reduction and oxidation of iron species in the CV of an electrolyte containing $FeCl_2$ and NH_4Cl are at −0.96 V and −0.63 V [24]. Fig. 43 shows the cyclic voltammogram of a mixture of 1 M $FeCl_2$ and 0.03 M $ZnCl_2$ in 2 M NH_4Cl. The CV for the Zn-Fe mixture exhibited two cathodic and anodic peaks. The first cathodic peak at −1.14 V is due to the electrodeposition of iron and the second cathodic peak at −1.23 V is due to the electrodeposition of zinc. The first and second anodic peaks were observed at potential values of −0.65 V and −0.5 V, respectively, which may be attributable to the dissolution of zinc and the dissolution of iron from the deposit. From the figure, it is observed that, in the presence of Zn^{2+}, the cathodic potential for iron deposition is shifted to more negative values in the forward scan. Thus it is confirmed that, in presence of Zn^{2+}, the iron deposition occurs at more negative potential. CVs at 1 M concentration were found to be very similar with low concentration CVs.

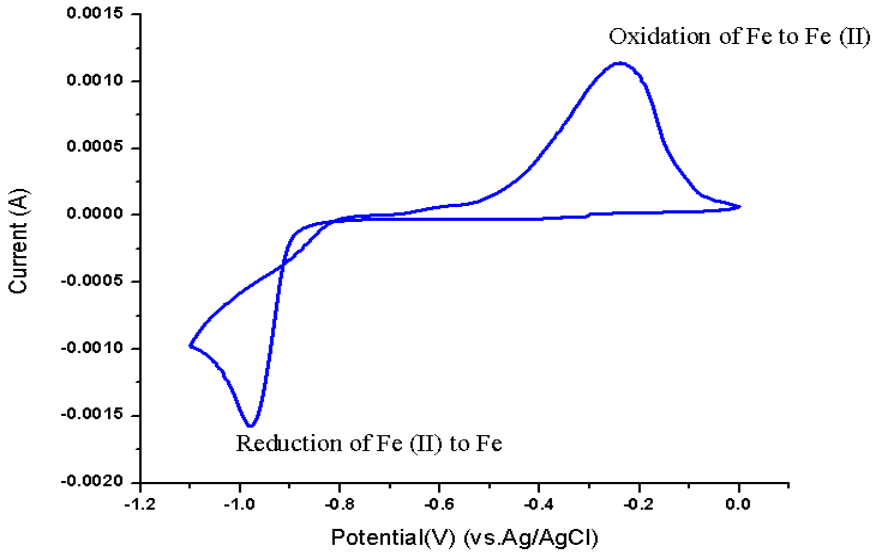

Fig. **42** Cyclic voltammogram of 1 M $FeCl_2$ and 2 M NH_4Cl at the scan rate of 50 mV s^{-1}.

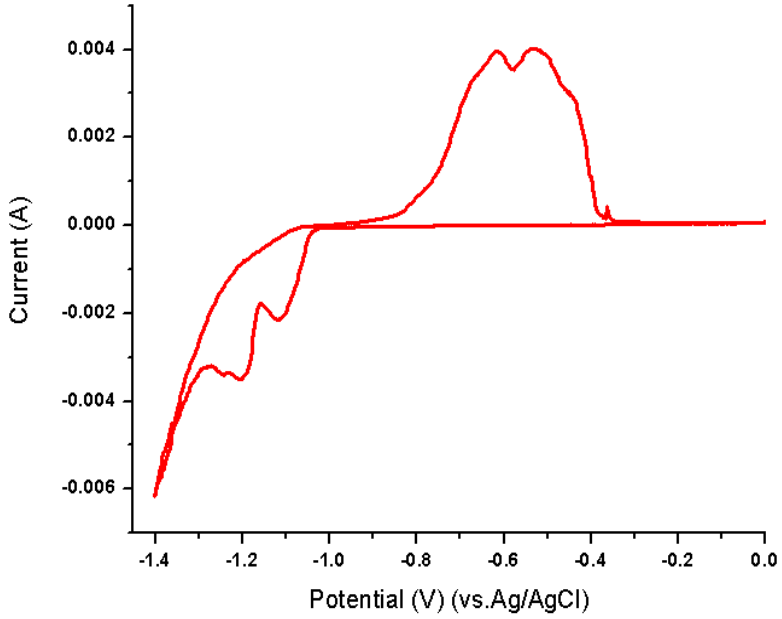

Fig. **43** Cyclic voltammogram of 1 M $FeCl_2$ and 0.03 M $ZnCl_2$ in 2 M NH_4Cl at the scan rate of 50 mV s^{-1}.

4.3.2 Charge-discharge cycle performance

The performances of the two all-Fe redox flow cells (A & B) were evaluated with constant-current charge-discharge measurements. During charging, the ferrous (Fe^{2+}) ion gains electrons and plates as solid iron on the graphite sheet. During discharge, the iron dissolves as ferrous ions and releases two electrons. The equilibrium potential for the iron deposition reaction is −0.44V. On the positive electrode, two Fe^{2+} ions lose two electrons to form Fe^{3+} ions during charge and two Fe^{3+} ions gain two electrons to form Fe^{2+} during discharge. Thus, both the reactions in the negative and positive electrodes in an all-iron redox flow battery are reversible. The equilibrium potential for Fe^{2+}/Fe^{3+} couple is +0.77 V. Fig. 44 and Fig. 45

represent the characteristic charge-discharge curves of the above two cells for 30 repeated cycles.

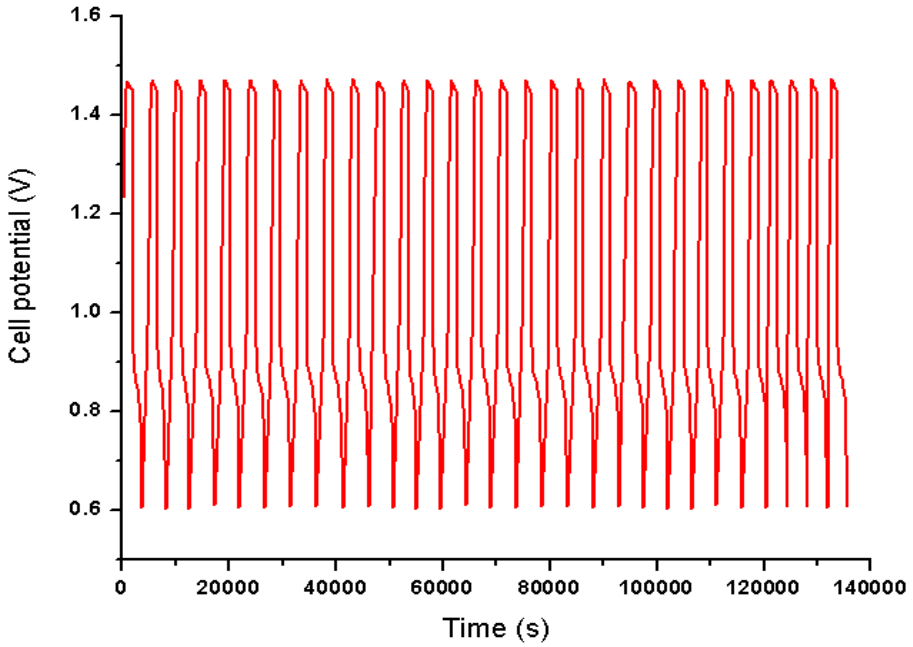

Fig. 44 Cell potential vs. time response for 30 cycles of cell A at 25 mA cm^{-2}.

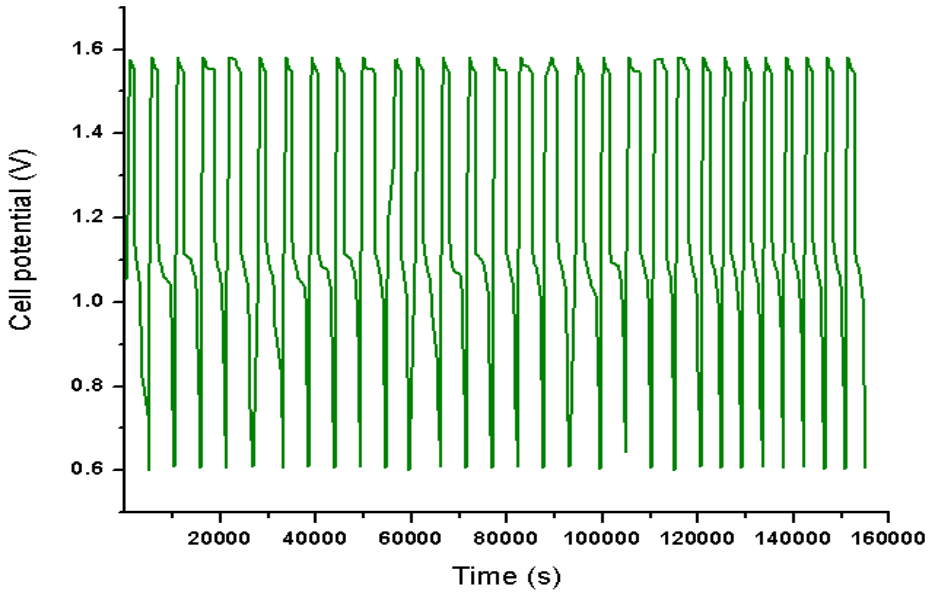

Fig. 45 Cell potential vs. time response for 30 cycles of cell B at 25 mA cm^{-2}.

The potential vs. time curves of the negative electrode was measured during cell charging and discharging using a negative electrolyte without and with $ZnCl_2$ additive is shown in Fig. 46 and Fig. 47 and the results obtained are tabulated in table 6. Comparing the overvoltage of cell A (without $ZnCl_2$) with the overvoltage required at the negative electrode during charging, it can be seen that 68.75% of the overvoltage of the cell is for charging of the negative electrode. For the same cell, a comparison of the voltage losses of the cell with that of the negative electrode during discharge shows that 88.09% of the voltage loss occurs at the negative electrode. For cell B (with $ZnCl_2$) the corresponding values during charging and discharging shift to 55.2% and 73.27%, respectively. Thus, the overvoltage of the negative electrode for charging is decreased by 13.55% and voltage loss during discharge is decreased by 14.82% by the addition of $ZnCl_2$.

Fig. 48 shows the 15^{th} charge-discharge curves with and without 0.03 M $ZnCl_2$ at 25 mA cm^{-2}. Without $ZnCl_2$, a relatively flat voltage profile for charge and discharge processes are observed and the plot shows an average charge voltage of 1.45 V and discharge voltage of 0.9 V. With 0.03 M $ZnCl_2$, the curves are identical in shape but the average charge and discharge voltages shifts to 1.55 V and 1.1 V approximately. The cell potential of the all-Fe redox flow cells with and without $ZnCl_2$ during charging and discharging are influenced by a number of factors particularly the activation and concentration polarization of the positive and negative electrodes along with the ohmic drop (IR).

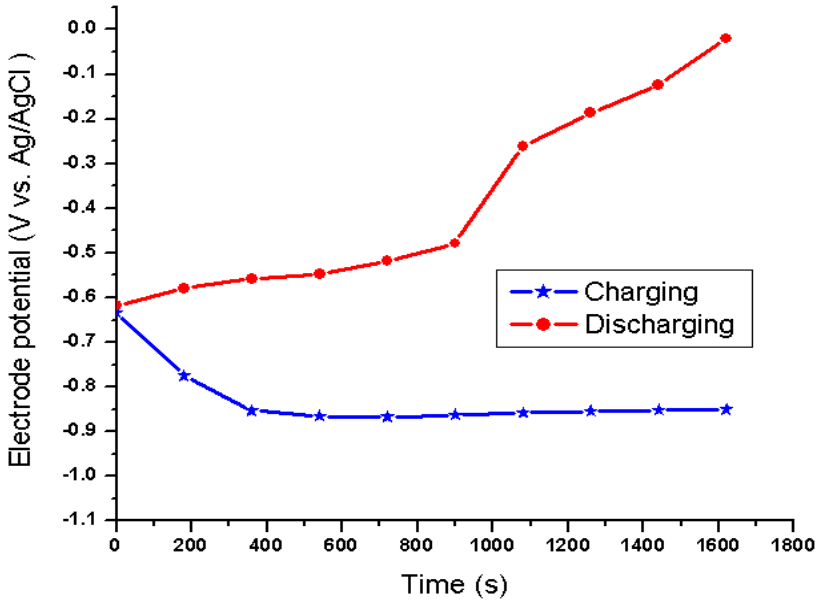

Fig. 46 Potential vs. time curves measured during the cell charging and discharging without $ZnCl_2$ additive in the negative electrolyte.

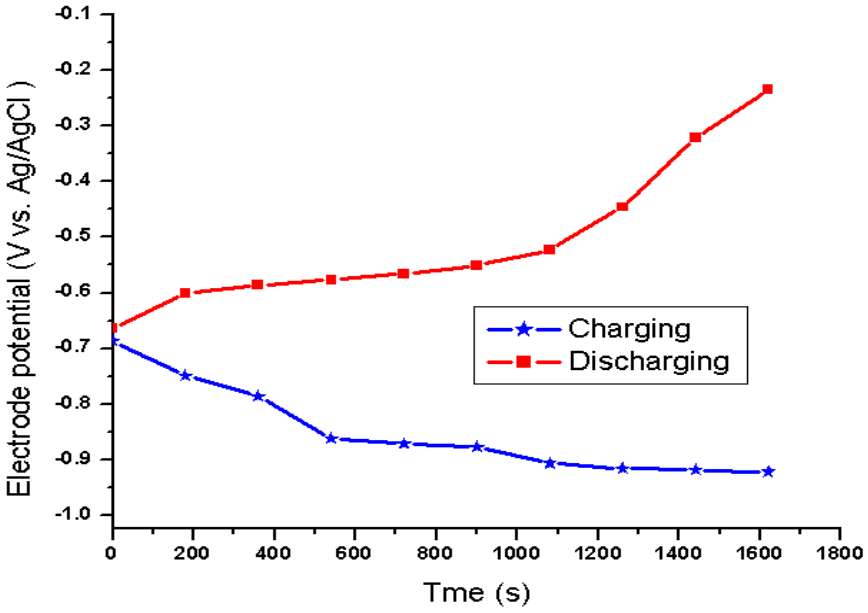

Fig. 47 Potential vs. time curves measured during the cell charging and discharging with $ZnCl_2$ additive in the negative electrolyte.

Table 6 Comparison of the overvoltage and voltage loss of the cell without and with $ZnCl_2$.

Charging				
Electrolyte in the anode compartment	**Overvoltage of negative electrode**	**Overvoltage of positive electrode**	**Total over voltage for charging**	**Percentage overvoltage of the negative electrode**
1 M $FeCl_2$ + 2 M NH_4Cl	0.165	0.075	0.24	68.75%
1 M $FeCl_2$ + 2 M NH_4Cl + 0.03 M $ZnCl_2$	0.1877	0.1523	0.34	55.2%
Discharging				
Electrolyte in the anode compartment	**Voltage loss at the negative electrode**	**Voltage loss at the positive electrode**	**Total voltage loss of the cell**	**Percentage voltage loss at the negative electrode**
1 M $FeCl_2$ + 2 M NH_4Cl	0.2731	0.0369	0.31	88.09%
1 M $FeCl_2$ + 2 M NH_4Cl+ 0.03 M $ZnCl_2$	0.0806	0.0294	0.11	73.27%

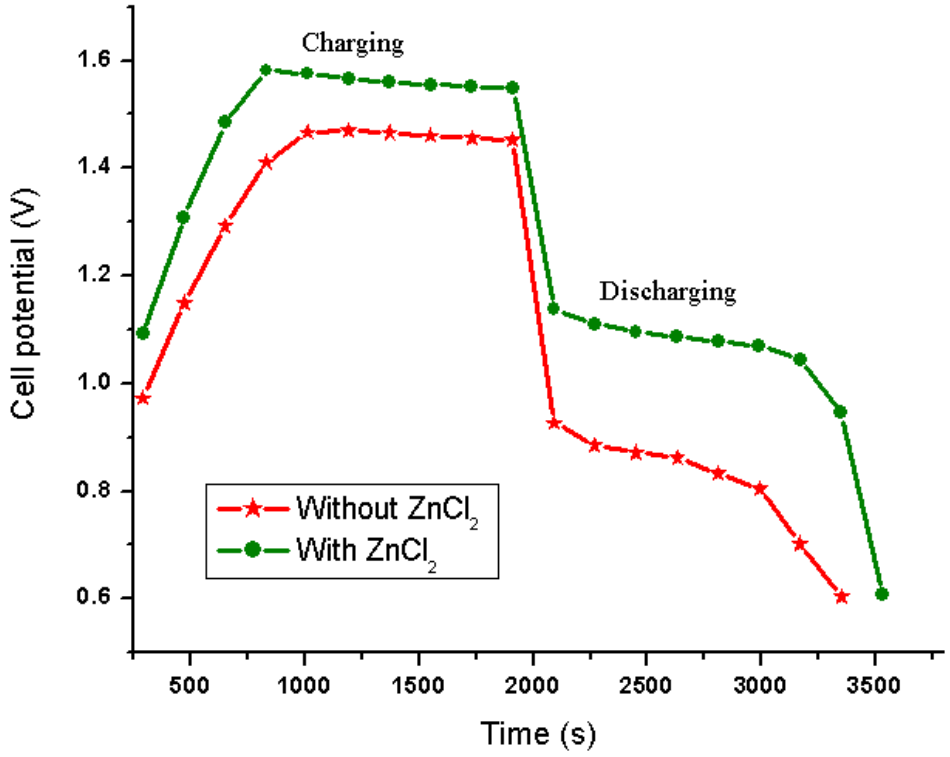

Fig. 48 Cell potential vs. time response for 15th charge-discharge cycle of cells A and B at 25 mA cm^{-2}.

The CE, EE and VE data obtained from the charge-discharge curves shown in Fig. 44 and 45 are plotted in Fig. 49 and listed in Table 7. The CE, VE and EE of the cell without $ZnCl_2$ are 80%, 62.06% and 49.64%, respectively. On adding $ZnCl_2$ these values increase to 90%, 70.96% and 63.86%, respectively. It is evident from Fig. 48 and table 7 that for the cell B containing $ZnCl_2$, there is an improvement of 0.2 V in the average cell voltage during discharge compared to that of the cell without $ZnCl_2$. However, there is an increase of 0.1 V in the charge voltage after the addition of $ZnCl_2$. Overall, there is a net gain of 0.1 V after the addition of $ZnCl_2$ leading to higher voltage efficiency for the cell B.

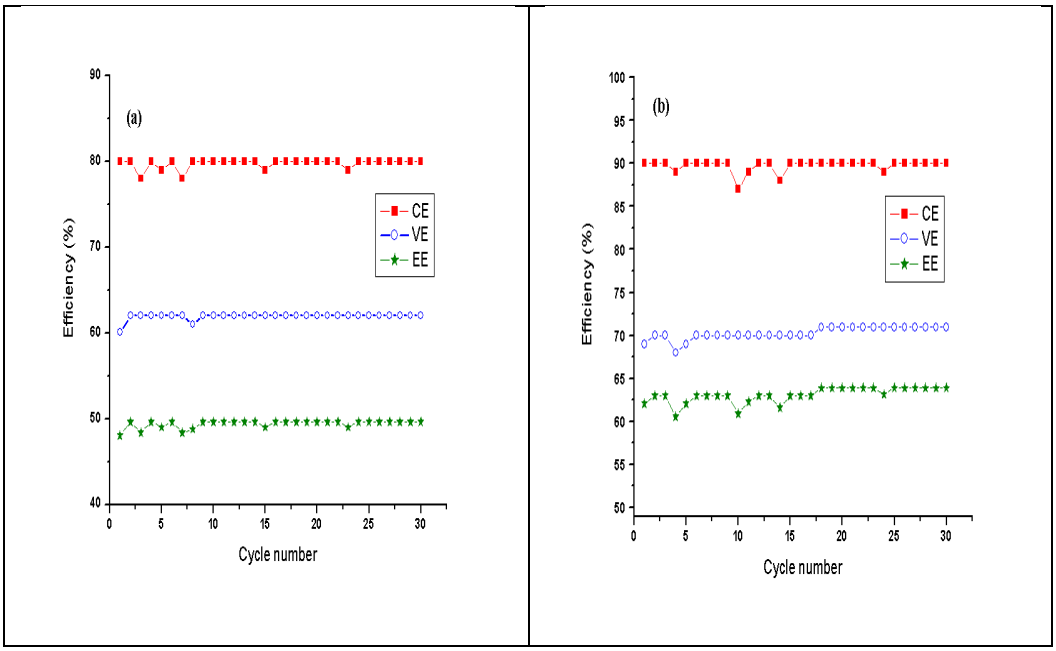

Fig. 49 Efficiencies of the all-Fe cell (a) without $ZnCl_2$ and (b) with 0.03 M $ZnCl_2$ under a current density of 25 mA cm^{-2}.

Table 7 Summary of the performance of two cells obtained at 25 mA cm^{-2}

The electrolyte in the anode compartment	OCV (V)	Avg. charge voltage (V)	Avg. discharge voltage (V)	CE (%)	VE (%)	EE (%)
1 M $FeCl_2$ + 2 M NH_4Cl	1.13	1.45	0.9	80	62.06	49.64
1 M $FeCl_2$ + 2 M NH_4Cl + 0.03 M $ZnCl_2$	1.27	1.55	1.1	90	70.96	63.86

The results show that the addition of small amounts of zinc with iron has a suppressing effect on the hydrogen evolution reaction and then leads to an increase in the CE of the cell. Since the reduction potential of Zn/Zn^{2+} at a Zn^{2+} concentration of 0.03 M is too low (~−0.85 V), the chance of co-deposition of zinc along with iron during charging can be neglected. Hence the reason for the improved performance of the cell after adding zinc ions may be explained as follows. When hydrogen is evolved at the negative electrode by the reduction of H^+ ions, the hydroxide ions left in the vicinity of the iron electrode combine with Zn^{2+} ions forming $Zn(OH)_2$. This $Zn(OH)_2$ layer on the iron electrode inhibits further hydrogen evolution [25]. Thus the addition of zinc ions in the negative electrolyte helps to increase the coulombic efficiency from 80% to 90% and has a beneficial effect on the overall performance of an all-iron flow battery.

4.4 Conclusions

In this work, the electrochemical performance of an all-iron redox flow battery with Fe/Fe(II) and Fe(III)/Fe(II) redox couples were studied. The densified graphite sheets were used both as positive and negative electrode current collectors and the two electrolyte solutions were separated by a self-made anion exchange membrane. The electrochemical performance of the cell was measured by conducting charge-discharge experiments at a constant current density of 25 mA cm^{-2}. The performance was also studied with the addition of 0.03 M $ZnCl_2$. The results show that the cell with 0.03 M $ZnCl_2$ as additive delivered a higher average discharge voltage of ~1.1 V compared to the cell without $ZnCl_2$ (~0.9 V). The CE, VE and EE of the cell with 0.03 M $ZnCl_2$ are higher (90%, 70.96% and 63.86%) than that of the cell without $ZnCl_2$ (80%, 62.06% and 49.64%). The overvoltage of the negative

electrode during charging is reduced by 13.55%, while voltage loss during discharge is reduced by 14.82% after the addition of $ZnCl_2$. During charge-discharge cycles, only chloride ions shuttle between anode and cathode compartments through AEM, which eliminates the issue of cross-contamination of electroactive materials and thus increases the coulombic efficiency of the battery. The increase in charging efficiency after the addition of zinc ions may be due to the inhibition of hydrogen evolution reaction by a layer of $Zn(OH)_2$ formed at the iron electrode. The hydroxide ions, formed by the removal of protons at the early stages of hydrogen evolution, combine with Zn^{2+} ions forming $Zn(OH)_2$. This $Zn(OH)_2$ layer on the iron electrode inhibits further hydrogen evolution resulting in an overall improvement in cell performance.

4.5 References

[1] D. Park, K. Jeon, C. Ryu, G. Hwang, Performance of the all-vanadium redox flow battery stack, J. Ind. Eng. Chem. (2016), 1-4. doi:10.1016/j.jiec.2016.10.007.

[2] D.J. Park, K.S. Jeon, C.H. Ryu, G.J. Hwang, Performance of the all-vanadium redox flow battery stack, J. Ind. Eng. Chem. 45 (2017) 387–390. doi:10.1016/j.jiec.2016.10.007.

[3] P. Taylor, C. Bae, E. Pelham, L. Roberts, H. Chakrabarti, M. Saleem, C. Bae, E. Pelham, L. Roberts, M.H. Chakrabarti, M. Saleem, International Journal of Green Energy All-Chromium Redox Flow Battery for Renewable Energy Storage, Int. J. Green Energy. 8 (2011) 37–41. doi:10.1080/15435075.2010.549598.

[4] J. Collins, X. Li, D. Pletcher, R. Tangirala, D. Stratton-campbell, F.C. Walsh, C. Zhang, A novel flow battery:A lead acid battery based on an electrolyte with soluble lead (II). Part IX : Electrode and electrolyte conditioning with hydrogen peroxide, 195 (2010) 2975–2978. doi:10.1016/j.jpowsour.2009.10.109.

[5] C.P. Zhang, S.M. Sharkh, X. Li , F.C. Walsh, C.N. Zhang, J.C. Jiang,The performance of a soluble lead-acid flow battery and its comparison to a static lead-acid battery, Energy Convers. Manag. 52 (2011) 3391–3398. doi:10.1016/j.enconman.2011.07.006.

[6] R. Suman, M.K. Ravikumar, J. Nandini, P. Satish, A.K. Shukla, Extending cycle life of the soluble lead redox flow battery with an auxiliary gas-diffusion electrode : a proof of concept study, Ionics (Kiel). 27 (2021) 3403–3414. doi:10.1007/ s11581-021-04127-5.

[7] S. Schaltin, Y. Li, N.R. Brooks, J. Sniekers, I.F.J. Vankelecom, K. Binnemans, J. Fransaer, Towards an all-copper redox flow battery based on a copper-containing ionic liquid, Chem. Commun. (2015), 1-4. doi:10.1039/C5CC06774J.

[8] L. Sanz, D. Lloyd, E. Magdalena, J. Palma, Description and performance of a novel aqueous all-copper redox flow battery, J. Power Sources J. 268 (2014) 121–128. doi:10.1016/j.jpowsour.2014.06.008.

[9] N. Yensen, P.B. Allen, Open source all-iron battery for renewable energy storage, HardwareX. 6 (2019) e00072, 1-11. doi:10.1016/j.ohx.2019.e00072.

[10] K. Gong, F. Xu, J.B. Grunewald, X. Ma, Y. Zhao, S. Gu, Y. Yan, All-Soluble All-Iron Aqueous Redox-Flow Battery, ACS Energy Lett. (2016) 89–93. doi:10.1021/acsenergylett.6b00049.

[11] M.C. Tucker, A. Phillips, A.Z. Weber, All-Iron Redox Flow Battery Tailored for Off-Grid Portable Applications, (2015) 3996–4004. doi:10.1002/cssc.201500845.

[12] L.W. Hruska, Investigation of Factors Affecting Performance of the Iron-Redox Battery, J. Electrochem. Soc. 128 (1981) 18-25. doi:10.1149/1.2127366.

[13] A. Dinesh, S. Olivera, K. Venkatesh, M. Sridhar, S. Murugesan, G. Priya, Iron‐based flow batteries to store renewable energies, Environ. Chem. Lett. (2018). doi:10.1007/s10311-018-0709-8.

[14] B.S. Jayathilake, E.J. Plichta, M.A. Hendrickson, S.R. Narayanan, Improvements to the Coulombic Efficiency of the Iron Electrode for an All-Iron Redox-Flow Battery, J. Electrochem. Soc. 165 (2018) 1630–1638. doi:10.1149/2.0451809jes.

[15] A.K. Manohar, K.M. Kim, E. Plichta, M. Hendrickson, S. Rawlings, S.R. Narayanan, A High Efficiency Iron-Chloride Redox Flow Battery for Large-Scale Energy Storage, J. Electrochem. Soc. 163 (2016) A5118–A5125. doi:10.1149/2.0161601jes.

[16] B.S. Jayathilake, E.J. Plichta, M.A. Hendrickson, S.R. Narayanan, Improvements to the Coulombic Efficiency of the Iron Electrode for an All-Iron Redox-Flow Battery, 165 (2018) 1630–1638. doi:10.1149/2.0451809jes.

[17] D.R. Gabe, The role of hydrogen in metal electrodeposition processes, J. Appl. Electrochem. 27 (1997) 908–915. doi:org/10.1023/A:1018497401365.

[18] D.M. Drazic and L.Z. Vorkapic, Inhibitory effects of manganeous, cadmium and zinc ions on hydrogen evolution reaction and corrosion of iron in sulphuric acid solutions, Corros. Sci. 18 (1978) 907–910. doi:10.1016/0010-938X(78)90011-2.

[19] M. Seo, Inhibition effect of underpotential deposition of metallic cations on aqueous corrosion of metals, 36 (2018) 17–33. doi:org/10.1515/corrrev-2017-0041.

[20] J. Shin, J. Lee, Y. Park, J. W. Choi, Aqueous Zinc Ion Batteries: Focus on Zinc Metal Anodes, Chem. Sci. (2020), 1-40. doi:10.1039/D0SC00022A.

[21] N.V. Mandich, pH, Hydrogen Evolution & Their Significance In Electroplating Operations, 89 (2002) 54–58. https://www.nmfrc.org.

[22] C.B. Jeena, P.J. Elsa, P.P. Moly, K.J.Ambily, V.T.Joy, A dendrite free Zn-Fe hybrid redox flow battery for renewable energy storage, Energy Storage. 4 (2022) 1–10. doi:10.1002/est2.275.

[23] J. Noack, M. Berkers, J. Ortner, K. Pinkwart, The Influence of Some Electrolyte Additives on the Electrochemical Performance of Fe/Fe^{2+} Redox Reactions for Iron/Iron Redox Flow Batteries, J. Electrochem. Soc. (2021), 1-10. doi:10.1149/1945-7111/abf5a3.

[24] K.L. Hawthorne, T.J. Petek, M.A. Miller, J.S. Wainright, R.F. Savinell, An Investigation into Factors Affecting the Iron Plating Reaction for an All-Iron Flow Battery, J. Electrochem. Soc. 162 (2015) A108–A113. doi:10.1149/2.0591501jes.

[25] R. Thornhill, Zinc, Manganese, and Chromic Salts as Corrosion, Inhibitors, Ind. Eng. Chem. 37 (1940) 706–708. doi:org/10.1021/ie50428a011.

CHAPTER 5

A Novel Chloride-Based Copper-Cerium Redox Flow Battery for Renewable Energy Storage

5.1 Introduction

Among various redox flow batteries (RFBs), the concept of a cerium based redox flow battery has resulted from the high positive standard potential of the Ce^{3+}/Ce^{4+} pair (between +1.28 and +1.72 V vs. NHE) [1–3]. The zinc-cerium [4,5], cerium-hydrogen [6], vanadium-cerium [7,8] and cerium-lead [9] cells, with a Ce^{3+}/Ce^{4+} pair as the positive electrode active material, have been extensively studied. Na et al. developed a novel cerium-lead redox flow battery that used Ce(IV)/Ce(III) and Pb(II)/Pb redox couples in methanesulfonic acid supporting electrolyte [9]. Lead is a toxic metal and may pollute the environment when the electrolyte is disposed of after usage. Although the methanesulfonic acid increased the solubility of the cerium species, it increases the cost of the flow battery [10]. G. Nikiforidis et al. studied the electrochemical activity of the Ce^{3+}/Ce^{4+} in the presence of various mixed acid electrolytes employing methanesulfonic acid as the base electrolyte along with hydrochloric, nitric and sulfuric acid. The results revealed that methanesulfonic acid (CH_3SO_3H) coupled with hydrochloric acid as the supporting electrolyte had better redox reversibility and reduction current density than pure CH_3SO_3H [11].

The all-copper redox flow batteries are more attractive because of the reason that copper is earth-abundant, non-toxic and cheap. Another advantage of using Cu/Cu^{2+} redox couple is that Cu^{2+} ions are highly soluble in water [12]. In

copper-based redox flow batteries, the hydrogen evolution reaction (HER) is a poor side reaction due to the very high hydrogen overvoltage (~−0.60 V) of metallic copper [13]. As a result, the coulombic efficiency for copper deposition and stripping is almost 100% [14].

In this work, we report a novel chloride-based copper-cerium redox flow battery system that uses a Ce(IV)/Ce(III) redox couple in the positive half-cell and a Cu/Cu(II) redox couple in the negative hall-cell to combine the advantages of both cerium and copper-based redox flow batteries. None of the previous works in copper-cerium RFBs have used chloride-based electrolytes for both half cells. The positive and negative electrolytes were separated by the self-made anion exchange membrane. Preparation of the membrane and its properties has been discussed in chapter 3.

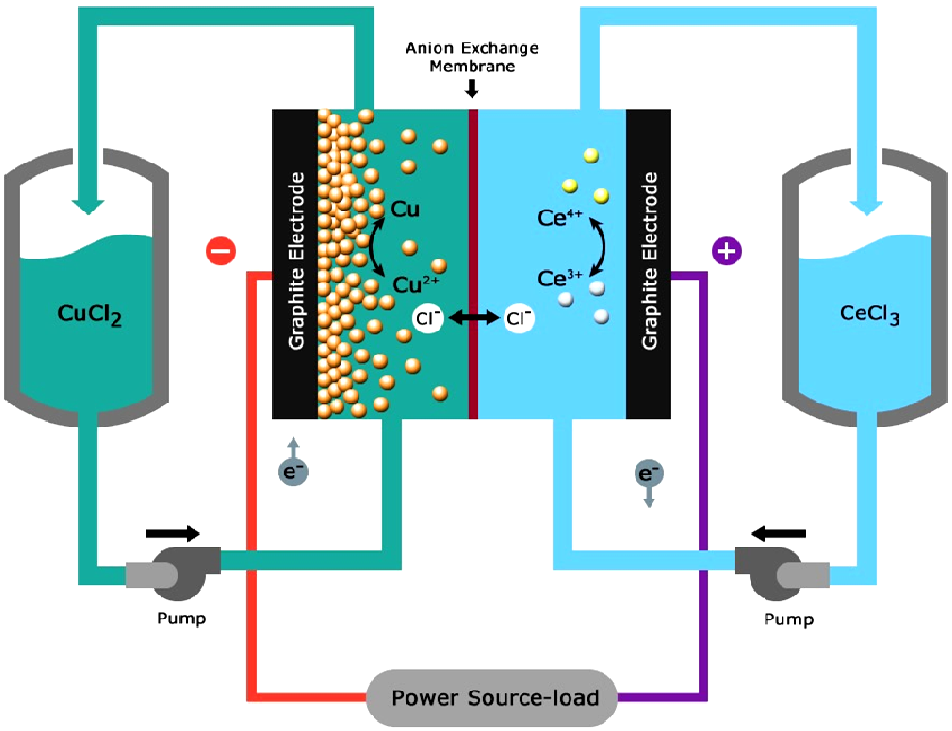

Fig. 50 Schematic representation of the Cu-Ce system.

At the positive electrode of the copper-cerium flow battery, the primary reaction during charging is the oxidation of the Ce(III) to form Ce(IV).

$$Ce^{3+} \rightleftharpoons Ce^{4+} + e^{-} \quad E^0 = 1.28 \text{ V vs. SHE [15]} \quad \ldots\ldots(5.1)$$

For the negative side, the cupric ions (Cu^{2+}) are reduced to copper metal (Cu^0).

$$Cu^{2+} + 2\,e^{-} \rightleftharpoons Cu \qquad E^0 = 0.34 \text{ V} \quad \ldots\ldots. (5.2)$$

The overall reaction of the copper-cerium flow cell is:

$$2Ce^{3+} + Cu^{2+} \rightleftharpoons 2Ce^{4+} + Cu \quad E_{cell} = 0.94 \text{ V} \quad \ldots\ldots. (5.3)$$

The reactions indicate that during the charging process, Cu^{2+} is electrodeposited as Cu at the negative electrode and Ce^{3+} is oxidized to Ce^{4+} at the positive electrode. During the discharge, the above electrochemical reactions are reversed. The theoretical voltage of the copper-cerium redox flow battery is 0.94 V, which is greater than that of the all-copper flow battery (~0.7 V) [16,17]. A schematic diagram of the battery system is shown in Fig. 50.

5.2 Experimental details

5.2.1 Chemicals

Cupric chloride dihydrate ($CuCl_2.\ 2H_2O$) and cerium(III) chloride heptahydrate ($CeCl_3.\ 7H_2O$) were obtained from Sigma Aldrich.

5.2.2 Electrolyte preparation

The positive electrolyte is an aqueous solution of 1 M copper(II) chloride ($CuCl_2$) and the negative electrolyte is an aqueous solution of 1 M cerium(III) chloride ($CeCl_3$).

5.2.3 Cyclic voltammetry

CV analysis was performed for both positive and negative electrolytes at a scan rate of 50 mV s^{-1} using the same experimental set-up as described in chapter 3 section 3.2.4.

5.2.4 Battery performance

A schematic diagram of the flow-cell arrangement used for the experimental studies is shown in Fig. 51 and the cell set-up is same as described in chapter 3 section 3.2.5. The concentration of negative and positive electrolytes was 1 M $CuCl_2$ and 1 M $CeCl_3$, respectively. The charging (coulombic) efficiency of the copper-cerium redox flow cell was evaluated by charging and discharging the cell for 1800 seconds at a constant current of 25 mA cm^{-2}.

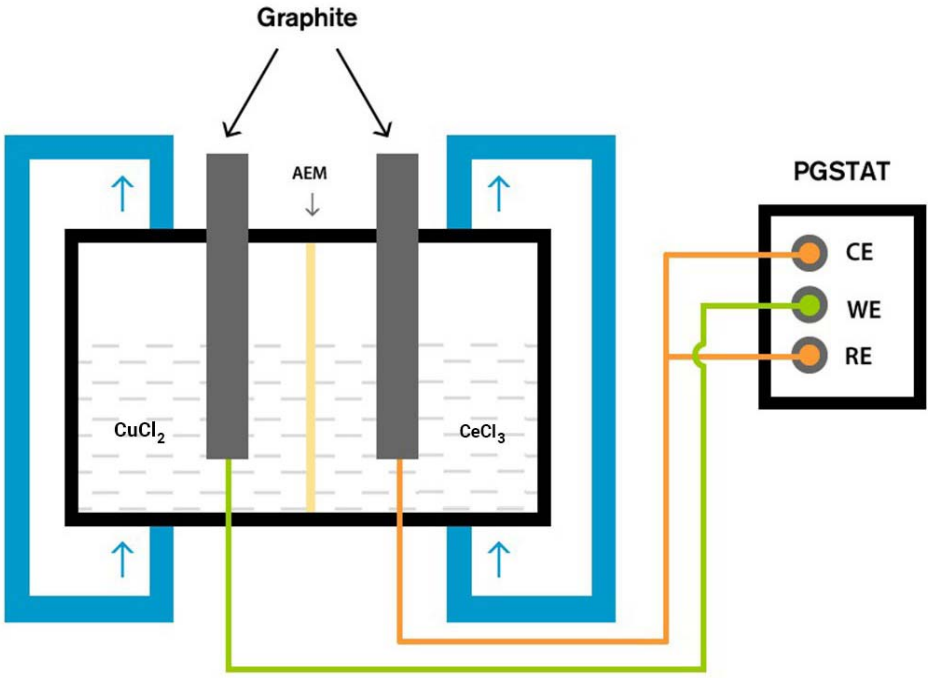

Fig. 51 The standard two-electrode setup for charge-discharge measurements.

5.3 Results and discussion

5.3.1 Cyclic voltammograms

The cyclic voltammogram of 0.085 M copper(II) chloride on a graphite sheet working electrode in the range between −0.8 to 1.25 V vs. Ag/AgCl at the scan rate of 50 mV s^{-1} is shown in Fig. 52. In this figure there is a cathodic peak (c_2) at 0.05 V and a corresponding anodic peak (a_2) at 0.62 V, indicating a reversible cupric-cuprous (Cu^{2+} to Cu^{+}) redox process at the electrode surface. The deposition/stripping of elemental copper on the electrode surface is shown by the cathodic peak (c_1) at −0.26 V and the corresponding anodic peak (a_1) at 0.31 V. The cyclic voltammogram of 0.085 M cerium(III) chloride on a graphite sheet working electrode in the range from 0.0 V to 2 V vs. Ag/AgCl at the scan rate of 50 mV s^{-1} is shown in Fig. 53. In this figure, the anodic and cathodic peaks of Ce(IV)/Ce(III) couple are observed at 1.31 V and 0.98 V, respectively. The anodic peak corresponds to the oxidation of Ce^{3+} to Ce^{4+} and the cathodic peak to the reduction of Ce^{4+} to Ce^{3+} [18]. By averaging the oxidation and reduction peak potentials, formal potentials for Cu/Cu(II) and Ce(IV)/Ce(III) redox couples are estimated to be 0.18 V and 1.15 V vs. Ag/AgCl, respectively.

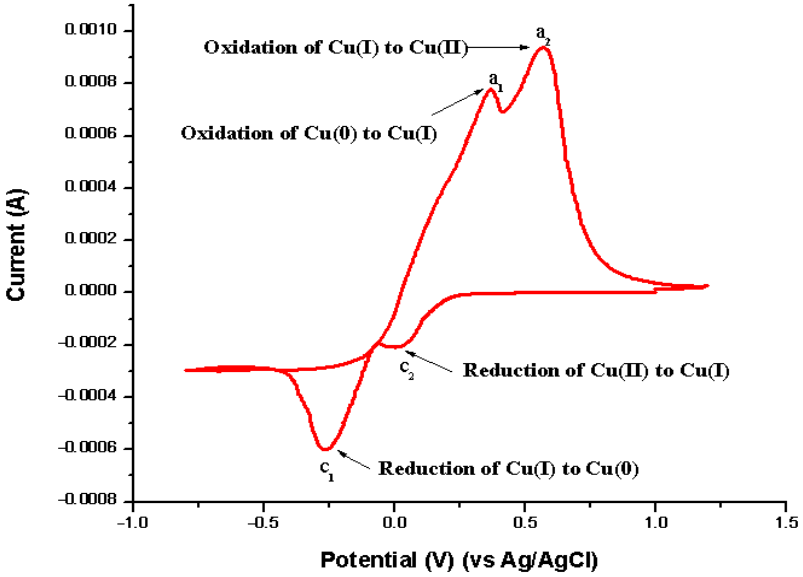

Fig. 52 CV of 0.085 M copper(II) chloride at a scan rate of 50 mV s^{-1}.

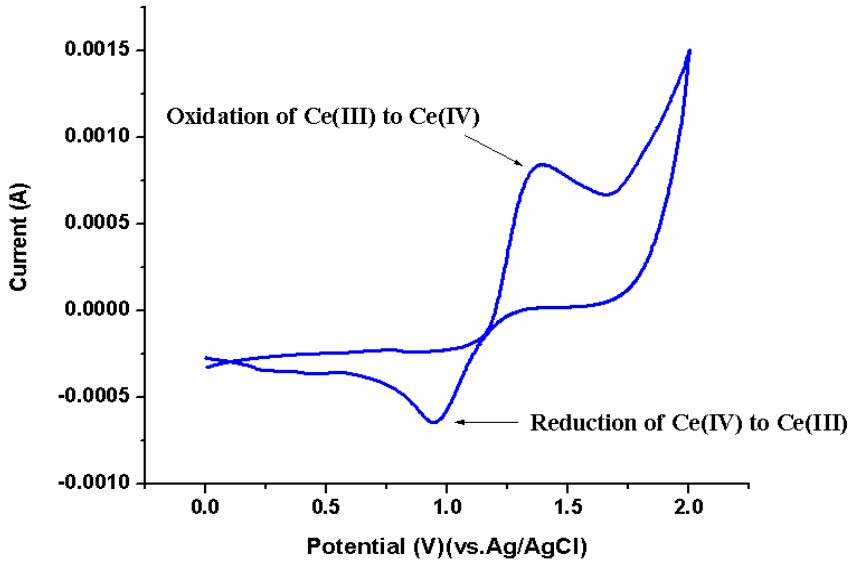

Fig. 53 CV of 0.085 M cerium(III) chloride at a scan rate of 50 mV s^{-1}.

5.3.2 Charge-discharge cycle performance

The charge-discharge measurement of the Cu-Ce RFB employing 1 M copper(II) chloride aqueous solution as negative active species and 1 M cerium(III) chloride aqueous solution as positive species was evaluated with constant-current charge-discharge measurements. Fig. 54 represents the charge-discharge curves for 30 repeated cycles. Fig. 55 shows the 15th charge-discharge curves at 25 mA cm^{-2}. The Fig. 54 shows that the electrochemical performance of the battery is relatively stable. The curves are identical with an average charge voltage of approximately 1.43 V and discharge voltage of 0.87 V.

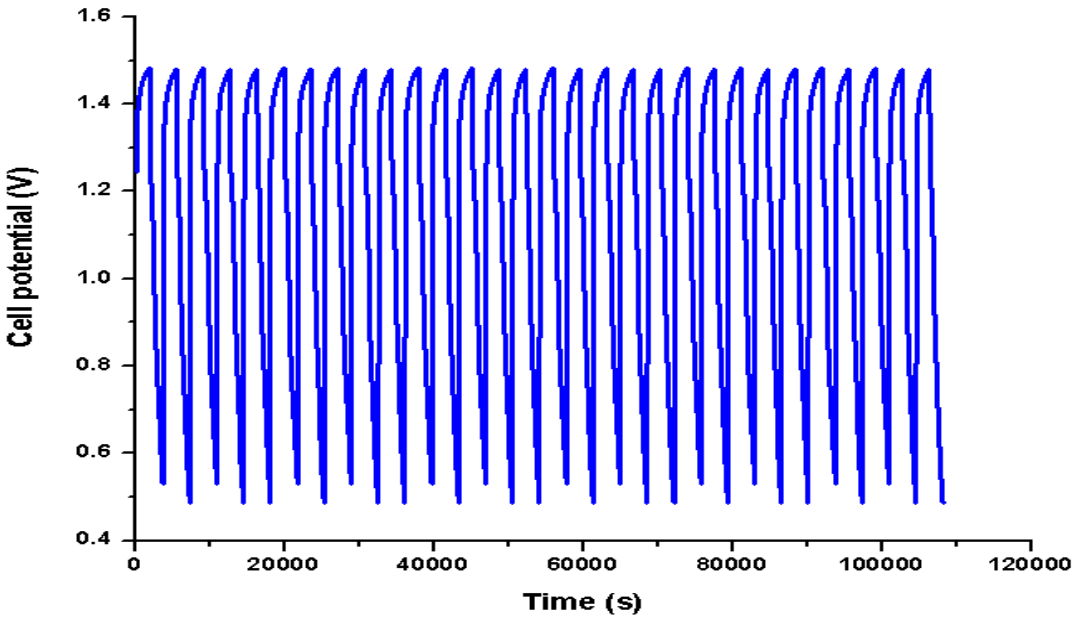

Fig. 54 Cell potential vs. time response for 30 cycles of the copper-cerium RFB at 25 mA cm^{-2}.

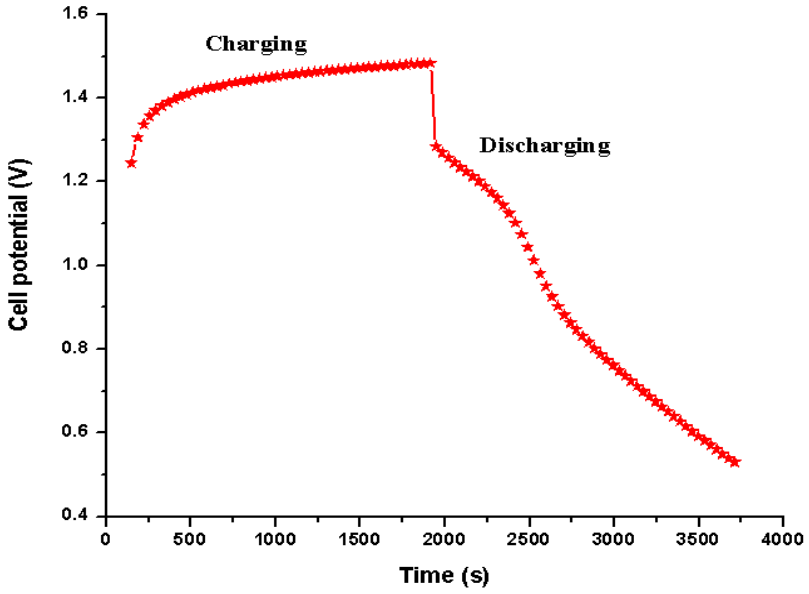

Fig. 55 Charge-discharge curves during 15th cycle of copper-cerium RFB at 25 mA cm^{-2}.

Galvanostatic charge-discharge experiments were performed at $CuCl_2$ concentrations of 1 M, 3 M and 5 M, at a current density of 25 mA cm^{-2}. The experiments were also performed at current densities of 15, 25 and 50 mA cm^{-2}, for 1 M $CuCl_2$. In all of the above experiments, the concentration of $CeCl_3$ was 1 M. The results of the above experiments are summarized in Tables 8 and 9. Table 8 shows that as the concentration of $CuCl_2$ increases from 1 to 5 M, the average discharge voltage decreases from 0.87 V to 0.74 V. The coulombic efficiency (CE) remains nearly constant at 99%, indicating the high anion selectivity of the membrane used and low hydrogen evolution during charging process. The decrease in energy efficiency (EE) from 60.22% to 56.82% is primarily due to a loss in voltage efficiency (VE) caused by increased electrolyte resistance arising from increased electrolyte concentration [19].

Table 8 Cu-Ce RFB performance as a function of $CuCl_2$ concentration at a current density of 25 mA cm^{-2}.

$CuCl_2$ (M)	**OCV (V)**	**Avg. charge voltage (V)**	**Avg. discharge voltage (V)**	**CE (%)**	**VE (%)**	**EE (%)**
1 M	1.22	1.43	0.87	99	60.83	60.22
3 M	1.01	1.38	0.81	99	58.6	58.01
5 M	0.9	1.34	0.74	99	57.4	56.82

Table 9 shows that when the current densities increases from 15 to 50 mA cm^{-2}, the voltage efficiency decreased from 69.23% to 45.06%. The reduction in VE may be attributed to mass transport limitation effects at higher current densities [9,20,21]. However, a constant CE of ~99% was obtained at all current densities. The EE reaches the highest value of 68.53% at 15 mA cm^{-2}, while the EEs were found to be 60.22% and 44.6% for current densities of 25 mA cm^{-2} and 50 mA cm^{-2}, respectively. The results indicate that current density influences RFB performance and that a moderate current density may be favorable for getting a high EE [9].

Table 9 The electrochemical performance of Cu-Ce cell with 1 M $CuCl_2$ and 1 M $CeCl_3$ run at different charge/discharge current densities.

Current density (mA cm^{-2})	**OCV (V)**	**Avg. charge voltage (V)**	**Avg. discharge voltage (V)**	**CE (%)**	**VE (%)**	**EE (%)**
15	1.25	1.3	0.9	99	69.23	68.53
25	1.22	1.43	0.87	99	60.83	60.22
50	1.1	1.62	0.69	99	45.06	44.6

From Fig. 54, the coulombic, voltage and energy efficiencies were calculated and the values obtained are plotted against the cycle number in Fig. 56. As shown in figure, the Cu-Ce RFB showed no decrease for coulomb efficiency (99%), voltage efficiency (60.83%) and energy efficiency (60.22%) on repeated charge-discharge cycles at 25 mA cm^{-2}. In all the cycles, the average coulombic efficiency was around 99%, showing that the products formed during battery charge return to their original state during discharge.

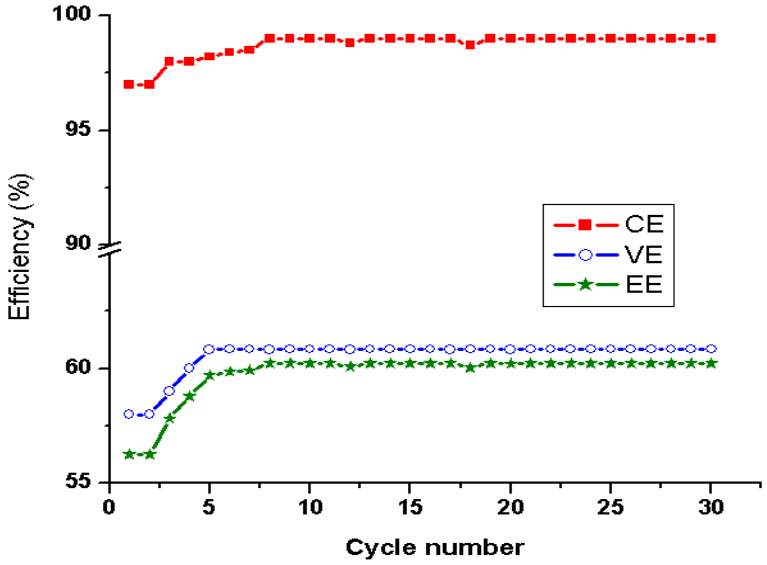

Fig. 56 Efficiency of the cell with 1 M $CuCl_2$ under the current density of 25 mA cm^{-2}.

5.4 Conclusions

In this work, a novel chloride-based copper-cerium redox flow battery system that uses Ce(IV)/Ce(III) and Cu/Cu(II) redox couples separated by a self-made anion exchange membrane has been demonstrated. The positive and negative electrodes were made from densified graphite sheets and the performance of the test cell was assessed using repeated constant current charge-discharge experiments. The cell delivered an average discharge voltage of ~0.87 V at 25 mA cm^{-2}, with a high average coulombic efficiency of 99%, voltage efficiency of 60.83% and energy efficiency of 60.22%, over 30 cycles at 298 K. During charge-discharge cycles, only chloride ions move between the anode and cathode compartments through an anion exchange membrane, preventing cross-contamination of electroactive materials and improving battery life and the performance.

The effect of concentration and current density on cell performance was also examined using galvanostatic charge-discharge cycles at various electrolyte concentrations (1 M, 3 M and 5 M) and at various current densities (15, 25 and 50 mA cm^{-2}). When the concentration is increased from 1 M to 5 M, the average discharge voltage reduces from 0.87 to 0.74 V, while the coulombic efficiency (CE) remains practically constant (99%). The strong anion selectivity of the AEM is confirmed by the high coulombic efficiency. However, when the electrolyte concentration increases, the energy efficiency (EE) values decline from 60.22% to 56.82%, due to the decreased voltage efficiency (VE) caused by increased electrolyte resistance. The coulombic efficiency remained nearly unchanged when current densities were increased from 15 to 50 mA cm^{-2}. However, voltage efficiency decreased from 69.23% to 45.06% and energy efficiency decreased from 68.53% to 44.6%. The results reveal that operating conditions have a significant impact on cell performance and the Cu-Ce RFB can perform well at low concentrations and low current densities. The overall results show that $Cu|CuCl_2\|CeCl_4|CeCl_3$ redox flow battery, in which the two electrolyte solutions are separated by an anion exchange membrane, could provide a new perspective for renewable energy storage.

5.5 References

[1] Z. Xie, F. Xiong, D. Zhou, Study of the Ce^{3+}/Ce^{4+} Redox Couple in Mixed-Acid Media (CH_3SO_3H and H_2SO_4) for Redox Flow Battery Application, Energy & Fuels. 25 (2011) 2399–2404. doi:org/10.1021/ef200354b.

[2] Y. Liu, X. Xia, Electrochemical Behavior of the Ce^{4+}/Ce^{3+} Couple in the Novel Ce-V Redox Flow Cell, in: Mater. Res. Soc., 2009: pp. 2–7. doi:10.1557/PROC-1127-T01-03.

[3] P. Modiba, M. Matoetoe, A.M. Crouch, Kinetics study of transition metal complexes (Ce-DTPA, Cr-DTPA and V-DTPA) for redox flow battery applications, Electrochim. Acta. 94 (2013) 336–343. doi:10.1016/j.electacta.2013.01.081.

[4] Z. Xie, Q. Liu, Z. Chang, X. Zhang, The developments and challenges of cerium half-cell in zinc–cerium redox flow battery for energy storage, Electrochim. Acta. 90

(2013) 695–704. doi:10.1016/j.electacta.2012.12.066.

[5] G. Nikiforidis, L. Berlouis, D. Hall, D. Hodgson, An electrochemical study on the positive electrode side of the zinc–cerium hybrid redox flow battery, Electrochim. Acta. 115 (2014) 621–629. doi:10.1016/j.electacta.2013.09.081.

[6] H. Hewa Dewage, B. Wu, A. Tsoi, V. Yufit, G. Offer, N. Brandona, A Novel Regenerative Hydrogen Cerium Fuel Cell for Energy Storage Applications, J. Mater. Chem. A. (2015), 1-6. doi:10.1039/C5TA00571J.

[7] S. Yun, J. Parrondo, V. Ramani, A Vanadium–Cerium Redox Flow Battery with an Anion- Exchange Membrane Separator, (2014) 1–11. doi:10.1002/cplu.201402096.

[8] M. Govindan, K. He, I. Moon, Evaluation of Dual Electrochemical Cell Design for Cerium- Vanadium Redox Flow Battery to Use Different Combination of Electrodes, Int. J. Electrochem. Sci. 8 (2013) 10265–10279. http://www.electrochemsci.org/papers/vol8/80810265.pdf.

[9] Z. Na, S. Xu, D. Yin, L. Wang, A cerium-lead redox flow battery system employing supporting electrolyte of methanesulfonic acid, J. Power Sources. 295 (2015) 28–32. doi:10.1016/j.jpowsour.2015.06.115.

[10] N. Kocyigit, A novel electrolytes for redox flow batteries : Cerium and chromium couples in aqueous system, Int. J. Energy Res. (2021) 1–13. doi:10.1002/er.6850.

[11] G. Nikiforidis, W.A. Daoud, Effect of Mixed Acid Media on the Positive Side of the Hybrid Zinc-Cerium Redox Flow Battery, Electrochim. Acta. 141 (2014) 255–262. doi:10.1016/j.electacta.2014.06.142.

[12] D.M. Kabtamu, L. Guan-Yi, C. Yu-Chung, C. Hsueh-Yu, H. Hsin-Chih, H. Ning-Yih, C. Yi-Sin, W. Hwa-Jou, W. Chen-Hao, The effect of adding Bi^{3+} on the performance of a newly developed iron–copper redox flow battery, RSC Adv. 8 (2018) 8537–8543. doi:10.1039/C7RA12926B.

[13] S. Anantharaj, T.S. Amarnath, E. Subhashini, S. Chatterjee, K.C. Swaathini, K. Karthick, S. Kundu, Shrinking the Hydrogen Overpotential of Cu by 1 V and Imparting Ultralow Charge Transfer Resistance for Enhanced H_2 Evolution, ACS Catal. 8 (2018) 5686–5697. doi:10.1021/acscatal.8b01172.

[14] H.K. Wainright Jesse, Savinell robert, Copper based flow batteries, US 2018/0233763 A1, 2018.

[15] A.W. Maverick, Q. Yao, The Cerium(IV)/Cerium(III) Electrode Potential in Hydrochloric Acid Solution, Inorg. Chem. Chem. 32 (1993) 5626–5628. doi:10.1021/ic00076a034.

[16] L. Sanz, D. Lloyd, E. Magdalena, J. Palma, Description and performance of a novel aqueous all-copper redox flow battery, J. Power Sources. 268 (2014) 121–128. doi:10.1016/j.jpowsour.2014.06.008.

[17] D. Lloyd, E. Magdalena, L. Sanz, L. Murtom, Preparation of a cost-effective , scalable and energy efficient all-copper redox flow battery, 292 (2015) 87–94. doi:10.1016/j.jpowsour.2015.04.176.

[18] Z. Xie, D. Zhou, F. Xiong, S. Zhang, K. Huang, Cerium-zinc redox flow battery : Positive half-cell electrolyte studies, J. Rare Earths. 29 (2011) 567–573. doi:10.1016/S1002-0721(10)60499-1.

[19] B. Li, Z. Nie, M. Vijayakumar, G. Li, J. Liu, V. Sprenkle, W. Wang, Ambipolar zinc-polyiodide electrolyte for a high-energy density aqueous redox flow battery, Nat. Commun. 6 (2015) 1–8. doi:10.1038/ncomms7303.

[20] V. Yufit, B. Hale, M. Matian, P. Mazur, N.P. Brandon, Development of a Regenerative Hydrogen-Vanadium Fuel Cell for Energy Storage Applications, J. Electrochem. Soc. 160 (2013) A856–A861. doi:10.1149/2.086306jes.

[21] R. Chen, S. Kim, Z. Chang, Redox Flow Flow Batteries : Fundamentals and Applications, in: Redox - Princ. Adv. Appl., 2017, 103–118. doi:10.5772/intechopen.68752.

CHAPTER 6

Summary and Conclusions

6.1 Summary and Conclusions

The thesis is divided into seven chapters, with a summary and conclusions chapter. In the following sessions, the summary of each chapter and the conclusions reached are briefly discussed.

6.1.1 Chapter 1: Introduction

The first chapter in this thesis presents a description about current energy resources, classification of energy sources, necessity of energy storage, batteries and their classifications, introduction and classification of flow batteries, electrochemistry of flow battery, advantages and disadvantages of flow batteries, structure, design and components of flow batteries, performance of redox flow batteries, types of redox flow batteries, limitations of hybrid redox flow batteries, objectives of the present work and thesis layout.

6.1.2 Chapter 2: Experimental Techniques

The second chapter discusses the various experimental techniques and methods used to characterize the redox flow batteries developed in this study. The working principles of the techniques are briefly explained here. Cyclic voltammetry, galvanostatic charge-discharge, electrochemical impedance spectroscopy and SEM techniques were used to analyze and characterize the flow batteries.

6.1.3 Chapter 3: A dendrite free Zinc-Iron hybrid redox flow battery for renewable energy storage

The third chapter describes a dendrite-free zinc-iron redox flow battery employing Zn/Zn(II) and Fe(III)/Fe(II) redox couples as positive and negative redox systems, respectively, separated by a self-made anion exchange membrane (AEM). This chapter explains the preparation of an anion exchange membrane and its properties. For 30 charge-discharge cycles, the battery provides a good discharge voltage of around 1.34 V at 25 mA cm^{-2}, with a coulombic efficiency (CE) of 92%, voltage efficiency (VE) of 85%, and energy efficiency (EE) of 78.2%. Repeated charge/discharge cycles reveal no degradation in performance, indicating excellent stability of the system. The present Zn-Fe hybrid redox flow battery has a significant advantage is that no zinc dendrite growth was observed on the electrode after repeated charge-discharge cycles, which was a major drawback in many previously reported zinc-based flow batteries.

6.1.4 Chapter 4: Improvement in the Performance of Fe/Fe^{2+} Electrode in an All-Iron Redox Flow Battery by the addition of Zn^{2+} ions

All-Iron redox flow batteries are a good choice among RFBs since iron is the second most abundant metal in the earth's crust and is both inexpensive and environmentally favorable. Low charging efficiency and the parasitic hydrogen evolution reaction (HER) of the negative Fe/Fe^{2+} electrode, self-discharge due to electrolyte cross-over and poor cycle life (due to ferric hydroxide precipitation) are the major technical challenges that must be overcome for all-iron redox flow batteries to be commercialized successfully. An all-iron redox flow battery with Fe/Fe(II) and Fe(III)/Fe(II) redox couples separated by a self-made anion exchange membrane is

described in this paper. The effect of Zn^{2+} ions on the electrochemical performance of Fe/Fe(II) redox couples was also investigated. The cell containing 0.03 M $ZnCl_2$ has higher coulombic efficiency, voltage efficiency and energy efficiency (90%, 70.96% and 63.86%, respectively) than the cell without $ZnCl_2$ (80%, 62.06% and 49.64%). The findings show that mixing small amounts of zinc with iron inhibits the hydrogen evolution reaction, resulting in improved cell performance.

6.1.5 Chapter 5: A novel Chloride-based Copper-Cerium Redox Flow Battery for Renewable Energy Storage

Chapter 5 of this thesis describes a copper-cerium redox flow battery, which employing Cu/Cu(II) and Ce(IV)/Ce(III) redox pairs as positive and negative redox systems separated by a self-made anion exchange membrane. The RFB uses kinetically favorable reactions and provides an appropriate discharge voltage of around 0.87 V, with a high average coulombic efficiency of 99% voltage efficiency of 60.8% and energy efficiency of 60.2% over 30 charge-discharge cycles at 25 mA cm^{-2}. The low-cost active materials, high cell performance and excellent capacity retention make the Cu-Ce flow battery a promising candidate for large-scale application for power storage. The results of this study may open up new possibilities for the use of alternate redox couples in redox flow batteries.

CHAPTER 7

Recommendations

7.1 Recommendations for future studies

Nowadays, there is a widespread demand to utilize renewable energy sources in order to reduce the greenhouse effect and the resulting climate changes. Battery storage systems are one of the key solutions to store energy harvested from renewable energy resources in power systems worldwide. Hence, in the current scenario of energy transition, there is a need for developing efficient, safe and affordable battery systems to store energy harvested from renewable energy resources. Redox-flow batteries are ideal choices for cost-effective stationary storage, especially when long discharge and storage times are required. The design and development of novel, efficient redox flow batteries employing various electroactive materials is now being researched extensively. In this work, we have fabricated various redox flow batteries by combining different electroactive species and studied their performance using charge-discharge experiments. In these redox flow batteries, a self-made anion exchange membrane was used as a separator for the electrolytes. The following are recommendations for future work, based on the results of this thesis work.

1. More research are needed to improve stability and performance of the redox flow cells on repeated long charge-discharge cycles by careful selection and optimization of cell components.

2. The stability and conductivity of the anion exchange membrane are critical components for long term use of the redox flow batteries. Hence, a systematic study of the long term stability of the membrane during repeated charge-discharge cycles are to be done for each redox flow systems.
3. The present work used a heterogeneous anion exchange membrane as a separator. In future, it would be more desirable to develop homogeneous anion exchange membranes as separators in redox flow systems due to its higher stability and easy methods for production on large scale.
4. In some redox flow systems, hydrogen evolution is a parasitic reaction, which reduces the coulombic efficiency of the cell. Hence, more effective methods are to be developed for the complete suppression of hydrogen evolution reaction.

I. PAPER PUBLICATIONS

1. **C.B. Jeena**, P.J. Elsa, P.P. Moly, K.J.Ambily, V.T.Joy, "A dendrite free Zn-Fe hybrid redox flow battery for renewable energy storage", *Energy Storage*, (2021) 1-10. doi:10.1002/est2.275.

2. K. Ambily Jacob, P. Moly Peter, P. Elsa Jose, **C. Jeena Balakrishnan**, V. Joy Thomas, "A simple method for the synthesis of anatase-rutile mixed phase TiO_2 using a convenient precursor and higher visible-light photocatalytic activity of Co–doped TiO_2", *Materials Today: Proceedings*, (2021) *49(5)*, 1408-1417. org/10.1016/j.matpr.2021.07.104

3. P.J. Elsa, **C.B. Jeena**, P.P. Moly**,** K.J. Ambily, "A Novel Synthetic Route For Cerium Nickel Mixed Oxide (Ceni0.5Oy) Nanoparticles And Study Of Its Hydrogen Storage Property", *International Journal Of Scientific & Technology Research*, Volume 8, Issue 08, August 2019 ISSN 2277-8616.

4. P.P. Moly**, C.B. Jeena**, P. J. Elsa, K.J. Ambily, V.T. Joy, "High performance polyvinyl alcohol/calcium titanate nanocomposite anion-exchange membranes as separators in redox flow batteries", *Polymer Bulletin*, 2018, doi:10.1007/s00289-018-2277-2.

II. PAPERS COMMUNICATED

1. **C.B. Jeena**, P.P. Moly, Daiphi Davis, A.K. Jibin, V.T. Joy, "Improvement in the Performance of Fe/Fe^{2+} Electrode in an All-Iron Redox Flow Battery by the addition of Zn^{2+} ions" Communicated to *ChemistrySelect*.

2. **C.B. Jeena**, Daiphi Davis, Dijo Damien, V.T. Joy, "A Novel Chloride-based Copper-Cerium Redox Flow Battery for Renewable Energy Storage" communicated to *International Journal of Green Energy*.

III. PAPERS PRESENTED IN SEMINARS

1. **C.B. Jeena**, V.T. Joy, "Impact of electrolyte concentration on the performance of the copper-cerium redox flow battery system" National seminar on *Nano materials for medical applications,* Post Graduate Dept. of Chemistry Little Flower College, Guruvayoor, 29th July 2017.

2. **C.B. Jeena**, P. J. Elsa, P.P. Moly, K.J. Ambily ,V.T.Joy, "Study of nanostructured Fe and Fe_3O_4 composite material as a negative electrode for Ni-Fe rechargeable batteries", National Seminar on *Emerging Trends in Chemical Research,* Sponsored by UGC, Research and Post Graduate Dept. of Chemistry, Christ College (Autonomous) Irinjalakuda, Thrissur Kerala, 28 Feb. and 1st March 2017.

3. **C.B. Jeena**, P.J. Elsa, P.P. Moly, K.J. Ambily, V.T. Joy, "Synthesis, characterization and performance study of Fe/Fe_3O_4 Nano composite material as negative electrode in Ni-Fe batteries", National seminar on *Green Chemistry For Environmental Sustainability,* PG & Research department of chemistry, Bharath Matha College, EKM, 7-8th Feb.2017.

4. **C.B. Jeena**, P.J. Elsa, P.P. Moly, K.J. Ambily,V.T. Joy, "Study on the performance of Graphene incorporated Fe/Fe_3O_4 Nano composite as negative electrode in Ni-Fe batteries" National seminar on *Current Trends in Chemistry*, PG & Research department of chemistry, Christ College, Irinjalakuda, 14-15th October2014.

5. P.P. Moly**, C.B. Jeena**, P.J. Elsa, K.J. Ambily, V.T. Joy, "Synthesis and characterization of perovskite nanopowder as anion exchange material by co-precipitation from simple precursors", National level seminar on *Nano materials for medical applications*, Post Graduate Dept. of Chemistry Little Flower College, Guruvayoor, 29th July 2017.

6. P.P. Moly**, C.B. Jeena**, P.J. Elsa, K.J. Ambily, V.T. Joy, "A novel anion-exchange membrane by chemical modification of polyvinyl alcohol for electrochemical devices", National Seminar on *Emerging Trends in Chemical Research*, Sponsored by UGC, Research and Post Graduate Dept. of Chemistry, Christ College (Autonomous) Irinjalakuda, Thrissur Kerala, 28 Feb. and 1st March 2017.

7. P.P. Moly**, C.B. Jeena**, P.J. Elsa, K.J. Ambily, V.T. Joy, Development of high performance anion exchange membranes by chemical modification of polyvinyl alcohol for electrochemical devices" Prof. K.V. Thomas Endowment International Symposium on *New Trends In Applied Chemistry* NTAC -2017, Post Graduate and Research Dept. of Chemistry, Sacred Heart College (Autonomous) Thevara Kochi, Kerala.

Received: 12 March 2021 | Revised: 7 July 2021 | Accepted: 18 July 2021

DOI: 10.1002/est2.275

RESEARCH ARTICLE

ENERGY STORAGE WILEY

A dendrite free Zn-Fe hybrid redox flow battery for renewable energy storage

C. Balakrishnan Jeena | **P. Jose Elsa** | **P. Peter Moly** | **K. Jacob Ambily** | **Vadakkan T. Joy**

Department of Chemistry, Christ College (Autonomous, affiliated to University of Calicut), Irinjalakuda, Kerala, India

Correspondence
Vadakkan T. Joy, Department of Chemistry, Christ College (Autonomous, affiliated to University of Calicut), Irinjalakuda, Kerala 680125, India.
Email: joyvthomas@christcollegeijk.edu.in; joyvthomas2002@gmail.com

Funding information
Council of Scientific and Industrial Research (CSIR), Govt. of India

Abstract

About two thirds of global greenhouse emissions is caused by burning of fossil fuels for energy purposes and this has spurred great research interest to develop renewable energy technologies based on wind, solar power, and so on. Redox flow batteries (RFB) are receiving wide attention as scalable energy-storage systems to address the intermittency issues of renewable energy sources. However, for widespread commercialization, the redox flow batteries should be economically viable and environmentally friendly. Zinc based batteries are good choice for energy storage devices because zinc is earth abundant and zinc metal has a moderate specific capacity of 820 mA hg^{-1} and high volumetric capacity of 5851 mA h cm^{-3}. We herein report a zinc-iron (Zn-Fe) hybrid RFB employing Zn/Zn(II) and Fe(II)/Fe(III) redox couples as positive and negative redox systems, respectively, separated by a self-made anion exchange membrane (AEM). The battery delivers a good discharge voltage of approximately 1.34 V at 25 mA cm^{-2}, with a coulombic efficiency (CE) of 92%, voltage efficiency (VE) of 85% and energy efficiency (EE) of ~78% for 30 charge-discharge cycles. Repeated galvanostatic charge/discharge cycles show no degradation in performance, confirming the excellent stability of the system. A key advancement in the present Zn-Fe hybrid redox flow battery with AEM separator is that no dendrite growth was observed on zinc electrode on repeated charge-discharge cycles, which was the serious drawback of many previously reported zinc based redox flow batteries.

KEYWORDS

anion-exchange membrane, dendrite growth suppression, energy storage, redox flow battery, renewable energy, zinc deposition

1 | INTRODUCTION

Global climate change resulting from greenhouse emissions is causing increasingly severe risks for ecosystems, human safety and health. This combined with the large-scale demand for electricity expected during the coming decades has aroused great interest in the development of new technologies for energy production from renewable energy sources, such as wind, solar, and so on. However, these renewable energy sources are intermittent in nature and hence the success of these new renewable energy harvesting technologies needs to be associated with the introduction of competitive energy storage devices for grid scale energy storage. Unlike traditional batteries, the

redox flow batteries (RFBs) are attractive electrochemical systems which store energy in two electrolyte solutions comprising of different redox couples separated by an ion-exchange membrane (IEM).[1–5] Among various traditional flow battery systems, the hybrid flow batteries involve the deposition of a metal coating on at least one of the electrodes.[4,6] The main advantages of RFBs over other battery systems are their safety, moderate cost, modularity, transportability and flexibility in charge-discharge cycles.[7–9] Unfortunately, the inadequate ionic selectivity of the existing IEMs leads to undesired crossover of redox species between negative and positive electrolytes through the membrane. This results a permanent loss of both coulombic efficiency (CE) and battery capacity and will lead to overall performance degradation of RFBs.[5,10–13]

There are many redox flow batteries under development and among which the vanadium redox flow battery (VRFB) reported by Skyllas-Kazacos et al. at the University of New South Wales (UNSW), Australia is considered as most successful RFBs to date but its commercialization is hindered mainly by the high costs of vanadium salts and perfluorosulfonic acid (PFSA) membrane.[14–16] Other RFBs that uses low-cost redox materials are all-copper,[17–20] all-iron[21,22] and all-lead[23–25] RFBs, but all these systems have low performances. Due to slow kinetics of Cu/Cu(I) redox couple, all-copper RFBs have low energy efficiency and low cell voltage.[17,26] In all-iron RFBs, the standard redox potential of Fe^{2+}/Fe (−0.44 V vs SHE) is more negative than that of hydrogen evolution reaction (HER) and lower hydrogen overpotential of iron causes hydrogen evolution and coulombic losses.[27–29]

Zinc-based redox flow batteries are generally more attractive due to favorable electrochemical properties of zinc such as its low cost, fast electrode kinetics, negative electrode potential ($E^0 = -0.76$ V vs SHE) and high overpotential for the hydrogen evolution reaction (HER).[30–32] A Zn-Fe flow battery system reported by Selverston et al. used mixed zinc-iron electrolytes and porous separator in place of expensive ion-exchange membranes.[31] Gong et al. reported a zinc-iron RFB based on double-membrane triple electrolyte design.[33] Yuan et al. reported a battery that employs $Zn(OH)_4^{2-}$/Zn and $Fe(CN)_6^{3-}$/Fe $(CN)_6^{4-}$as the negative and positive redox couples, respectively, while a self-made polybenzimidazole (PBI) membrane was used as a separator. Xie et al. reported an energy efficiency of 71.1% over 50 cycles for a zinc-ferrum redox flow battery (Zn/Fe RFB) employing an ion exchange membrane as a separator.[34] Wu et al. developed a chloride acid-based tin-iron hybrid flow battery with good rate and cycle performance.[35,36] Wang and co-workers developed a zinc-polyiodide flow battery and reported high energy density.[29] During the charging process of Zn based flow batteries, zinc dendrites form and ultimately pierce the separator, causing a short circuit and battery failure.[37–40] Additionally, zinc dendrites can easily fall from anodes, reducing efficiency, capacity and life time of the cell.[41] As a result, inhibiting the formation of zinc dendrites is essential for the successful commercialization of zinc based RFBs. Researchers have recently focused their efforts on modifying the electrolyte, anodes, electric field, and rate of zinc ion transfer to solve zinc dendrite formation.[37,39] To prevent negative effects of zinc dendrites on the performance and lifetime of zinc-based batteries, the separator should also have good mechanical stability to prevent the direct contact of the anode and cathode.[42] Thus, developing a high efficiency, dendrite free zinc based RFB electrical energy storage system having negligible crossover of the electroactive materials between the anode and cathode compartments, is an important goal towards widespread use of renewable energy sources.

Herein we report a novel zinc-iron hybrid redox flow battery (Zn/Fe hybrid RFB), in which Zn/Zn (II) and Fe(II)/Fe(III) redox couples act as negative and positive redox materials and the two redox couples are separated by a self-made anion exchange membrane. Both zinc and iron are the two advantageous elements for energy storage due to their low cost and high abundance.[33] The ferric/ferrous chloride redox pair, which has been used in a variety of flow battery systems, is promising as an active material on the positive side due to its rapid kinetics.[27] Electrodes were densified graphite sheets and cell housings were made of acrylic sheets. A schematic representation of the Zn-Fe hybrid redox flow battery is shown in Figure 1. The electrochemical reaction through which Zn-Fe RFB stores and releases electricity can be expressed by following reactions:

$$\text{At anode}: \quad Zn^{2+} + 2e^- \rightleftharpoons Zn \qquad E^0 = -0.76\,V \quad (1)$$

$$\text{At cathode}: \quad 2Fe^{2+} \rightleftharpoons 2Fe^{3+} + 2e^- \qquad E^0 = +0.77\,V \quad (2)$$

$$\text{The overall reaction is}: \quad Zn^{2+} + 2\,Fe^{2+} \rightleftharpoons Zn + 2Fe^{3+}$$
$$E^0 = 1.53\,V \quad (3)$$

During the charging process, the Fe(II) ions at the positive electrode release the electrons, and get oxidized to Fe(III) ions; the Zn(II) ions at the negative electrode acquire these electrons from the external circuit, and electrodeposits onto the electrode as metallic Zn. The chloride ions move through the anion-exchange membrane from zinc compartment to the iron compartment, to maintain charge neutrality. During the discharge, the above electrochemical processes are reversed. At the

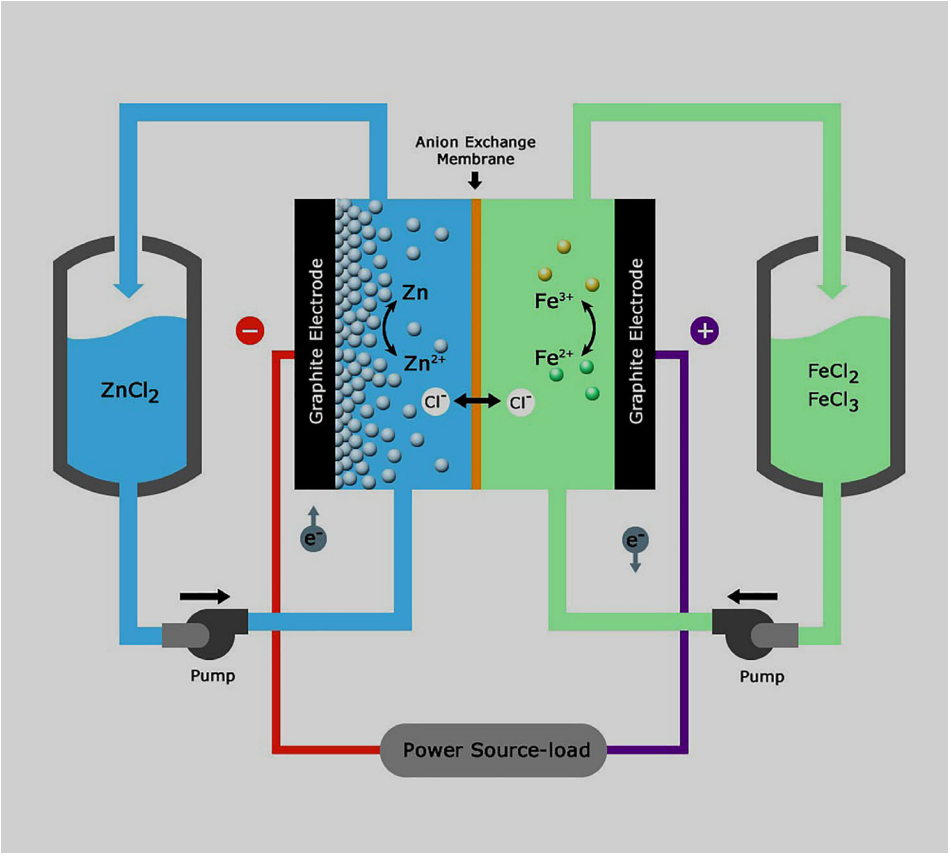

FIGURE 1 Schematic of a Zn-Fe flow battery

positive electrode, the Fe(II)/Fe(III) redox couple have good solubility in acidic media and exhibits facile kinetics.[33] At the negative electrode, the Zn/Zn(II) redox couple also exhibit fast kinetics and has high overpotential for hydrogen evolution reaction.

2 | EXPERIMENTAL

2.1 | Chemicals

All chemicals were of reagent grade and the electrolytes were prepared with deionized water. Iron(II) chloride tetrahydrate ($FeCl_2{\cdot}4H_2O$), iron(III) chloride ($FeCl_3$), ammonium chloride (NH_4Cl) and zinc chloride ($ZnCl_2$) were obtained from Merck India.

2.2 | Preparation of electrolyte

1 M Zn/Zn(II) electrolyte is prepared by dissolving Zn(II) chloride in deionized water (pH = 5.8). The positive electrolyte is a mixture of 0.5 M $FeCl_2$ and 0.5 M $FeCl_3$ with 2 M NH_4Cl in deionized water (pH = 1.7). The NH_4Cl was added to the positive electrolyte as a supporting electrolyte in order to improve conductivity of the solution.

2.3 | Preparation of anion-exchange membrane

The anion-exchange membrane was prepared by condensing guanidine carbonate with formaldehyde followed by cross-condensation with melamine. The dried powder was mixed with a polymer powder as a binder and made in to a homogeneous suspension and converted in to membrane by solvent casting method. The prepared membranes were highly flexible and had a thickness of ~120 μm. The prepared membranes exhibited hydroxide ion conductivity around 80 mS^{-1} at room temperature. The ion exchange value of the membrane was 1.2 mmol/g. To study the alkaline stability, the membranes were kept immersed in 2 M NaOH at room temperature for 2 weeks. The FT-IR and weight loss measurements of the washed, dried membrane after alkali treatment show no signs of degradation and weight loss indicating high alkaline stability. Figure 2 shows the SEM images of the membrane. More details about the membrane will be published elsewhere.

2.4 | Cyclic voltammetry

Cyclic voltammetry (CV) experiments were conducted in a three-electrode cell as shown in Figure 3, using a

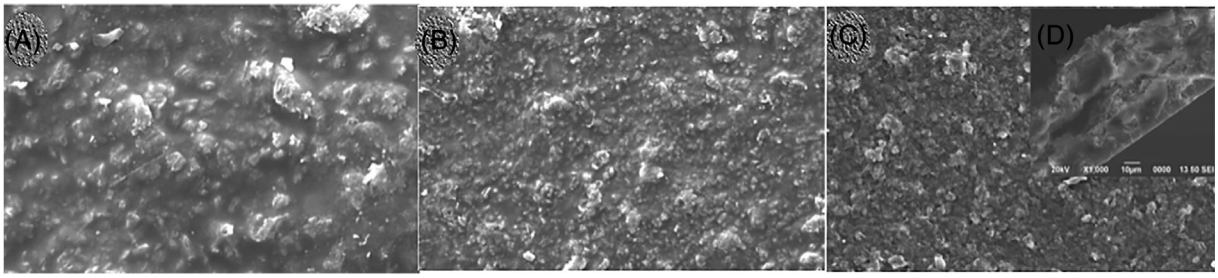

FIGURE 2 (A-C) The SEM images of the membrane and (D) cross-sectional image of membrane

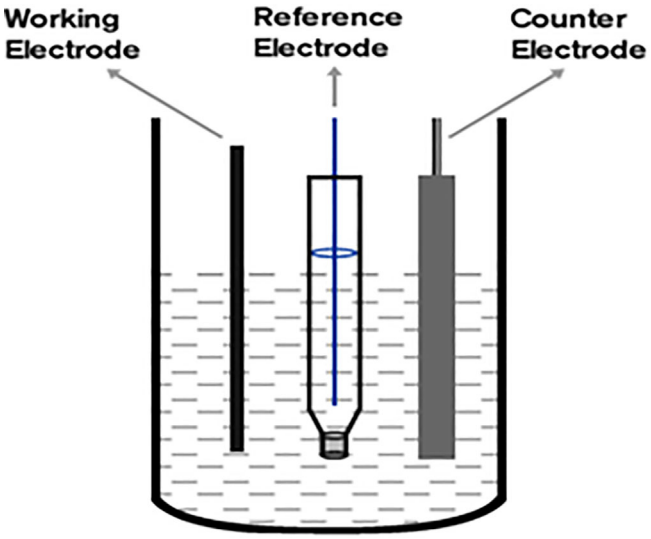

FIGURE 3 The electrochemical set-up of a three-electrode cell

potentiostat/galvanostat (Autolab PGSTAT, Metrohm 50519) instrument. A graphite sheet, platinum sheet and an Ag/AgCl electrode were used as working, counter and reference electrodes, respectively. The CV was measured from −1.6 to −0.2 V vs Ag/AgCl reference electrode using 0.085 M $ZnCl_2$ as the electrolyte at a scan rate of 50 mV/s. The measurement was performed at room temperature.

2.5 | Battery test

The redox flow battery consists of a reaction chamber (cell) and two reservoirs to store electrolytes externally. The cell was made of acrylic sheet and the positive and negative electrodes were densified graphite sheets with an area of 16 cm^2 and thickness of 2 mm. The negative and positive electrodes were separated by the self-made anion-exchange membrane. The total volume of each compartment of the cell is 3 cm × 3 cm × 1 cm. The negative electrolyte of this zinc-iron flow cell consisted of 1 M $ZnCl_2$ and the positive electrolyte is a mixture of 0.5 M $FeCl_2$ and 0.5 M $FeCl_3$ with 2 M NH_4Cl. The electrolytes were stored in two external reservoirs (each of 75 mL volume). Both positive and negative electrolytes were circulated through the cell using two peristaltic pumps. The cell performance was measured under a constant current charge-discharge measurement using an Autolab PGSTAT (Metrohm 50519 with NOVA 1.11 software) instrument connected to a PC. The charge-discharge measurements were carried out using a standard two-electrode setup as shown in Figure 4, in which the graphite sheets act as both working electrode and counter electrode, respectively.

The charge-discharge experiment of the zinc-iron redox flow cell is performed by charging the cell at a constant current of 25 mA cm^{-2} for 1800 seconds followed by discharge at the same current, until the cell reached a voltage of 0.0 V to completely strip off any deposited zinc. The cell parameters like coulombic efficiency (CE), voltage efficiency (VE) and energy efficiency (EE) of the battery are calculated using the following equations[43]:

$$CE = \frac{t_d}{t_c} \times 100\% \quad (4)$$

$$VE = \frac{V_d}{V_c} \times 100\% \quad (5)$$

$$EE = VE \times CE \quad (6)$$

Here t_d represents the discharge time; t_c represents the charge time; V_d represents the average discharge voltage; and V_c represents the average charge voltage.

2.6 | Zn electrodeposit characterization

Electrodeposits are analyzed using scanning electron microscope (JEOL-JSM 6390 JED 2300 scanning electron microscope).

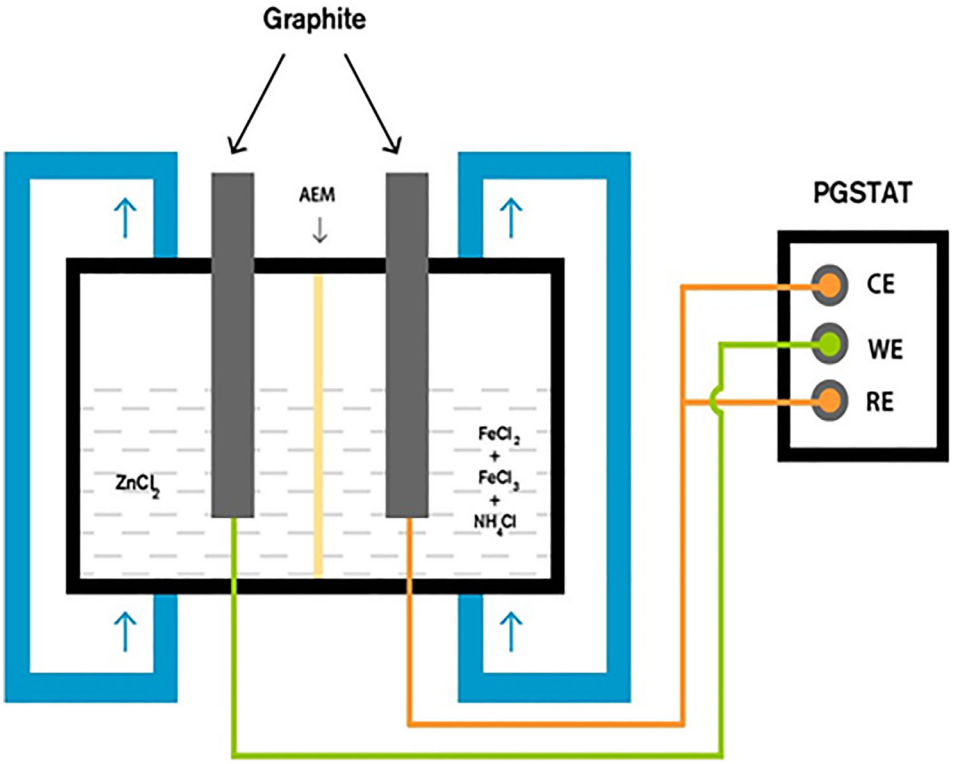

FIGURE 4 The standard two-electrode setup for charge-discharge measurements

3 | RESULTS AND DISCUSSION

3.1 | Cyclic voltammograms

A cyclic voltammogram of 0.085 M electrolyte of $ZnCl_2$ on a graphite sheet working electrode in the range of −1.6 to −0.2 V (vs Ag/AgCl) at the scan rate of 50 mV s^{-1} is shown in Figure 5. From figure, it is clear that the cathodic peak at −1.28 V corresponds to the electrodeposition of zinc and the anodic peak at −0.74 V corresponds to the dissolution of zinc to the solution.

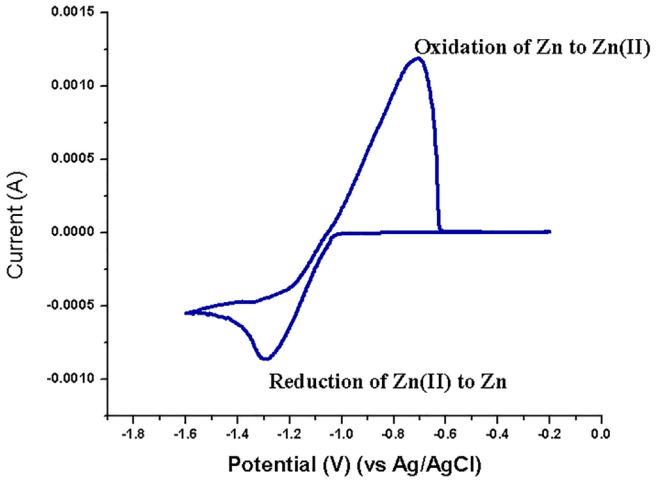

FIGURE 5 CV of 0.085 M $ZnCl_2$ on a graphite electrode at the scan rate of 50 mV s^{-1}

3.2 | Battery performance

The performance of a Zn-Fe RFB employing 1 M Zn(II) chloride aqueous solution as negative active species and 0.5 M $FeCl_2$ and 0.5 M $FeCl_3$ with 2 M NH_4Cl aqueous solution as positive species was evaluated with constant-current charge-discharge measurements. Figure 6 represents the characteristic charge/discharge curves during the 15th cycle at 25 mA cm^{-2}. This curve was obtained from 30 minutes of charging followed by 30 minutes of discharging under a current density of 25 mA cm^{-2} using graphite electrodes. It shows a relatively flat voltage profile for charge and discharge process. The charge-discharge measurements were repeated over 30 cycles and are shown in Figure 7. The cycling studies at 25 mA cm^{-2} revealed good stability of the battery, without any evidence of degradation. The curves are identical with a charge voltage of approximately 1.59 V and a discharge voltage of 1.34 V.

Any crossover of Fe^{2+}/Fe^{3+} through the membrane to the anodic compartment will result in a gradual fading of coulombic efficiency on repeating the charge-discharge cycles.[31,34] However, this phenomenon is not observed in the present redox flow system indicating that the crossover of Fe^{2+}/Fe^{3+}does not occur appreciably. This may be due to the good cation-blocking ability of the anion exchange membrane. In this case, during charging,

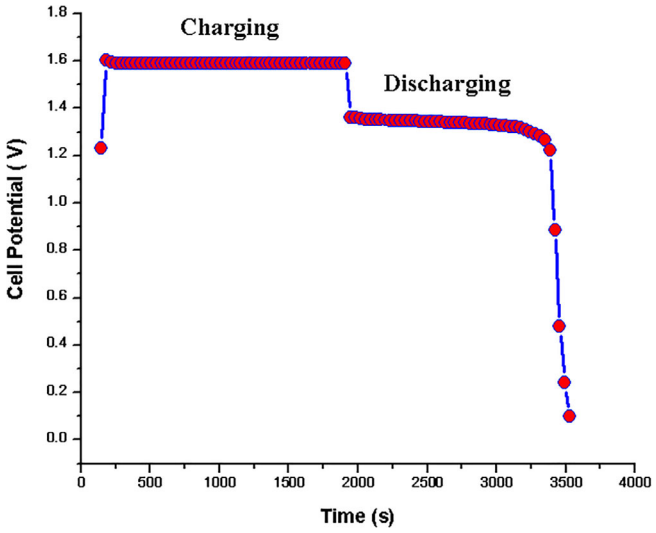

FIGURE 6 Cell potential vs time response for the 15th charge-discharge cycle at 25 mA cm^{-2}

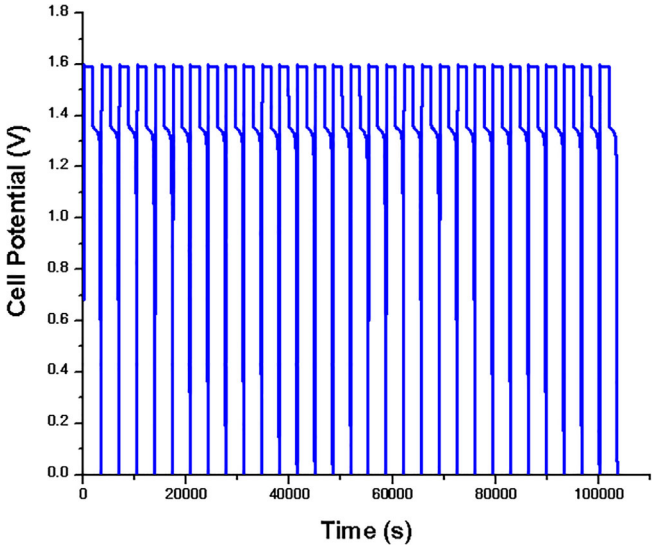

FIGURE 7 Cell potential vs time response for 30 cycles of Zn-Fe RFB at 25 mA cm^{-2}

excess chloride ions left in the anode compartment move towards cathode compartment through the membrane for electrical neutrality. During discharge process, opposite changes take place. When we repeated the experiments with a porous PVC membrane instead of an AEM, dendrite formation was observed on zinc electrodes even on first charging step. When an AEM is used, only chloride ions can diffuse from anode compartment to the cathode compartments through the AEM, during charging. From the above observations it clear that selective migration of chloride ions has a strong influence on the uniform deposition of the zinc. Similar results of suppression of dendrite formation in zinc RFBs with different kinds of membranes have been reported by many other groups.[44–46]

The dependences of cell performance on concentration and current density were also investigated by performing the galvanostatic charge-discharge measurement at different electrolyte concentrations (1 M, 3 M and 5 M) and at different current densities (15, 25 and 50 mA cm^{-2}). The results are tabulated in Table 1 and 2.

From Table 1, it is found that the average discharge voltage decreases from 1.34 to 1.01 V on increasing concentration of $ZnCl_2$ from 1 M to 5 M, while the coulombic efficiency (CE) remains nearly constant at ~92 to 90%, which indicates the high anion selectivity of the membrane. A higher CE compared to that of the cells reported by other researchers is mainly due to the negligible crossover of Fe^{3+} ions through AEM used in our redox flow battery. This result also confirms the high anion selectivity of our anion exchange membrane when used as a separator in Zn-Fe redox flow battery. The decrease in energy efficiency (EE) values from 78.2% to 53.46% with increase in electrolyte concentration is mainly due to the decreasing voltage efficiency (VE) arising from the increased electrolyte resistance.[47,48]

The electrochemical performance of the Zn-Fe system with 1 M $ZnCl_2$ at different current densities (such as 15, 25, and 50 mA cm^{-2}) is given in Table 2. The coulombic efficiency is mainly influenced by three key factors: temperature, current and state-of-charge. The relationship between charge or discharge currents and coulomb efficiency can be expressed by the Peukert equation.[20] This states that the overall battery capacity or the total energy supplied by the battery, decreases disproportionately as the discharge current rises.

$$\eta_c = \frac{Q_d}{Q_N} = \left(\frac{I_d}{I_N}\right)^{1-n} \tag{7}$$

where I_d is discharge current, I_N is base current, Q_d is the capacity discharged by I_d and Q_N is the capacity discharged by base current I_N. The equation relating internal resistance, discharge current and energy efficiency can be written as

$$\eta_w = \eta_c \eta_v = \left(\frac{I_d}{I_N}\right)^{1-n} \frac{V_B - R_i I_d}{V_B + R_i I_c} \tag{8}$$

From Equations (7) and (8), it is clear that the internal resistance and discharge current values are obviously two key factors that reduce energy efficiency. Reducing internal resistance and maintaining an optimum charge and

TABLE 1 Zn-Fe RFB performance as a function of $ZnCl_2$ concentration at a current density of 25 mA cm^{-2}

$ZnCl_2$ (M)	OCV (V)	Avg. charge voltage (V)	Avg. discharge voltage (V)	CE (%)	VE (%)	EE (%)
1 M	1.44	1.58	1.343	92	85	78.2
3 M	1.31	1.65	1.138	92	68.9	63.38
5 M	1.09	1.7	1.01	90	59.4	53.46

TABLE 2 The electrochemical performances for Zn-Fe cell with 1 M $ZnCl_2$ run at different charge/discharge current density

Current density (mA cm^{-2})	OCV (V)	Avg. charge voltage (V)	Avg. discharge voltage (V)	CE (%)	VE (%)	EE (%)
15	1.52	1.55	1.4	90	90	81
25	1.44	1.58	1.343	92	85	78.2
50	1.38	1.71	1.27	92	74	68.08

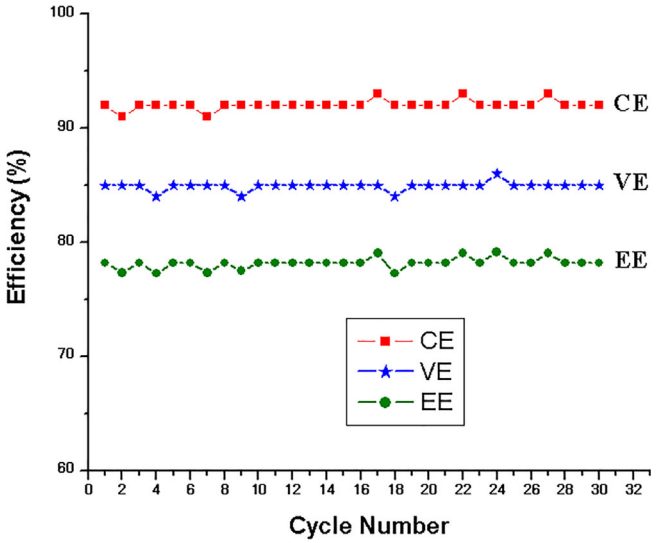

FIGURE 8 Efficiency of the cell with 1 M $ZnCl_2$ under the current density of 25 mA cm^{-2}

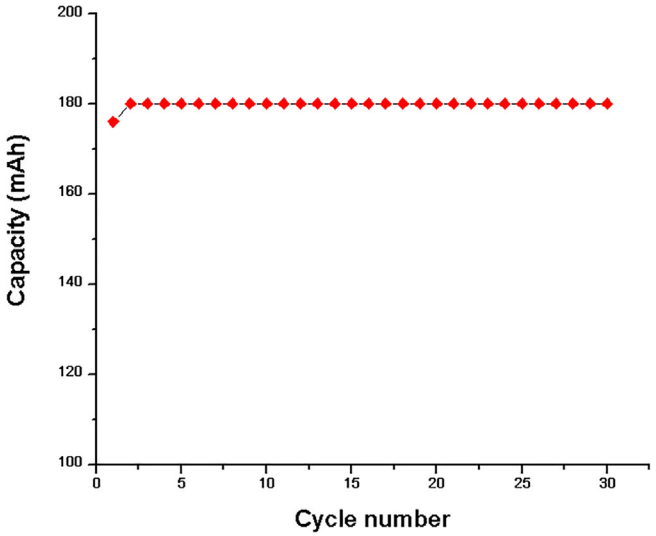

FIGURE 9 Discharge capacity vs number of cycles at a current density of 25 mA cm^{-2}

discharge current will help to increase the energy efficiency.

From charge-discharge plot, the coulombic, voltage and energy efficiencies were calculated and plotted vs cycle number in Figure 8. From the figure, it is clear that the Zn-Fe RFB shows no decrease of coulomb efficiency (92%), voltage efficiency (85%) or energy efficiency (78.2%) on 30 repeated charge-discharge cycles at 25 mA cm^{-2}. The average coulombic efficiency of about 92% in all the cycles indicates that the products formed during battery discharge return almost completely to their initial conditions on charging. Low coulombic efficiency in aqueous electrolytes is generally attributed to the side reactions due to water electrolysis.[5] The standard reduction potential of zinc in acid media is −0.76 V vs the standard hydrogen electrode (SHE). During the charging process, proton or water reduction leading to H_2 evolution is the preferred reaction, thermodynamically. However zinc is a relatively poor electrocatalyst for the H_2 evolution and hence high overpotential of zinc for hydrogen evolution increase the overall cell efficiency by suppressing hydrogen evolution reaction.[30] After repeated charge-discharge cycles, no appreciable changes in pH were observed. Hydrogen evolution reaction ($2H^+ + 2e^- \rightarrow H_2$ (g)) is a side reaction that decrease the efficiency of many redox flow batteries. This will also increase the pH of the anolyte. Higher coulombic efficiency and near consistency of the pH values after many charge-discharge cycles indicates that the hydrogen evolution on the anode is negligible in the present system. The cell capacity is also calculated for each discharge cycles at a current density of 25 mA cm^{-2} and plotted vs cycle number in Figure 9. From the figure, it is clear that the discharge capacity is almost constant even after

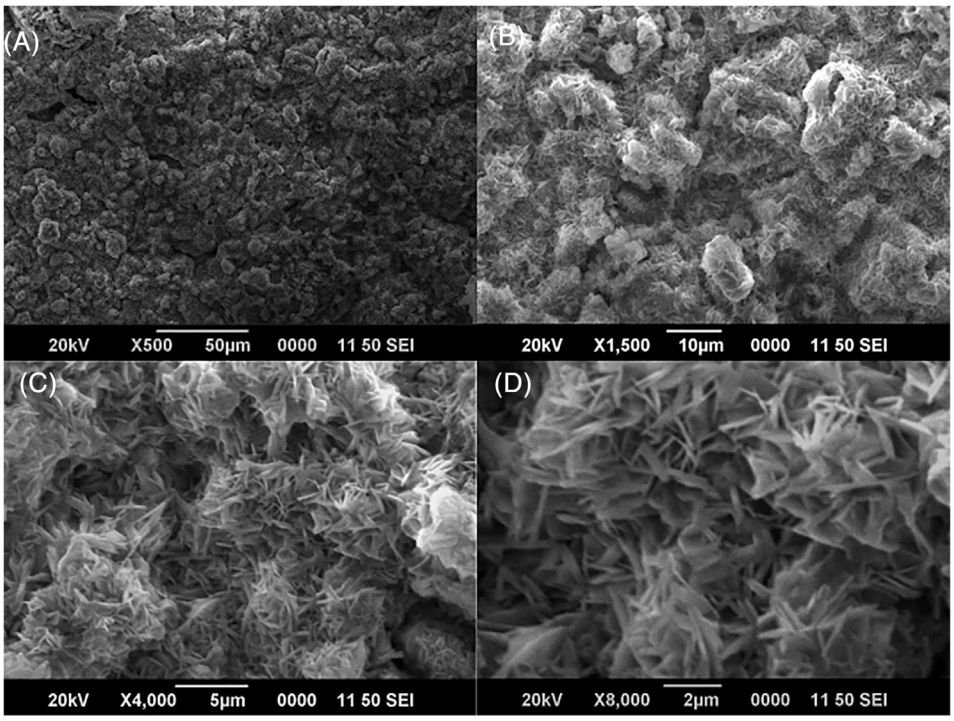

FIGURE 10 (A-D) SEM images of zinc deposition at various magnifications

30 charge-discharge cycles. No zinc dendrite formation was observed on increasing the current densities to 15, 25, 50, 100 and 150 mA cm^{-2}.

3.3 | SEM Analysis

The deposition of a uniform, thick zinc layer onto an inert current collector has become a necessity in all zinc-based redox flow batteries. Figure 10 shows SEM micrograph of zinc electrodeposit obtained during the charging phase of the zinc half-cell under a current density of 25 mA cm^{-2}. Visually, all the electrodeposited Zn coatings were homogeneous and metallic gray. It is pertinent to note that no dendrite growth occurs on the zinc electrode which was a severe drawback of previously reported zinc based rechargeable batteries. Absence of dendrite growth might be due to the fact that, only the chloride ions shuttles between two electrolyte solutions through AEM and this probably promotes uniform zinc deposition and prevent the dendrite growth.

4 | CONCLUSION

In conclusion, the feasibility of a Zn-Fe RFB system utilizing Zn(II)/Zn and Fe(III)/Fe(II) redox couples and an anion exchange membrane as a separator has been demonstrated. Densified graphite sheets were used both as positive and negative electrode current collectors and the performance of the test cell was evaluated with repeated constant current charge-discharge experiments. The cell delivered an average discharge voltage of ~1.34 V at 25 mA cm^{-2}, with a high average coulombic efficiency of 92%, voltage efficiency of 85% and energy efficiency of 78.2% over 30 cycles at 298 K. During charge-discharge cycles, only chloride ions shuttle between anode and cathode compartments through AEM, which eliminates the issue of cross contamination of electroactive materials and thus increase the performance of the battery. From SEM images, it was clear that the Zn coatings were homogeneous and dendrite-free.

The dependence of cell performance on concentration and current density was also investigated by performing the galvanostatic charge-discharge measurements at different electrolyte concentrations (1 M, 3 M and 5 M) and at different current densities (15, 25 and 50 mA cm^{-2}). The results show that the average discharge voltage decreases from 1.34 to 1.01 V on increasing concentration of $ZnCl_2$ from 1 M to 5 M, while the coulombic efficiency (CE) remains nearly constant (90-92%). Higher coulombic efficiency confirms negligible hydrogen evolution side reaction and high anion selectivity of AEM. The energy efficiency (EE) values, however, decrease from 78.2 to 53.46% with increase in electrolyte concentration and this is mainly due to the decreasing voltage efficiency (VE) arising from the increased electrolyte resistance. On increasing the current densities to 15 to 50 mA cm^{-2} the coulombic efficiency remained almost same (90-92%). However, voltage efficiency decreased from ~90% to 74%

and energy efficiency decreased from ~81% to 68%. The results show that the operating conditions are crucial impact factors for the cell performance and the Zn-Fe RFB can exhibit good performance at low concentration (1 M) and at low current density (15 mA cm^{-2}). Thus, we have successfully demonstrated working of a high efficiency and stable Zn-Fe hybrid redox flow battery with no dendrite growth during zinc deposition by optimizing charge-discharge conditions and employing an anion exchange membrane as separator.

ACKNOWLEDGEMENT

C.B. Jeena and P.J. Elsa gratefully acknowledge Council of Scientific and Industrial Research (CSIR), Govt. of India for Senior Research Fellowships.

DATA AVAILABILITY STATEMENT

Data sharing is not applicable to this article as no new data were created or analyzed in this study.

ORCID

C. Balakrishnan Jeena https://orcid.org/0000-0001-7228-5891
P. Jose Elsa https://orcid.org/0000-0003-1427-1138
P. Peter Moly https://orcid.org/0000-0002-7549-4952
K. Jacob Ambily https://orcid.org/0000-0002-7499-4453
Vadakkan T. Joy https://orcid.org/0000-0001-9871-2900

REFERENCES

1. Bartolozzi M. Development of redox flow batteries. A historical bibliography. *J Power Sources*. 1989;27:219-234. https://doi.org/10.1016/0378-7753(89)80037-0
2. Noack J, Roznyatovskaya N, Herr T, Fischer P. The chemistry of redox-flow batteries. *Angewandte*. 2015;54(34):9776-9809. https://doi.org/10.1002/anie.201410823
3. Skyllas-kazacos M, Kazacos G, Poon G, Verseema H. Recent advances with UNSW vanadium-based redox flow batteries. *Energy Res*. 2010;34(2):182-189. https://doi.org/10.1002/er
4. Leung P, Li X, De Leo P, Berlouis L, John CT, Walsh FC. Progress in redox flow batteries, remaining challenges and their applications in energy storage. *RSC Adv*. 2012;2:10125-10156. https://doi.org/10.1039/c2ra21342g
5. Soloveichik GL. Flow batteries: current status and trends. *Chem Rev*. 2015;115(20):11533-11558. https://doi.org/10.1021/cr500720t
6. Van Nguyen T, Savinell RF. Flow batteries. *Electrochem Soc Interface*. 2010;19:54-56. https://doi.org/10.1021/ac200156s
7. Chen R, Kim S, Chang Z, Chen R, Kim S. Redox flow batteries: Fundamentals and applications. *Principles Adv Appl*. Rijeka, Croatia: InTech; 2017. https://doi.org/10.5772/intechopen.68752
8. De Le CP, Walsh FC. Redox flow cells for energy conversion. *J Power Sources*. 2006;160:716-732. https://doi.org/10.1016/j.jpowsour.2006.02.095
9. Shigematsu T. Recent development trends of redox flow batteries. *SEI Techn Rev*. 2019;89:5-11.
10. Zhang C, Zhang L. Progress and prospects of next-generation redox flow batteries. *Energy Storage Mater*. 2018;15:324-350. https://doi.org/10.1016/j.ensm.2018.06.008
11. Small LJ, Soc JE, Small LJ, Iii HDP, Anderson TM. Crossover in membranes for aqueous soluble organic redox flow batteries. *J Electrochem Soc*. 2019;166(12):A2436-A2542. https://doi.org/10.1149/2.0681912jes
12. Prifti H, Parasuraman A, Winardi S, Lim TM, Skyllas-kazacos M. Membranes for redox flow battery applications. *Membranes*. 2012;2(2):275-306. https://doi.org/10.3390/membranes2020275
13. Weber AZ, Mench MM, Meyers JP, Ross PN, Gostick JT, Liu Q. Redox flow batteries: a review. *J Appl Electrochem*. 2011;41:1137-1164. https://doi.org/10.1007/s10800-011-0348-2
14. Wei L, Zhao TS, Zeng L, Zhou XL, Zeng YK. Copper nanoparticle-deposited graphite felt electrodes for all vanadium redox flow batteries. *Appl Energy*. 2016;180:386-391. https://doi.org/10.1016/j.apenergy.2016.07.134
15. Mohammadi T, Kazacos MS. Evaluation of the chemical stability of some membranes in vanadium solution. *J Appl Electrochem*. 1997;27:153-160. https://doi.org/10.1023/A:1018495722379
16. Sukkar T, Skyllas-kazacos M. Membrane stability studies for vanadium redox cell applications. *J Appl Electrochem*. 2004;03430:137-145. https://doi.org/10.1023/B:JACH.0000009931.83368.dc
17. Sanz L, Lloyd D, Magdalena E, Palma J. Description and performance of a novel aqueous all-copper redox flow battery. *J Power Sources*. 2014;268:121-128. https://doi.org/10.1016/j.jpowsour.2014.06.008
18. Schaltin S, Li Y, Brooks NR, et al. Towards an all-copper redox flow battery based on a copper-containing ionic liquid. *Chem Commun*. 2015;52(2):414-417. https://doi.org/10.1039/C5CC06774J
19. Lloyd D, Magdalena E, Sanz L, Murtom L. Preparation of a cost-effective, scalable and energy efficient all-copper redox flow battery. *J Power Sources*. 2015;292:87-94. https://doi.org/10.1016/j.jpowsour.2015.04.176
20. Sanz L, Lloyd D, Magdalena E, Palma J, Anderson M. Study and characterization of positive electrolytes for application in the aqueous all-copper redox flow battery. *J Power Sources*. 2015;278:175-182. https://doi.org/10.1016/j.jpowsour.2014.12.034
21. Yensen N, Allen PB. HardwareX Open source all-iron battery for renewable energy storage. *HardwareX*. 2019;6:e00072. https://doi.org/10.1016/j.ohx.2019.e00072
22. Tucker MC, Phillips A, Weber AZ. All-iron redox flow battery tailored for off-grid portable applications. *ChemSusChem*. 2015;8(23):3996-4004. https://doi.org/10.1002/cssc.201500845
23. Banerjee A, Saha D, Row TNG, Shukla AK. A soluble-lead redox flow battery with corrugated graphite sheet and reticulated vitreous carbon as positive and negative current collectors. *Bull Mater Sci*. 2013;36:163-170.
24. Collins J, Li X, Pletcher D, et al. A novel flow battery: a lead acid battery based on an electrolyte with soluble lead (II). Part IX: Electrode and electrolyte conditioning with hydrogen peroxide. *J Power Sources*. 2010;195:2975-2978. https://doi.org/10.1016/j.jpowsour.2009.10.109
25. Cheng J, Gao C, Wen YH, Pan JQ, Xu Y, Cao GP. Performance improvement of the all—lead redox flow battery in fluoroboric acid electrolyte. *Int J Energy Sci*. 2013;3:165-168.

26. Ventosa E, Guarnieri M, Trov A, et al. Redox flow batteries: status and perspective towards sustainable stationary energy storage. 2021;481. https://doi.org/10.1016/j.jpowsour.2020.228804
27. Manohar AK, Kim KM, Plichta E, Hendrickson M, Rawlings S, Narayanan SR. A high efficiency iron-chloride redox flow battery for large-scale energy storage. *J Electrochem Soc*. 2016;163:A5118-A5125. https://doi.org/10.1149/2.0161601jes
28. Gong K, Xu F, Grunewald JB, et al. All-soluble all-iron aqueous redox-flow battery. *ACS Energy Lett*. 2016;1(1):89-93. https://doi.org/10.1021/acsenergylett.6b00049
29. Jayathilake BS, Plichta EJ, Hendrickson MA, Narayanan SR. Improvements to the coulombic efficiency of the iron electrode for an all-iron redox-flow battery. *J Electrochem Soc*. 2018;165:1630-1638. https://doi.org/10.1149/2.0451809jes
30. Li X, De Le CP. Zinc-based flow batteries for medium- and large-scale energy storage. *Advances in Batteries for Medium and Large-Scale Energy Storage*. Woodhead Publishing; 2015;293-315. https://doi.org/10.1016/B978-1-78242-013-2.00008-X
31. Selverston S, Savinell RF, Wainright JS. Zinc-iron flow batteries with common electrolyte. *J Electrochem Soc*. 2017;164:1069-1075. https://doi.org/10.1149/2.0591706jes
32. Arenas LF, Loh A, Trudgeon DP, et al. The characteristics and performance of hybrid redox flow batteries with zinc negative electrodes for energy storage. *Renew Sustain Energy Rev*. 2018;90:992-1016. https://doi.org/10.1016/j.rser.2018.03.016
33. Gong K, Ma X, Conforti KM, et al. A zinc-iron redox-flow battery under $100 per kW h of system capital cost. *Energ Environ Sci*. 2015;8:2941-2945. https://doi.org/10.1039/C5EE02315G
34. Xie Z, Su Q, Shi A, et al. High performance of zinc-ferrum redox flow battery with Ac−/HAc buffer solution. *J Energy Chem*. 2016;25(3):1-5. https://doi.org/10.1016/j.jechem.2016.02.009
35. Zhou X, Lin L, Lv Y, Zhang X, Fan L, Wu Q. Elucidating effects of component materials and flow fields on Sn-Fe hybrid flow battery performance. *J Power Sources*. 2020;450:227613. https://doi.org/10.1016/j.jpowsour.2019.227613
36. Zhou X, Lin L, Lv Y, Zhang X, Wu Q. A Sn-Fe flow battery with excellent rate and cycle performance. *J Power Sources*. 2018;404:89-95. https://doi.org/10.1016/j.jpowsour.2018.10.011
37. Xie C, Zhang H, Li X. Zinc dendrites inhibition for zinc-based battery. *ChemSusChem*. 2018;11:1-2. https://doi.org/10.1002/cssc.201801657
38. Wang K, Pei P, Ma Z, et al. Dendrite growth in the recharging process of zinc-air batteries. *J Mater Chem A*. 2015;3:22648-22655. https://doi.org/10.1039/C5TA06366C
39. Guo L, Guo H, Huang H, Tao S, Cheng Y. Inhibition of zinc dendrites in zinc-based flow batteries. *Front Chem*. 2020;8:1-8. https://doi.org/10.3389/fchem.2020.00557
40. Li C, Zhang X, He W, Xu G, Sun R. Cathode materials for rechargeable zinc-ion batteries: From synthesis to mechanism and applications. *J Power Sources*. 2020;449:227596. https://doi.org/10.1016/j.jpowsour.2019.227596
41. Cheng Y, Lai Q, Li X, Xi X, Zheng Q. Electrochimica Acta Zinc-nickel single flow batteries with improved cycling stability by eliminating zinc accumulation on the negative electrode. *Electrochim Acta*. 2014;145:109-111.
42. Li Q. Dendrites issues and advances in Zn anode for aqueous rechargeable Zn-based batteries. *EcoMat*. 2020;2(3):1-14. https://doi.org/10.1002/eom2.12035
43. Zeng YK, Zhao TS, Zhou XL, Wei L, Ren YX. A novel iron-lead redox flow battery for large-scale energy storage. *J Power Sources*. 2017;346:97-102. https://doi.org/10.1016/j.jpowsour.2017.02.018
44. Yuan Z, Liu X, Xu W, Duan Y, Zhang H, Li X. Negatively charged nanoporous membrane for a dendrite-free alkaline zinc-based flow battery with long cycle life. *Nat Commun*. 2018;9:1-11. https://doi.org/10.1038/s41467-018-06209-x
45. Lee B, Cui S, Xing X, et al. Energy, environmental, and catalysis applications dendrite suppression membranes for rechargeable zinc batteries dendrite suppression membranes for rechargeable zinc batteries. *ACS Appl Mater Interfaces*. 2018;10(45):38928-38935. https://doi.org/10.1021/acsami.8b14022
46. Hao X, Hu J, Zhang Z, et al. Interfacial regulation of dendrite-free zinc anodes through a dynamic hydrophobic molecular. *J Mater Chem A*. 2021;9:14265-14269. https://doi.org/10.1039/d1ta01697k
47. Li B, Nie Z, Vijayakumar M, et al. Ambipolar zinc-polyiodide electrolyte for a high-energy density aqueous redox flow battery. *Nat Commun*. 2015;6:1-8. https://doi.org/10.1038/ncomms7303
48. Lu R, Yang A, Xue Y, Xu L, Zhu C. Analysis of the key factors affecting the energy efficiency of batteries in electric vehicle. *World Electr Veh J*. 2010;4:9-13.

How to cite this article: Jeena CB, Elsa PJ, Moly PP, Ambily KJ, Joy VT. A dendrite free Zn-Fe hybrid redox flow battery for renewable energy storage. *Energy Storage*. 2021;e275. https://doi.org/10.1002/est2.275